**Dissertationes Forestales 22**

# Radiative transfer, interception and scattering in coniferous forests: models and applications for production ecology and remote sensing

Sampo Smolander
Department of Mathematics and Statistics
Faculty of Science
University of Helsinki

Academic dissertation

To be presented, with the permission of the Faculty of Science
of the University of Helsinki, for public criticism in Auditorium B123,
Exactum (Gustaf Hällströmin katu 2b), on June 16th, 2006, at 12 o'clock.

Radiative transfer, interception and scattering in coniferous forests: models and applications for production ecology and remote sensing

Author: Sampo Smolander

Dissertationes Forestales 22

Supervisors: Docent Pauline Stenberg
Department of Forest Ecology
University of Helsinki
Finland

Professor Elja Arjas
Department of Mathematics and Statistics
University of Helsinki
Finland

Pre-examiners: Professor Yuri Knyazikhin
Department of Geography
Boston University
USA

Professor Olevi Kull
Institute of Botany and Ecology
University of Tartu
Estonia

Opponent: Professor Ranga B. Myneni
Department of Geography
Boston University
USA

Cover drawing by Petri Hiltunen

ISSN 1795-7389
ISBN-13: 978-951-651-132-3 (PDF)
ISBN-10: 951-651-132-5 (PDF)

Paper copy printed:
Yliopistopaino
Helsinki 2006

Publishers:
The Finnish Society of Forest Science
Finnish Forest Research Institute
Faculty of Agriculture and Forestry of the University of Helsinki
Faculty of Forestry of the University of Joensuu

Editorial Office:
The Finnish Society of Forest Science
Unioninkatu 40A, 00170 Helsinki, Finland
http://www.metla.fi/dissertationes/

Smolander, Sampo 2006. Radiative transfer, interception and scattering in coniferous forests: models and applications for production ecology and remote sensing. University of Helsinki. Department of Mathematics and Statistics.

# ABSTRACT

This work develops methods to account for shoot structure in models of coniferous canopy radiative transfer. Shoot structure, as it varies along the light gradient inside canopy, affects the efficiency of light interception per unit needle area, foliage biomass, or foliage nitrogen. The clumping of needles in the shoot volume also causes a notable amount of multiple scattering of light within coniferous shoots. The effect of shoot structure on light interception is treated in the context of canopy level photosynthesis and resource use models, and the phenomenon of within-shoot multiple scattering in the context of physical canopy reflectance models for remote sensing purposes.

*Light interception.* A method for estimating the amount of PAR (Photosynthetically Active Radiation) intercepted by a conifer shoot is presented. The method combines modelling of the directional distribution of radiation above canopy, fish-eye photographs taken at shoot locations to measure canopy gap fraction, and geometrical measurements of shoot orientation and structure. Data on light availability, shoot and needle structure and nitrogen content has been collected from canopies of Pacific silver fir (*Abies amabilis* (Dougl.) Forbes) and Norway spruce (*Picea abies* (L.) Karst.). Shoot structure acclimated to light gradient inside canopy so that more shaded shoots have better light interception efficiency. Light interception efficiency of shoots varied about two-fold per needle area, about four-fold per needle dry mass, and about five-fold per nitrogen content. Comparison of fertilized and control stands of Norway spruce indicated that light interception efficiency is not greatly affected by fertilization.

*Light scattering.* Structure of coniferous shoots gives rise to multiple scattering of light between the needles of the shoot. Using geometric models of shoots, multiple scattering was studied by photon tracing simulations. Based on simulation results, the dependence of the scattering coefficient of shoot from the scattering coefficient of needles is shown to follow a simple one-parameter model. The single parameter, termed the recollision probability, describes the level of clumping of the needles in the shoot, is wavelength independent, and can be connected to previously used clumping indices. By using the recollision probability to correct for the within-shoot multiple scattering, canopy radiative transfer models which have used leaves as basic elements can use shoots as basic elements, and thus be applied for coniferous forests. Preliminary testing of this approach seems to explain, at least partially, why coniferous forests appear darker than broadleaved forests in satellite data.

Keywords: shoot structure, light interception, leaf area index, forest reflectance model, multiple scattering, photon recollision probability

# PREFACE

This work begun in 1997, when I – then a second year biology student – was working as a summer trainee for Pauline Stenberg. She had the dataset of paper **II** and had outlined the method described in paper **I**. I spent the summer developing the method, programming, and analysing the data. Pauline introduced me to the study of light and canopy structure, and especially to the problem of describing and modelling the coniferous shoots. Her continuing guidance and support has made this work possible.

In 2000, Ranga Myneni invited me to visit his group in Boston. There, he and Yuri Knyazikhin introduced me to the radiative transfer theory. After all the work with Pauline to describe light interception at the shoot level, it was natural for me to think the scattering process at the shoot level as well. One afternoon we had a long discussion with Yuri on the definitions of the basic scattering element and the elementary volume in numerical radiative transfer computations. Papers **IV** and **V** are basically a late argument to supplement that discussion. I am sorry it took me such a long time to explicate my thoughts.

Discussions with and writings by the old Estonian masters of vegetation radiative transfer, late Juhan Ross, Tiit Nilson and Andres Kuusk, have been a great source of information and inspiration.

I wish to thank my supervisors Pauline Stenberg and Elja Arjas, and all my coauthors. Comments from the pre-examiners Yuri Knyazikhin and Olevi Kull were valuable and really helped to improve the composition of the summary part, for which I am thankful. My father, an ecologist himself, has been a great support and given me lots help and advice.

Financial support from the Graduate School in Computational Biology, Bioinformatics, and Biometry (ComBi), the MaDaMe research programme of the Academy of Finland, the University of Helsinki, the Ella and Georg Ehrnrooth foundation, the Emil Aaltonen foundation, and the Niemi foundation is gratefully acknowledged.

# LIST OF ARTICLES

This thesis is based on the following original articles:

**I** **Smolander, S.** and Stenberg, P. 2001. A method for estimating light interception by a conifer shoot. Tree Physiology 21(12/13):797-803.
(Errata: On page 799 some units are wrong. Both kJ and KJ should always be MJ.)

**II** Stenberg, P., Smolander, H., Sprugel, D., and **Smolander, S.** 1998. Shoot structure, light interception and distribution of nitrogen in an *Abies amabilis* canopy. Tree Physiology 18(11): 759-767.

**III** Palmroth, S., Stenberg, P., **Smolander, S.**, Voipio, P. and Smolander, H. 2002. Fertilization has little effect on light-interception efficiency of *Picea abies* shoots. Tree Physiology 22(15/16): 1185-1192.

**IV** **Smolander, S.** and Stenberg, P. 2003. A method to account for shoot scale clumping in coniferous canopy reflectance models. Remote Sensing of Environment 88(4): 363-373.
(Errata: on page 367, in the line following Eq. 9, $\omega_{\mathrm{L}}$ should be leaf scattering coefficient, not reflectance.)

**V** **Smolander, S.** and Stenberg, P. 2005. Simple parameterizations of the radiation budget of uniform broadleaved and coniferous canopies. Remote Sensing of Environment 94(3): 355-363.



## Author's contribution

I am fully responsible for the summary part of this thesis. In paper **I** I did model development, implementation and computations and a major part of the writing. In paper **II** I did the computations applying the model described in paper **I**, and a minor part of the writing. In paper **III** I did part of the field work and part of the computations. In papers **IV** and **V** I did model development, implementation and computations and an equal part of the writing.

# CONTENTS

# 1 INTRODUCTION

Mathematical modelling of radiative transfer and photosynthesis in plant canopies is generally seen to date back to the seminal paper by Monsi and Saeki (1953). Solar radiation provides energy for plant photosynthesis, and the energy and carbon derived from photosynthesis, the primary production, drive most of the biological processes in Earth's biosphere. Canopy structure determines the part of the available light that plants are able to absorb. Other factors, such as water and nutrient conditions, may limit the capacity with which plants are able to utilize absorbed light in photosynthesis, but the description of the amount of absorbed light is of prime importance in studies of canopy photosynthesis and production ecology.

Since the light response of leaf photosynthesis is non-linear, and generally varies in shape in different parts of a canopy (Larcher 2003), knowing only the total amount of light absorbed by a canopy is sufficient only for rather approximate estimates of canopy photosynthesis (Friend 2001). If we assume canopy geometrical structure and incoming light to be known, we can, in principle at least, calculate the distribution of absorbed light in the canopy. If we also assume the photosynthetic light response in different parts of the canopy as known, using this and the distribution of light, we can calculate canopy photosynthesis. In practice all of the three problems (measuring and modelling canopy structure, calculating canopy radiation regime when structure is known, and measuring and modelling the distribution of photosynthetic capacity in different parts of a canopy) are nontrivial, and empirical and theoretical research of these problems has proceeded iteratively.

Canopy structure, together with the properties of the underlying ground, also determines how vegetation reflects radiation. Understanding the process of radiation reflection, in different wavelengths, from vegetation forms physical basis for the interpretation of vegetation properties from satellite images and other remotely sensed signals (such as satellite radars and lidar). Since in the PAR[1]-wavelengths reflectance and transmittance of leaves and needles is low[2], the models of radiative transfer in plant canopies that have been developed for the purposes of light absorption and photosynthesis usually neglect light scattering and concentrate only on the penetration of direct sunlight and skylight into the canopy. In the radiative transfer models for canopy reflectance, on the other hand, scattered radiation is the main interest and accurate values for leaf or needle optical properties in different wavelengths are important input data.

In their current state of development, canopy reflectance models assume canopy structure and element optical properties to be known, and aim to solve the radiation field inside canopy (e.g. Knyazikhin et al. 1998b, 1999, Gobron et al. 1999, Kuusk and Nilson 2000). The upward radiation leaving the top of the canopy constitutes then the canopy reflectance. The estimation of vegetation properties from remote sensing data is then based on either comparing the observed signal to a database of previously computed reflectances for a wide selection of different canopies, and choosing the closest matches (Knyazikhin et al. 1998b, 1999, Gobron et al. 1999), or iteratively optimizing model input parameters to match the observed signal as closely as possible (Kuusk and Nilson 2000).

Several aspects of the structure of coniferous trees distinguish them from broadleaved plants. The leaves of conifers are needles in shape, not planar like those of broadleaved plants. The needles of conifers are closely grouped together as shoots. While there is shoot

[1] Photosynthetically Active Radiation, 400-700 nm

[2] Generally less than 10%, except for a peak in green that may reach over 20% in a narrow waveband (Walter-Shea and Norman 1991, Middleton et al. 1997)

level grouping also in broadleaved canopies (e.g. Kull and Tulva 2002), the phenomenon is much more pronounced in conifers (Oker-Blom 1986, Oker-Blom et al. 1991, Nilson 1992). Also higher level grouping, shoots in branches and branches in tree crowns, is usually more pronounced in conifers than in broadleaved trees.

The mathematical description of radiative transfer in an interacting medium has traditionally been based on the so called turbid medium assumption (Chandrasekhar 1950, Ross 1981). This means that there should be a length scale in which the locations of absorbing and scattering elements (leaves) in the medium (canopy) are amenable to be described using the concept of statistical density distribution. This is indeed the case in the fields where the radiative transfer theory has been developed (astrophysics, atmospheric physics, nuclear physics). The assumption also holds true relatively well to facilitate describing the radiative regimes of broadleaved canopies (Ross 1981, Myneni et al. 1989).

However, if there is no such length scale, the concept of statistical density distribution is not good for describing the properties of the medium (Mandelbrot 1983). The main motivation of this work has been the notification that this is the case in coniferous canopies. The length scale of the size of the basic elements, needles, is in the order of centimeters. The density distribution of needles in the canopy also varies greatly at the essentially same length scale; needle density is high inside a shoot volume, and then within a distance of a couple of centimeters, outside of a shoot, it can be zero.

The first hierarchy level of grouping is the grouping (or clumping) of needles into shoots. In this work, the effect of shoot scale grouping and the variations in shoot structure on the processes of light absorption (papers **I**, **II** and **III**) and scattering (papers **IV** and **V**) are studied. The effect of grouping in higher hierarchy levels (branches, whorls, tree crowns) is outside the scope of this work and remains subject to further studies.

In paper **I**, a method for estimating light interception by conifer shoots is described. Shoot structure alone can introduce many-fold variation in the efficiency of light interception by unit needle surface or unit needle dry mass (papers **II** and **III**), so it clearly needs to be included in accurate models of canopy light absorption, photosynthesis and resource use. Papers **II** and **III** present empirical work describing the variation in shoot structure and physiology in relation to shoot light interception. Theories and models of canopy photosynthesis and resource use should confirm to this kind of empirical observations.

In paper **IV**, the phenomenon of multiple scattering of light within a coniferous shoot is described using a detailed simulation model. Based on the results of the simulations, a simple algebraic formula is presented that should describe the amount of within-shoot multiple scattering to a very good approximation, and could be used as an easy way to correct for the within-shoot scattering in the traditional leaf-based canopy radiative transfer models. The effect of including within-shoot multiple scattering into canopy level radiative transfer models is described in papers **IV** and **V**, albeit using only simple model canopies with homogeneous higher level structure. The effect is found to be notable, and in the right direction, to explain the observed higher absorption and lower reflectance of coniferous forests, when compared to broadleaved forests (Williams 1991, Zhang et al. 2002, Roberts et al. 2004).

# 2 RADIATIVE TRANSFER

Radiative transfer theory is the study of radiation inside a medium which absorbs, emits and scatters radiation. Historically, it was developed in the early 1900's by astrophysicists and meteorologists studying electromagnetic radiation in planetary, stellar and terrestrial atmospheres (Simpson 1928, Chandrasekhar 1950, Sobolev 1970, Thomas and Stamnes 1999). From the mid 1900's the theory has also been applied and developed by physicists and engineers studying neutron radiation in nuclear reactors (Case and Zweifel 1967, Bell and Glasstone 1970). Transfer theory is also known by the name transport theory.

A more complete description of interaction of radiation with matter would include the Maxwell equations and the wave nature of photons (Ishimaru 1999), or also quantum mechanical behavior of particles. However, in the areas where radiative transfer theory is applied (e.g. atmospheric physics, nuclear reactor theory, radiative transfer in plant canopies), wave nature, polarization, etc. are usually not important and photons, or neutrons, can be treated as point particles.

The theory of radiative transfer inside vegetative canopies started with the interest in modelling canopy photosynthesis (Ross 1981, Hirose 2005), and for that purpose radiation scattering is relatively unimportant and can be mostly ignored. The advent of satellite imaging and remote sensing (Campbell 1996) has made the scattering of photons by vegetation an important area of study.

The radiative transfer equation describes the propagation and scattering of point particles inside an absorbing and scattering medium (Chandrasekhar 1950, Bell and Glasstone 1970, Ross 1981, Myneni et al. 1989, Myneni and Ross 1991). It is based on the following assumptions: (i) that there is a sufficient number of particles so that mean particle flux, as described by the radiation field, is a sufficient description and statistical fluctuations can be ignored, (ii) the particles do not interact with each other, and do not alter the properties of the medium, and (iii) the medium can be described as a continuous turbid medium.

## 2.1 Basic definitions

A position in space is described by vector $\mathbf{r} = (x, y, z)$. A direction is described by unit vector $\mathbf{\Omega}$. A direction can also be specified in polar coordinates by polar angle $\theta$ and azimuth angle $\phi$. In this case $\mathbf{\Omega} = (\sin\theta\cos\phi, \sin\theta\sin\phi, \cos\theta)$. Particle angular density $N(\mathbf{r}, \mathbf{\Omega}, E, t)$ gives the density of particles in point $\mathbf{r}$ propagating to direction $\mathbf{\Omega}$ with energy $E$ at time $t$. Thus,

$$N(\mathbf{r}, \mathbf{\Omega}, E, t)\, dV\, d\mathbf{\Omega}\, dE \tag{1}$$

is the number of particles in the volume element $dV$ about $\mathbf{r}$, having directions within solid angle $d\mathbf{\Omega}$ about $\mathbf{\Omega}$, energies within $dE$ about $E$, at time $t$. If polar coordinates are used for directions, the differential element of solid angle $d\mathbf{\Omega} = \sin\theta\, d\theta\, d\phi$.

Particle angular flux $I$ is the particle angular density $N$ multiplied by the particle velocity $v$. Another view of the particle flux is that

$$I(\mathbf{r}, \mathbf{\Omega}, E, t)\, dA\, d\mathbf{\Omega}\, dE\, dt \tag{2}$$

gives the number of particles having directions within $d\mathbf{\Omega}$ about $\mathbf{\Omega}$ and energies within $dE$ about $E$ that cross area $dA$, being perpendicular to $\mathbf{\Omega}$, in time interval $dt$ about $t$. In photometric terminology (Bell and Rose 1981), angular photon flux is also called radiance.

Radiation traversing a medium will be weakened by its interaction with matter. The total interaction cross section $\sigma$ is the probability that a particle will undergo an interaction, per distance traversed, for differentially small distances. Using differential notation, flux $I$ becomes $I + dI$ after traversing a distance $ds$, and

$$dI = -\sigma I \, ds. \tag{3}$$

$\sigma$ can depend on location and also on the direction of incoming radiation. A part of the radiation interacting with the medium is absorbed, this is given by the absorption cross section $\sigma_{\mathrm{a}}$. Another part is scattered to other directions, this is given by the scattering cross section $\sigma_{\mathrm{s}}$. These two constitute the total interaction cross section, $\sigma = \sigma_{\mathrm{a}} + \sigma_{\mathrm{s}}$. The ratio $\sigma_{\mathrm{s}}/\sigma$ gives the probability of scattering for one interaction, and is called the scattering coefficient.[3] The scattering coefficient is here denoted by $\omega$. A scattered particle shall appear in a new direction. This is described by a probability distribution $f(\mathbf{r}, \mathbf{\Omega}' \rightarrow \mathbf{\Omega})$, giving the probability density that a particle coming from $\mathbf{\Omega}'$ and scattered at $\mathbf{r}$ shall continue to direction $\mathbf{\Omega}$. Naturally,

$$\int_{4\pi} f(\mathbf{r}, \mathbf{\Omega}' \rightarrow \mathbf{\Omega}) \, d\mathbf{\Omega} = 1 \tag{4}$$

since $f$ is a probability distribution. Here integration over all directions (all vectors $\mathbf{\Omega}$ on the surface of the unit sphere) is denoted by $4\pi$. The directional distribution $f$ multiplied by the scattering coefficient $\omega$ is called the scattering phase function. Some authors (e.g. Chandrasekhar 1950) prefer to normalize $f$ to $4\pi$ rather than to 1. This has the advantage that $f \equiv 1$ for uniform scatterers, and the disadvantage that a term $\frac{1}{4\pi}$ has to be included in the scattering term in the equations.

The term $\sigma(\mathbf{r}, \mathbf{\Omega}') \, \omega(\mathbf{r}, \mathbf{\Omega}') \, f(\mathbf{r}, \mathbf{\Omega}' \rightarrow \mathbf{\Omega})$ is written together as $\sigma_{\mathrm{s}}(\mathbf{r}, \mathbf{\Omega}' \rightarrow \mathbf{\Omega})$ for brevity. In this form it is called the differential scattering cross section. In the case of $f$ normalized to $4\pi$, the differential scattering cross section gives the probability per length traversed and per solid angle, for differentially small length and solid angle, that a particle traversing a unit length to direction $\mathbf{\Omega}'$ shall be scattered to direction $\mathbf{\Omega}$.

## 2.2 The radiative transfer equation

The general form of the radiative transfer equation is

$$\frac{1}{v}\frac{\partial I}{\partial t} = -\mathbf{\Omega} \cdot \nabla I - \sigma I + \int_0^\infty \int_{4\pi} \sigma \omega f I \, d\mathbf{\Omega}' \, dE' + Q. \tag{5}$$

Here $v$ denotes particle velocity, $I(\mathbf{r}, \mathbf{\Omega}, E, t)$ is the flux of particles in point $\mathbf{r}$ to direction $\mathbf{\Omega}$ with energy $E$ at time $t$. The total interaction cross section $\sigma(\mathbf{r}, \mathbf{\Omega}, E)$ describes the rate at which particles in point $\mathbf{r}$ traversing to direction $\mathbf{\Omega}$ are removed (absorbed or scattered) from the beam. The scattering coefficient $\omega(\mathbf{r}, \mathbf{\Omega}, E)$ describes the proportion of interactions that lead to scattering, and $f(\mathbf{r}, \mathbf{\Omega}' \rightarrow \mathbf{\Omega}, E)$ describes the probability density that a scattered particle will continue to direction $\mathbf{\Omega}$. The term $Q(\mathbf{r}, \mathbf{\Omega}, E, t)$ describes particle source. The del operator $\nabla$ operates only on the spatial coordinates $\mathbf{r}$. Boundary conditions can be included in the terms for source, interaction and scattering, or given separately.

[3] This probabilistic interpretation is valid here with photons, as collisions do not produce new particles. A more general interpretation is used with neutron scattering, when the production of new particles is possible.

## 2.3 Time-independent form

In photon-vegetation interactions the particle velocity, the speed of light, is so great that the radiation field can usually (with some exceptions, like lidar studies, e.g. Kotchenova et al. 2003) be assumed to be in a steady state, that is $\frac{\partial}{\partial t} I = 0$. The collisions can be assumed not to change photon energies, so the steady state solution can be constructed for different photon energies independently. Additionally, instead of energy, photons are usually characterized by their wavelength. Photon wavelength $\lambda$ is completely determined by photon energy by $E = hc/\lambda$, where $h$ is the Planck's constant and $c$ is the speed of light. The time-independent form of the radiative transfer equation is

$$\mathbf{\Omega} \cdot \nabla I_\lambda(\mathbf{r}, \mathbf{\Omega}) = -\sigma(\mathbf{r}, \mathbf{\Omega}) I_\lambda(\mathbf{r}, \mathbf{\Omega}) + \int_{4\pi} \sigma_{\mathrm{s}\lambda}(\mathbf{r}, \mathbf{\Omega}' \rightarrow \mathbf{\Omega})\, d\mathbf{\Omega}' + Q_\lambda(\mathbf{r}, \mathbf{\Omega}). \qquad (6)$$

When defining the boundary conditions, a canopy is usually considered infinite in horizontal directions. The assumption that $\sigma$ does not depend on wavelength is well justified in plant canopies.

## 2.4 Limitations of the turbid medium assumption

When the traditional radiative transfer theory, as developed for astrophysical, atmospheric and nuclear engineering applications, is applied for plant canopies, three complications appear: anisotropy, spatial inhomogeneity and the large size of the scattering elements.

A good description of plant canopy anisotropy and inhomogeneity is given by Ross (1981). In many areas of application, the properties of the scattering medium are isotropic, i.e. the scattering properties of the medium in a point do not depend on the direction. However, numerical methods for anisotropic scattering also have been developed e.g. in nuclear reactor theory (Bell and Glasstone 1970).

It has been common to assume plant canopies to be horizontally homogeneous. For example the review by Myneni et al. (1989) mainly describes computational methods based on this assumption. At that time available computer resources may indeed have limited feasible numerical methods to horizontally homogeneous cases. Later there has been numerical work also covering horizontally inhomogeneous canopies (Knyazikhin et al. 1997, 1998a,b).

The first two of the above mentioned complications, anisotropy and inhomogeneity, are not inherent limitations in the turbid medium approach, they just have somewhat limited the direct applicability of numerical methods developed in other fields of radiative transfer.

A more serious limitation of the turbid medium approach is encountered with the large size of the scattering elements in plant canopies. In atmospheric and nuclear reactor applications the scattering elements are usually single atoms or molecules. In these cases the element size is many orders of magnitude smaller than the length scale in which the properties of the medium change. This kind of medium is well amenable to the statistical description. In plant canopies the element (leaf, needle) size is in the order of centimeters, and the density and distribution of these elements may change along distances of decimeters or meters. This phenomenon is especially pronounced in conifers, where needles are grouped together as shoots. The geometry of conifers is further discussed in section 3.2. In conifers, the element density varies from high, inside shoot volume, to zero, outside shoot volume, at essentially the same length scale as the element (needle) size. In this case, there is no length scale in which the medium could be considered continuous enough to warrant the use of the turbid medium approximation. Work based on this observation is further discussed in section 5 and in papers **IV** and **V**.

## 2.5 Photon tracing

The method of photon tracing involves generating photons at the light sources and following their paths as they interact with the elements of the scene (Glassner 1995, Jensen 2001). Photon tracing[4] falls under a family of simulation methods called Monte Carlo ray tracing (Disney et al. 2000).

In photon tracing, photons are generated to enter the scene from a specified directional distribution. Their paths are traced until they escape out of the scene, or until an interaction happens. The outcome of an interaction may be absorption, reflection or transmission, and for a particular interaction the outcome is randomly sampled from the respective probabilities. In the case of scattering (i.e. reflection and transmission), the new direction is sampled from a directional distribution describing the scattering properties of the target object, and the path is traced further. The scene can consist of solid objects, as was the case with the shoot level simulation in paper **IV**. In this case the point of first interaction along a photon path is solved by geometric means. The scene can also include objects filled with random turbid medium. In this case the length of the path penetrating into the medium before first collision is sampled from the exponential distribution. This method was used in the canopy level simulations in papers **IV** and **V**.

Since the first publication on the Monte Carlo methods (Metropolis and Ulam 1949), they have developed into a versatile tool in a large variety of applications. An interesting piece of history, as described by Metropolis (1987), is that the Monte Carlo methods were first developed and applied specifically for problems in radiative transfer theory.

# 3 CANOPY ARCHITECTURE AND RADIATION REGIME

The photosynthetic production of a vegetated area is determined by the total amount of foliage, and its photosynthetic performance. If we assume the spatial distribution of the parameters that govern photosynthesis locally to be known, calculating the whole vegetation stand photosynthetic production is reduced to the problem of describing the distribution of light on the photosynthetic surfaces (e.g. Ross 1981, Oker-Blom 1986, Oker-Blom et al. 1991, Gutschick 1991). On the other hand, if we assume that the radiation regime is known, we can ask the question which distribution of photosynthetic resources over different parts of foliage would maximize photosynthetic production (e.g. Kull 2002, and references therein). The matter is further complicated by that fact that plants can alter the total amount of foliage in a canopy, and they can alter the radiation penetration to the lower parts of the canopy by controlling the structure of the higher parts of the canopy (e.g. Anten et al. 1995b, Stenberg 1996b). Also, competition between individuals seems to add the condition that the optimal solution for maximal photosynthetic production is not evolutionary stable strategy (Schieving and Poorter 1999, Anten and Hirose 2001).

[4]Some sources (such as Disney et al. 2000) use the term forward ray tracing instead of photon tracing. However, Foley et al. (1990) point out that that term may be misleading, since usually ray tracing involves tracing the paths of photons from camera to the light sources. Thus the method of tracing photon paths from light sources to camera has also been called backward ray tracing, while it is also know to some as forward ray tracing. To avoid this confusion, I follow the terminology of Glassner (1995) and Jensen (2001) and use the term photon tracing here.

## 3.1 Development of canopy radiation regime models

The now classical mathematical model of canopy light regime and photosynthesis was published by Monsi and Saeki (1953). They measured light attenuation, under overcast sky, in herbaceus plant communities, and found that it was well described by the Beer's law, equation:

$$I(L) = I_0 e^{-kL}, \tag{7}$$

where $I$ is the photosynthetic photon flux density (PPFD) on a horizontal plane, $I_0$ is the PPFD at the top of canopy, $L$ is the leaf area index (LAI) cumulated from the top of the canopy and $k$ is the attenuation coefficient per unit cumulated leaf area. Monsi and Saeki (1953) noted that for randomly located horizontal leaves $k$ should be equal to 1. If leaf distribution is more even than random, it increases $k$, and if leaves are clumped together, it decreases $k$. The amount of light that leaves in a certain infinitesimal layer receive, is given by the derivative of Eq. 7.

The light response $A(I)$ of photosynthetic carbon assimilation was described by a Michaelis-Menten (or rectangular hyperbola) type equation (Michaelis and Menten 1913),

$$A(I) = \frac{bI}{1 + aI} - r, \tag{8}$$

where $a$ and $b$ are some parameters describing photosynthesis light response ($b$ gives the initial slope for small values of $I$, $b/a$ gives the saturated value for large $I$) and $r$ is the respiration rate. Combining 8 and the derivative of 7, and integrating from 0 to maximum LAI ($L_{\max}$), Monsi and Saeki got productivity $P$ as

$$\begin{aligned} P &= \int_0^{L_{\max}} \left( \frac{bkI_0 e^{-kL}}{1 + akI_0 e^{-kL}} - r \right) dL \\ &= \frac{b}{ka} \ln \left( \frac{1 + akI_0}{1 + akI_0 e^{-kL_{\max}}} \right) - rL_{\max}. \end{aligned} \tag{9}$$

An important observation form Eq. 9 is that under some fixed light conditions, there will be some $L_{\max}$ for which the productivity is maximized.

This model of Monsi and Saeki (1953) is perhaps the simplest canopy photosynthesis model that one can think of. For example, the light intercepted by leaves in layer $L + \Delta L$ is assumed to be distributed evenly on the leaf surfaces. This assumption is clearly non-realistic. In reality the light available at a certain depth in a canopy consists of an interplay of spots of sunlight, shadow and penumbra. Leaf orientation, as it usually departs from the horizontal, also effects the irradiance on the surface of a leaf. Additionally, all leaves of the canopy are assumed to have the same photosynthetic capacity, and also this assumption contradicts general empirical knowledge (e.g. Larcher 2003).

The main determinant of the leaf photosynthetic capacity is the leaf nitrogen content[5] (Mooney and Gulmon 1979, Field and Mooney 1986, Evans 1989, Evans and Seeman 1989, Hirosaka and Terashima 1996). Usually, leaves developed in low-light conditions are thinner, and have a smaller amount of photosynthetic apparatus and nitrogen per unit area. Leaves developed in full sunlight are thicker, and have more of photosynthetic apparatus and nitrogen per unit area. Studies on leaf level light acclimation have shown both light saturated photosynthesis rates and respiration rates to be higher in sun leaves than in shade

[5]Leaf nitrogen content = amount of nitrogen per leaf area

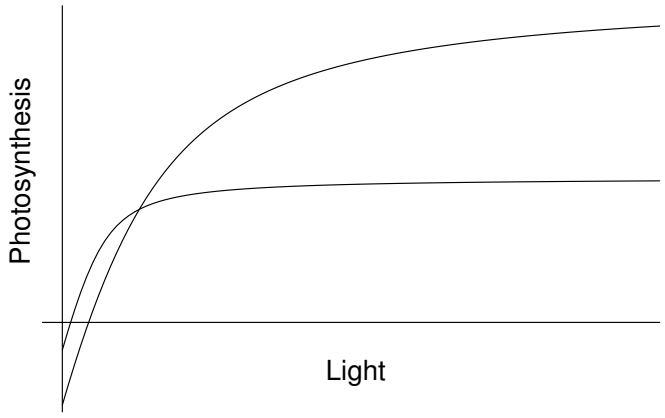


**Figure 1:** A schematic illustration of the typical photosynthesis light response curves of sun and shadow leaves. A sun leaf (higher curve) has higher photosynthesis when there is abundant light, but at low light levels the higher respiration cost causes the sun leaf to photosynthetize less than a shadow leaf (lower curve). The curves follow the form of a widely used model for photosynthesis light response, the non-rectangular hyperbola

$$P = \frac{\phi I + P_{\max} - \sqrt{(\phi I + P_{\max})^2 - 4\theta\phi I P_{\max}}}{2\theta} - r$$

(Thornley 1976). Here, $P$ is photosynthesis, $I$ is light, $P_{\max}$ is the maximum level of photosynthesis, $\phi$ is the initial slope of the photosynthesis light response, and $\theta$ controls the convexity of the curvature between the initial slope and the final saturation.

leaves (e.g. Hollinger 1989, Marek et al. 1989, Ellsworth and Reich 1993, Bassow and Bazzaz 1998). This difference in the photosynthetic light response curves of sun and shade leaves is illustrated in Fig. 1.

The seminal work of Monsi and Saeki has resulted in theories being developed on the optimal distribution of nitrogen in plant canopies, and in experimental work testing the theories. Mooney and Gulmon (1979) proposed a framework of cost-benefit analysis in plant resource use studies. The idea is that sequestering nitrogen (and also other nutrients, but nitrogen is the most important one) and synthesizing proteins for building the photosynthetic apparatus consumes energy, and the energy gain from photosynthesis by this apparatus should exceed the energy invested in its construction.

Field (1983) formulated leaf nitrogen allocation as a variational problem. The optimal distribution of nitrogen among the leaves would be such that no redistribution could increase productivity. Charles-Edwards et al. (1987) and Farquhar (1989) made the assumption that photosynthetic capacity is linearly related to nitrogen content and thus proposed that the optimal nitrogen distribution would be linearly related to intercepted light. Leaf nitrogen distribution has been studied extensively (e.g. Field 1983, DeJong and Doyle 1985, Field and Mooney 1986, Hirose and Werger 1987a,b, Evans 1989, Hirose et al. 1989, Hollinger 1989, Pons et al. 1990, Leuning et al. 1991, Werger and Hirose 1991, Schieving et al. 1992, Ellsworth and Reich 1993, Evans 1993, Kull and Niinemets 1993, Anten et al. 1995a, Hollinger 1996, Dang et al. 1997, Bond et al. 1999, Wilson et al. 2000, Meir et al. 2002, Han et al. 2004) and in nearly all cases nitrogen per unit leaf area varies in parallel with light availability. However, it does not decrease sharply enough to remain proportional to light at lower levels of canopies (Kull 2002, Anten 2005). A more detailed theory of

nitrogen allocation should also take into account the partitioning of leaf nitrogen into different components of the photosynthetic machinery (e.g. Laisk et al. 2005, Eichelmann et al. 2005).

## 3.2 Structural properties of conifers

The geometrical structure of trees has been studied from many viewpoints, including biomechanics (e.g. Niklas 1992), water relations (e.g. Kramer 1995, Kirkham 2005) and light conditions (e.g. Ross 1981, Myneni and Ross 1991). For the study of radiative transfer in vegetative canopies, the main interest lies in the spatial and angular distribution of phytoelements (plant parts: leaves, branches, stems).

Coniferous trees have a geometrical structure that is hierarchical in several levels (e.g. Oker-Blom 1986, Oker-Blom et al. 1991, Nilson 1992, Stenberg et al. 1995b, Bégin and Filion 1999). The space filled by the foliage and the branches of a tree is called a tree crown. It is quite normal for coniferous tree species to have rather distinct tree crowns (Gelderen and Van Hoey Smith 1996). This is especially pronounced in species which have conical crown shapes, such as spruces (genera *Picea*) and firs (genera *Abies*), and somewhat less pronounced in species which have more ellipsoidal crown shape, such as pines (genera *Pinus*). In general, the division of the space of a forest stand into tree crowns filled with foliage, and the empty space between the tree crowns, is important in determining the light conditions of the stand (Anderson 1966, Oker-Blom et al. 1991).

Within a crown, the foliage is divided into branches. Usually most first order lateral branches (lateral branches extending from the main stem) developed in a certain year start growth from the trunk at the same height. This collection of branches attached to tree trunk at the same height is called a whorl (Zimmerman and Brown 1971).

In the context of the conifer species that are treated in this work (*Abies amabilis* (Dougl.) Forbes), *Picea abies* (L.) Karst., and *Pinus sylvestris* L.), the basic unit of one year's growth is called a shoot. In these species, there usually is no branching within a single shoot, but branching takes place when new shoots grow from the buds at the end of previous year's shoots. However, it is also possible that some buds form along the length of a shoot, and new shoots can start to grow from these. The buds can even stay dormant for several years before a new shoot starts to elongate from them (Ishii and Ford 2001). The grouping of shoots into spatially distinct branches can be very pronounced, with empty spaces between the branch volumes, as in many spruces. Or the spaces of individual branches can join together to form a rather continuous crown, as is many pines (Gelderen and Van Hoey Smith 1996).

Perhaps the most distinct structural property of conifers is the aggregation of narrow needles into shoots (e.g. Norman and Jarvis 1974, Leverenz and Jarvis 1980, Carter and Smith 1985, Smith and Carter 1988). Because of the mutual shading of the needles in shoots, a certain amount of needle area, when clumped together into shoots, intercepts less light than would be the case when an equal amount of leaf area were independently distributed in canopy space[6]. Models of coniferous canopy light interception have thus used shoots as the basic elements, and described the canopy structure in terms of the spatial and angular distribution of shoots (Oker-Blom and Kellomäki 1983, Stenberg et al. 1993, Cescatti 1998, Nilson et al. 1999). This requires specifying how shoot silhouette areas, and thus the shoot level attenuation coefficient, depend on the amount of needle area in the shoot and the shoot

[6]That is, following a spatial Poisson process with constant intensity.

structure.

Norman and Jarvis (1974) may have been the first to measure shoot silhouette areas. They also sampled comprehensively from the directions of hemisphere. They called it the attached needle area, projected at an angle. Later, Carter and Smith (1985) defined the silhouette to total area ratio (STAR) as the silhouette area of the shoot divided by the total surface area of needles in the shoot. Since the shoot silhouette area varies as a function of the view direction, so should the STAR, but apparently Carter and Smith (1985) used only one view direction, directly from above the dorsal ("upper") side of the shoot, in their measurements. Measurement from this direction, but normalized to projected rather than total needle area, was later termed $R_{max}$ by Leverenz and Hinckley (1990) and $SPAR_{max}$ by Stenberg et al. (1995a), but as noted in paper **II** it usually does not represent the true maximum.

Next, Oker-Blom and Smolander (1988) explicitly noted the dependence of STAR on the angle between shoot axis and view direction. They worked with Scots pine (*Pinus sylvestris*) and assumed that the shoot structure is cylinder symmetric. They defined the spherical average of STAR as $\overline{\mathrm{STAR}}$ and calculated it for shoots that they had measured from several different view directions. For Scots pine, the assumption of cylinder symmetry in the shoots is rather good, but not perfect, as can be seen from Fig. 5 in paper **I**. For other species, such as Pacific silver fir (*Abies amabilis*) (Fig. 1 in paper **II**), or Norway spruce (*Picea abies*), it does not hold true at all.

Generally, to be able to estimate the value of the average silhouette area of an irregularly shaped object, silhouette area measurements from the directions of half of the the full sphere are required. Since the silhouette area is the same for a direction and its opposite direction, the full sphere is not required. Smolander and Oker-Blom (1989), Smolander et al. (1994) and Stenberg et al. (1995a) included also different angles of rotation of shoot axis in their measurements but they took measurements from one half (Smolander and Oker-Blom 1989, Smolander et al. 1994) or one fourth (Stenberg et al. 1995a) of the hemisphere only. Paper **II** may be the first work since Norman and Jarvis (1974) to present measurements of shoot silhouette areas with comprehensive sampling of all the hemisphere.

The level of needle clumping in shoots, as quantified by STAR, is generally higher in the topmost parts of canopy, and decreases with decreasing light availability (e.g. Sprugel 1989, Leverenz and Hinckley 1990, Schoettle and Smith 1991, Smolander et al. 1994, Niinemets and Kull 1995, Sprugel et al. 1996, Stenberg et al. 2001, paper **II**, paper **III**). Since projected needle area[7] is somewhat easier to measure than total needle surface area, it is sometimes used instead. In this case instead of STAR we have SPAR (silhouette to projected area ratio) (Stenberg et al. 1995a).

In a similar manner, usually needle thickness also decreases with the decreasing light availability from the top to the bottom of the canopy (e.g. Kellomäki and Oker-Blom 1981, Sprugel 1989, Niinemets and Kull 1995, Sprugel et al. 1996, paper **II**, paper **III**). This is illustrated in Fig. 1 of paper **III**.

As STAR increases and needle thickness decreases with the decreasing light availability, they both have the effect of decreasing the amount of needle dry mass per unit shoot silhouette area. We can think that there is more dry biomass "behind" a certain amount of shoot silhouette area in the top, better illuminated, parts of the canopy than in the lower, more shaded, parts.

[7] Area of the projection of needles when they are detached and laid non-overlapping on a flat surface.

# 4 RADIATION INTERCEPTION AND PHOTOSYNTHESIS

The theoretical models of canopy light interception and photosynthesis, as mentioned in section 3.1, are based on several simplifying assumptions on canopy structure and the process of light interception. To facilitate the comparison of theories to nature, we have developed a method to estimate seasonal light interception by real conifer shoots (paper **I**). Papers **II** and **III** describe studies on the effect of needle and shoot structure and shoot light interception efficiency to distributions of light and nitrogen in coniferous canopies, and on how shoot structure and light interception efficiency differ in canopies of different nutritional status.

## 4.1 Light interception at shoot level

The amount of photosynthetically active radiation (PAR) intercepted by leaves or shoots cannot be directly measured by the traditional method of placing horizontal sensors in the canopy (Anderson 1966). Only in the case of strictly horizontal leaves, the reading of a horizontal sensor would correspond to the amount of energy a leaf would receive. In the general case of non-horizontal leaves, or 3-dimensional objects such as shoots, the amount of intercepted radiation depends on the shape and orientation of the object, and the directional distribution of the incoming radiation field. While directional measurements of incoming radiation fields are technically possible (Kuusk et al. 2002), they require lots of effort and special equipment. This kind of directional data are very rare to date.

Our approach in paper **I** was to simulate the directional distribution of incoming radiation from sky during a growing period, based on the equations of motion for the sun, the Beer's law for atmospheric attenuation, and an assumption of simple uniform distribution for the diffuse radiation. The simulated distribution was calibrated to agree with total amounts on direct and diffuse radiation obtained from meteorological field data.

The radiation fields at the locations of shoots were reconstructed by taking a fish-eye photographs at the specific shoot locations, and using these to analyze gap fraction (fraction of visible sky) in different directions as seen from the shoot location. An example is shown in Fig. 3 of paper **I**. In paper **III**, a simpler method was used: The gap fraction of the whole fish-eye photo taken at the location of a shoot was analyzed. This parameter, termed openness (Eq. 1 in paper **III**), provides an indirect measure that correlates strongly with available light.

To describe the shoot geometry, the shoot orientation was measured before detaching the shoot from the tree. Then the shoot silhouette area from different directions was photographically measured in laboratory, and appropriate interpolation and coordinate rotation procedures were applied to reconstruct the shoot silhouette area as it would have been seen from different directions of the sky.

Finally, to calculate the amount of light intercepted by the shoot, the simulated directional distribution of skylight, the directional gap fractions as analyzed from the fish-eye photograph, and the directional distribution of shoot silhouette area were combined.

The main motivation in paper **I** was to describe the process of light interception of a coniferous shoot in a, hopefully, realistic way by including shoot geometry and the directionality of the radiation field in the description. This is done in order to demonstrate that the process of light interception is, especially in conifers, more complex than models of the type described in section 3.1 assume. The model by Monsi and Saeki (1953) is half a century old,

but similar models are also currently used in canopy photosynthesis modelling (e.g. Thornley 2002, Medlyn et al. 2003). When modelling large scale processes, model properties such as simplicity and easy integrability with remote sensing information are of course desirable properties. However, also simpler models for upscaling purposes benefit from comparisons with more detailed models. Our description of the shoot level light interception is hopefully useful when estimating the accuracy of the simpler large scale models.

The shoot seasonal light interception data in paper **II**, as obtained by the method described in paper **I**, is to my knowledge the first to consider both the directionality of the incoming radiation field and shoot geometry. This level of detail is required when testing the theories which predict the relation of leaf nitrogen to intercepted light. Many earlier works have compared sampled leaf nitrogen content with some indirect measure that correlates with the seasonal light interception. For example, Hirose et al. (1989) have used measurements from horizontal light sensors, Hollinger (1989) height in canopy, Ellsworth and Reich (1993) cumulative LAI and Kull and Niinemets (1993) canopy openness.

The theories on nitrogen use optimization describe how nitrogen should be distributed in relation with intercepted light, but they do not usually specify further e.g. the time interval and illumination conditions for light interception. In paper **II** the amount of light intercepted by shoots during one growth period was chosen as the level of detail for comparison with the theories. A more complete description of shoot photosynthesis would also include the distribution of irradiance on the needle surface of the shoot (Oker-Blom 1985, Smolander et al. 1987, Oker-Blom et al. 1992, Cescatti and Zorer 2003) and the effect of penumbra (Stenberg 1995). As the light response of leaf photosynthesis is non-linear (see Fig. 1), similar amounts of seasonal light interception can lead to different amounts of photosynthetic production if their spatial, temporal, or both distributions are different (Lappi and Smolander 1984, Smolander 1984). It remains unknown whether light interception at shoot scale and during one growth period is an adequate level of detail for comparing with the theories, or whether describing light interception at needle level, and accounting for different illumination conditions (e.g. clear and overcast days), would be essential in this context.

## 4.2 Morphology and physiology along light gradient

The study in paper **II** describes variation in shoot and needle structure and their effect on the distributions of light and nitrogen in the canopy of a Pacific silver fir (*Abies amabilis*) stand. Shoots were collected from different heights in the canopy, shoot seasonal light interception was modelled using the method described in paper **I**, shoot and needle structure was measured, and shoot nitrogen content was analyzed.

The radiation regime around the shoots, as obtained by modelling, was clearly multidirectional (Figs. 2, 3 and 4 in paper **II**), also for the shoots from lower locations. This makes accounting for shoot orientation and shape necessary when aiming for accurate estimates of intercepted light. The amount of light available to shoots was quantified by the amount of seasonal interception by a spherical surface if it had been at the place of a shoot. The seasonal light interception of a spherical surface, $\mathrm{SLI_O}$ (Eq. 4 in paper **I**, Eq. 3 in paper **II**), as averaged at the locations of the five most sunlit shoots was about 40 times greater than that averaged at the locations of five most shaded shoot. This is indicative of the variation of available light inside the canopy.

From the top to the bottom of the canopy, SPAR increased about 1.5-fold (Fig. 5A in paper **II**). This, together with the interplay of shoot orientations and the radiation fields

surrounding the shoots (Fig. 8 in paper **II**), reduced the 40-fold variation in $\mathrm{SLI_O}$ to about 20-fold variation in shoot seasonal light interception (SLI), expressed in this case on projected needle area basis. Needle thickness decreased about two-fold from top to bottom (Fig. 6A in paper **II**), resulting in a corresponding increase in specific needle area[8] (SNA) (Fig. 6B in paper **II**). The responses in SPAR, shoot orientation and specific projected needle area together resulted in about four-fold response in shoot silhouette area per dry weight (Fig. 6C in paper **II**) and in reducing the initial 40-fold variation in available light (as measured by $\mathrm{SLI_O}$) to about 10-fold variation in the intercepted light per dry mass.

Needle nitrogen content[9] increased linearly with seasonal light interception (Fig. 9 in paper **II**), albeit with a positive intercept at zero light interception. On mass basis, needle nitrogen concentration (nitrogen per dry mass) increased about 1.5-fold from the bottom to top of the canopy in the dominant and codominant trees. However, the largest nitrogen concentrations were observed in the suppressed trees, which had foliage only in the shaded parts of the canopy. Thus, in the data as a whole, there was no correlation between light availability and needle nitrogen concentration (Fig. 7A in paper **II**). The lowest observed nitrogen concentrations were about 5.5 – 7.5 mg/g. In a survey of 21 species of $C_3$ plants, Field and Mooney (1986, p. 37) present a rough approximate value of 0.5 mmol/g = 7 mg/g for the point where photosynthesis (in abundant light) just compensates for respiration, but commenting that there is much variation in the data between species.

Paper **III** presents a study on shoot and needle morphology and nitrogen concentration along light gradient in Norway spruce (*Picea abies*), with the added dimension that these properties were compared between trees from an irrigated and fertilized and a control ("natural") stand. Generally, shoot silhouette to dry mass ratio (SMR) increased three-fold from the most sunlit to the most shaded shoots in the data (Fig. 7 in paper **III**). However, in the irrigated and fertilized stand more of the variation in SMR resulted from variation in specific needle area (SNA), and less from variation in STAR. In the control stand, STAR caused more variation in SMR than SNA (Figs. 5 and 6 in paper **III**). The proximate reason for this was that the shoots in the control stand had smaller needles and lower needle density. Foliar nitrogen concentration was consistently higher in the irrigated and fertilized stand, and it increased with increasing openness about 1.3-fold in the irrigated and fertilized stand and about 1.2-fold in the control stand (Fig. 3 in paper **III**). The lowest new shoots were found at 2% openness in the irrigated and fertilized stand, and at 10% openness at the control stand.

## 4.3 Discussion and conclusions

It is important to note the difference between available light and intercepted light. There is theoretical (e.g. Stenberg 1996b) and experimental (among others, papers **II** and **III**) evidence that it may be advantageous for trees to have smaller light interception efficiency in the higher parts of canopy so that more light penetrates to the lower parts. In this way, a higher total leaf area can be maintained. The data in papers **II** and **III** suggest that the shoot light interception efficiency can vary about two-fold per needle area, about four-fold per dry mass, and about five-fold per nitrogen. This plasticity is not limited to conifers, also broadleaved trees can control the amount of intercepted light by altering leaf angle and branch structure (e.g. Kull and Tulva 2002). Branch structure at the higher level than shoot structure supposedly also has an effect in conifers, but studies on this are rare.

[8](In this case, projected) needle area divided by needle dry weight

[9]Amount of nitrogen per (projected) needle area

It is also notable that the spherically averaged shoot silhouette area is not an accurate measure of shoot light interception efficiency (Fig. 8 in paper **II**). Especially in the lower part of canopy the radiation field, while not unidirectional, is concentrated near the top part of the hemisphere (Figs. 3B and 4 in paper **II**). At the same time, the shoots in species like *Abies amabilis* and *Picea abies* in the lower canopy tend to be flat and horizontal, which makes the shoot orientation more favourable to light interception than a spherically distributed orientation would be.

Direct measurement of light intercepted by shoots in natural conditions is a technical problem that has not yet been solved. The work in paper **I** presents a solution combining modelling and relatively easy measurements to achieve the result without direct measurements. As the intercepted light is the concept which is used in the nitrogen-use optimization theories, obtaining measured values for it is needed for direct comparison between theories and nature.

The basic prediction of the nitrogen-use optimization theories is that trees should distribute nitrogen in relation to intercepted light. The details of the distribution vary somewhat between different theories. Papers **II** and **III** detail the mechanisms (changes in shoot structure, needle structure, and nitrogen concentration) controlling the nitrogen distribution and that they can lead up to five-fold difference in the amount of nitrogen per unit of light intercepting shoot silhouette area in the observed canopies.

# 5 RADIATION SCATTERING AND REMOTE SENSING

In coniferous canopies the density of scattering elements changes in the shoot scale, and also in larger scales (branches, tree crowns). It is not feasible to include such small scale variation into the leaf area density function, when formulating the radiative transfer problem for coniferous canopies, since that would require specifying the location of each shoot in the canopy. For example, Knyazikhin et al. (1997) used a density function that is piecewise constant in a mesh of 0.5 m sided cubes. When the leaf area density function varies in a length scale that is larger than the length scale in which needles are clumped into shoots, we need an additional method to account for the shoot scale clumping in the models.

If we assume no scattering, i.e. that the canopy elements are optically black, the description of radiation inside canopy is reduced from Eq. 6 to Eq. 3. This assumption is rather common when modelling radiation penetration into canopy for the purposes of photosynthesis modelling or leaf area index measurements. In these models, the phenomenon of needle grouping into shoots has been dealt with by introducing a grouping (or clumping) coefficient (e.g. Oker-Blom and Kellomäki 1983, Oker-Blom 1986, Stenberg 1996a, Chen et al. 1997, Nilson 1999). This coefficient, STAR (see section 3.2) or something similar, has the effect of decreasing the total interaction cross section $\sigma$ (see section 2) for a given amount of needle area density. Using this kind of correction coefficient for shoot level clumping is conceptually equivalent to using shoots as the basic units (scattering elements), and the statistical density function then describes shoot density, not needle density (Nilson and Ross 1997). Some recent canopy reflectance models (Knyazikhin et al. 1998b, Kuusk and Nilson 2000) have used this kind of parameterization.

What seemingly has gone unnoticed in previous models, is that when a shoot level grouping index is used to reduce the area interaction cross section, meaning that shoots, not needles, are treated as the basic scattering elements, optical properties (usually transmittance and reflectance) measured from needles can no longer be used to describe the scattering

properties of the basic elements.

In paper **IV**, the process of light scattering from coniferous shoots is studied using photon tracing and a geometric model of shoot structure, and a simple wavelength dependent correction to scattering is proposed. In paper **V** the consequences of this correction at canopy scale are explored using simple model canopies.

## 5.1 The recollision probability

The key concept in papers **IV** and **V** is the recollision probability. It is defined as the probability that a photon inside a canopy, after being scattered, will collide with the canopy again. A similar definition is applied for recollisions within a shoot, in this case regarding the shoot as a mini-canopy. The probability of hitting the canopy again is supposedly different for photons in different locations and flying to different directions. However, the methods developed in this work are based on the simplifying assumption that these differences do not matter much, and that we can use just one value of recollision probability when modelling the amount of multiple scattering that takes place within a certain canopy (or a shoot). It turns out that this simplifying assumption gives very good results.

Similar ideas have been used in nuclear reactor theory. The key objective in nuclear engineering is to keep the number of neutrons in a reactor stable. Neutrons are lost to absorption, and new neutrons are created in collisions (that is, scattering events). In this process, the changes in the number of neutrons in successive generations is of interest. In nuclear reactor theory literature, the ratio of the number of neutrons in two successive generations is known as the "multiplication factor" or the "multiplication factor eigenvalue" (see sec. 1.5 in Bell and Glasstone 1970), albeit it is not really an eigenvalue in the usual linear algebra sense. For a photon flying inside a canopy to pass from one generation to the next one, both recollision and a subsequent scattering are required. Thus, recollision probability multiplied by scattering probability gives the multiplication factor.

In thermal engineering, the concept of recollision probability is known as view factor or shape factor, giving the proportion of radiation emitted by a body that hits the body again (e.g. Holman 1986). It is important when calculating the capacity of cooling elements to lose heat by thermal radiation. The idea of radiation from one needle hitting the neighboring needles within the same shoot, in the context of heat transfer, has been mentioned by Gates and Benedict (1963).

Knyazikhin et al. (1998b) used the concept of multiplication factor eigenvalue, calling it the "unique positive eigenvalue of the radiative transfer equation", to develop a simple formula for relating canopy absorption in one wavelength to that in another, when leaf absorption was assumed to be known in both wavelengths. Panferov et al. (2001) noted that when the multiplication factor is divided by the element scattering coefficient, the remaining term should be independent of wavelength, and thus be related only to the geometrical structure of a canopy. They termed this factor as the "canopy spectral invariant $p_{\mathrm{i}}$". This is the same concept that is termed the recollision probability here.

The recollision probability is applied to calculate multiple scattering within a canopy as follows. In this example, ground reflectance is assumed to be zero. The part of photons passing through the canopy without colliding is called zero order transmission ($t_0$). The part of photons that collide is called zero order interception ($i_0$). Together, $i_0 + t_0 = 1$. Following the fates of the collided photons ($i_0$), part of them will be absorbed in the first collision ($a_1$). The part of the photons that are scattered at least once before absorption is called the scattered component of absorption ($a_{\mathrm{s}}$). Photons that are scattered at least once

and then escape the canopy downwards, are the scattered component of transmission ($t_\mathrm{s}$), and photons that escape upwards constitute the reflection ($r$). Naturally there is no uncollided component in the reflection. Noting that the components are wavelength dependent, except $i_0$, we get

$$a_1(\lambda) + a_\mathrm{s}(\lambda) + r(\lambda) + t_\mathrm{s}(\lambda) + t_0 = 1. \tag{10}$$

Under the simplifying assumption that the recollision probability is constant in successive scatterings, we can write the total absorptions as a series

$$\begin{aligned} a &= i_0 \left[ (1-\omega) + \omega p (1-\omega) + \omega^2 p^2 (1-\omega) + \ldots \right] \\ &= i_0 \frac{1-\omega}{1-\omega p}, \end{aligned} \tag{11}$$

where $\omega$ is the element scattering coefficient, and $p$ the recollision probability for the canopy. (The dependence of $a$ and $\omega$ on $\lambda$ is not written, to shorten the notation). The fraction of photons that are absorbed at the first collision, $a_1$, is given by $i_0 (1-\omega)$. Thus, we can write Eq. 11 also as

$$\begin{aligned} a &= a_1 + i_0 \left[ \omega p (1-\omega) + \omega^2 p^2 (1-\omega) + \ldots \right] \\ &= a_1 + i_0 \frac{\omega p (1-\omega)}{1-\omega p} \end{aligned} \tag{12}$$

and here the last term gives the multiply scattered part of absorption, $a_\mathrm{s}$. Now we see that the multiply scattered part of the total absorption simplifies to

$$\frac{a_\mathrm{s}}{a} = \frac{\omega p (1-\omega)}{1-\omega p} \Big/ \frac{1-\omega}{1-\omega p} = \omega p. \tag{13}$$

The approach of Eq. 11 can also be interpreted as a Markov chain, and it is illustrated in Fig. 1 in paper **V**.

The above parameterization was based on a simple probabilistic model of multiple scattering. Knyazikhin et al. (1998b) and Panferov et al. (2001) used different methods (they expanded the solution to the radiative transfer equation (Eq. 6) in series of orthogonal functions and truncated the series focusing on the coefficient of the first, dominating term) and arrived at a similar parameterization.

Knyazikhin et al. (1998b) and Panferov et al. (2001) also presented a similar parameterization for the fraction of scattered radiation in canopy transmission. This parameterization was later formulated by Shabanov et al. (2003) into the form

$$\frac{t_\mathrm{s}}{t} = \omega p_\mathrm{t}, \tag{14}$$

where $t = t_0 + t_\mathrm{s}$ is the total canopy transmission, and $p_\mathrm{t}$ is a wavelength independent, canopy structure related parameter describing canopy transmittance.

Both Eqs. 13 and 14 assume that the scattered part in total canopy absorption and transmission depends linearly on the element scattering coefficient. The coefficients $p$ (termed $p_\mathrm{i}$ by Panferov et al. (2001)) and $p_\mathrm{t}$ are postulated to be related to the canopy structure. The following sections, and papers **IV** and **V**, show that the parameterization for absorption, at both shoot scale and canopy scale, conforms well with results from simulations, while the parameterization for transmission does not conform with the simulations.

## 5.2 Multiple scattering at shoot level

In paper **IV**, measured data and a geometric model of a Scots pine (*Pinus sylvestris*) shoot structure by Stenberg et al. (2001) is used. An illustration of the model shoot is shown in Fig. 1 in paper **IV**. The main assumptions in the light scattering simulations were the following: needles were cylindrical in shape, needles followed a Fibonacci phyllotactic arrangement, needle reflectance and transmittance were always equal to each other, and both reflected and transmitted light followed the Lambert distribution. The idea of recollision probability was applied here at shoot level, and the recollision probability was denoted by $p_{\mathrm{sh}}$.

The scattering properties of the model shoot was studied using the photon tracing technique (see section 2.5). The constructed scattering phase functions for a model shoot are shown in Fig. 3 in paper **IV**. Multiple scattering within a shoot was found to be considerable. For example, using the value $p_{\mathrm{sh}} = 0.6$ from Fig. 6 in paper **IV** (this is for a shoot from top canopy) in Eq. 5 in paper **IV**, and using needle scattering coefficient $\omega_{\mathrm{L}} = 0.9$ to represent near infrared (NIR) radiation, we get the result that a photon hitting the shoot will interact with it 2.17 times on the average. Or, for the shoot illustrated in Fig. 1 (which was taken from the middle canopy) in paper **IV**, $p_{\mathrm{sh}} = 0.47$ and the average number of NIR interactions is 1.73.

The recollision probability was used to construct a very simple model of multiple scattering as a geometric series (Eqs. 4 and 5 in paper **IV**) to relate shoot scattering coefficient to needle scattering coefficient at the same wavelength. This simple formula agreed remarkably well at all wavelengths with the values of shoot scattering coefficient obtained from photon tracing simulations (Fig. 5 in paper **IV**). Further, the shoot level recollision probability ($p_{\mathrm{sh}}$) was shown to be approximately equal to $1 - 4\,\overline{\mathrm{STAR}}$. This means that the values of $\overline{\mathrm{STAR}}$ already reported in the literature for several species (papers **II** and **III**, Stenberg et al. 1999, 2001, Cescatti and Zorer 2003) can be directly utilized in parameterizing within-shoot multiple scattering.

## 5.3 Multiple scattering at canopy level

The consequences on canopy level of accounting for the within-shoot shoot multiple scattering (previous section, paper **IV**) are explored briefly in paper **IV** and in more detail in paper **V**. Simple model canopies with homogeneous structure were constructed with either leaves or shoots as the basic scattering elements. In the simulations, photons were fired into the canopy, and the absorption and scattering processes were sampled accordingly. With leaf canopy, scattering was sampled from the scattering phase function for spherically oriented leaves (Eq. 9 in paper **IV**). With shoot canopy, the scattering process was simulated by using the shoot level photon tracing model of paper **IV** as a sub-model for the canopy level simulations.

The fates of the photons were followed and statistics were collected of the number of photons that (i) went through the canopy with no interactions, (ii) were absorbed after zero, one or more interactions, or (iii) were scattered out of the canopy (either upwards or downwards) after one or more interactions (see Fig. 2 in paper **V** for an example). These simulations were performed for canopies of several leaf area indices, and with varying leaf/needle scattering coefficients (which represented different wavelengths).

With these statistics, the idea by Panferov et al. (2001) of using one parameter to describe the wavelength dependency of canopy absorption was tested, and found to be good with both

leaf and shoot canopies. This parameter, the canopy level recollision probability, was shown to be decomposable between shoot level and higher level multiple scattering (Eq. 5 and Fig. 5 in paper **V**).

Knyazikhin et al. (1998b) and Panferov et al. (2001) have also proposed a parameter similar to $p_{\mathrm{i}}$ (which describes wavelength dependent canopy absorption), the $p_{\mathrm{t}}$, to describe wavelength dependent canopy transmission. With absorption and transmission known, the most relevant property from the remote sensing point of view, reflection, is easy to calculate as 1–absorption–transmission. The $p_{\mathrm{t}}$-parameterization, when compared with the simulations, performed relatively well with the leaf canopies, but not well with the shoot canopies.

As an example of including the shoot level correction for a general radiative transfer model, a simple two-stream model by Ross (1981, section II.6.4) was chosen. With this correction included, Ross' model compared rather well with all the simulations (Figs. 7 and 8 in paper **V**).

## 5.4 Implications for remote sensing

As already implemented in some canopy reflectance models (Knyazikhin et al. 1998b, Kuusk and Nilson 2000), the effect of shoot level clumping for the amount of light a canopy intercepts can be implemented by multiplying the leaf area density of the canopy by a clumping index. In this way we get an "effective leaf area density" that describes the efficiency of shoot silhouette area to intercept and attenuate light traversing inside the canopy. In this work I propose that such a correction should logically be accompanied by a wavelength dependent correction for the degree of within-shoot multiple scattering.

For example, if a canopy consists of shoots with a clumping index STAR = 0.133, the effective leaf area index of the canopy is reduced by 4 STAR = 0.532. When performing radiative transfer modelling for this canopy at, say, NIR wavelengths with a needle scattering coefficient of 0.9, we should – since we have chosen shoots as the scattering elements in the model – use shoot level scattering coefficient in the model. The shoot scattering coefficient obtained using values $\omega_{\mathrm{L}} = 0.9$ and $p_{\mathrm{sh}} = 1 - 4\,\mathrm{STAR}$ in Eq. 6 in paper **IV** is 0.829, instead of the needle level value of 0.9.

This correction for the shoot level multiple scattering causes a wavelength dependent increase in canopy absorption (Fig. 3 in paper **V**) and an accompanying decrease in reflection and transmission (Fig. 7 in paper **V**). The increase in canopy absorption is largest when scattering is high but not perfect, corresponding to needle scattering coefficients of around 0.7 – 0.9. This is the situation in NIR wavelengths.

Interestingly, when Kuusk and Nilson (2000, 2001) compared their canopy radiative transfer model to measured data, they note that it specifically seems to underestimate the NIR and MIR (middle infrared) absorption in coniferous canopies, and discuss that this could be related to the inadequacy of their algorithm to calculate multiple scattering when canopies contain clustered structures.

## 5.5 Discussion and conclusions

The specific values chosen for needle reflectance and transmittance in paper **IV** may not be the most realistic. Especially the assumption that needle reflectance always equals transmittance was made more in order to achieve simplicity than realism. Measuring these values for conifer needles is somewhat complicated technically (Daughtry et al. 1989, Mesarch et al. 1999), but some values have been reported (Daughtry et al. 1989, Williams 1991, Rock et al.

1994, Middleton et al. 1997, Mesarch et al. 1999) and generally needle reflectance is larger than transmittance. Additionally, I think that the concepts of needle reflectance and transmittance – needles mostly not being even remotely planar shaped objects – would benefit from careful definition. This would help to clarify what is actually being measured, and whether light escaping from the sides of needles is counted as reflectance, transmittance, or whether it escapes from the measurement system is such a way that it is not included in either. I am not aware of any reported measurements of the specular reflectance of needle surface. However, measurements by Brakke (1994) on some broadleaved species indicate that specular reflectance may not be negligible. The existence of the phenomenon of needle specular reflection is also easy to qualitatively verify by visually observing needles. An improved model of shoot level scattering would include realistic values for needle optical properties, and needle surface specular reflectance.

The recollision probability holds potential to be the single parameter needed to describe how canopy spectral absorption depends on the absorption of canopy elements (leaves, needles). Present results show this approach to adequately describe absorption in homogeneous canopies, and with the inclusion of shoot level clumping when the higher level structure remains homogeneous. The final usefulness of the concept depends on whether the same approach can be successfully used to describe absorption in canopies with several intermediate levels of hierarchical grouping.

The results in paper **V** (Fig. 8) show that while the $p_{\mathrm{t}}$-parameterization of Panferov et al. (2001) performs well in the simple case of homogeneous leaf canopy, the introduction of shoot level clumping in the canopy causes the $p_{\mathrm{t}}$-based description to deviate from the simulation results. This gives reason to assume that the $p_{\mathrm{t}}$-parameterization might not perform well with canopies with grouping in several hierarchy levels. Also, the assumptions behind $p_{\mathrm{t}}$ as seen from Eq. 14 seem suspicious since it is assumed that the fraction of scattered radiation in total canopy transmission depends linearly on the element scattering coefficient. This assumption is not supported by the simulations (Fig. 2 in paper **V**). Still, Fig. 8D in paper **V** indicates regularity in the fractions of upwards and downwards scattered radiation. Perhaps it would be possible to develop another simple parameterization for this process.

Satellites mostly measure reflectances from a single direction, or from a limited set of directions. The models in this work have mostly considered the total reflection to the upper hemisphere. Forest directional reflectance varies for different measurement and solar directions, and is also influenced by crown structure (e.g. Rautiainen et al. 2004) and, according to simulations by Disney et al. (2006), by needle shape and shoot structure.

To conclude, papers **IV** and **V** demonstrate that accounting for multiple scattering at the shoot scale is important for accurate models of coniferous canopy radiative transfer and scattering. One way to handle clumped structures in modelling is to simulate their spectral scattering properties in isolation (paper **IV**) and use the results to derive parameterizations for scattering to be used in models of higher structural level (papers **IV** and **V**). Another way, as has recently been demonstrated by Disney et al. (2006), is to model complete forest canopies to needle level precision, and directly simulate light scattering in the model canopies by photon tracing techniques. Using any approach, the effect that the canopy structural properties at different hierarchy levels have on the canopy reflectance should be described in a way that is helpful in model inversion, i.e. estimating LAI or other structural information from canopies with varying level of clumping using reflectance data.

# REFERENCES

Anderson, M.C. 1966. Stand structure and light penetration, II. A theoretical analysis. Journal of Applied Ecology 3: 41–54.

Anten, N.P.R. 2005. Optimal photosynthetic characteristics of individual plants in vegetation stands and implications for species coexistence. Annals of Botany 95: 495–506.

— & Hirose, T. 2001. Limitations on photosynthesis of competing individuals in stands and the consequences for canopy structure. Oecologia 129: 186–196.

— , Schieving, F. & Werger, M.J.A. 1995a. Patterns of light and nitrogen distribution in relation to whole canopy carbon gain in $C_3$ and $C_4$ mono- and dicotyledonous species. Oecologia 101: 504–513.

— , Schieving, F., Medina, E., Werger, M.J.A. & Schuffelen, P. 1995b. Optimal leaf area indices in $C_3$ and $C_4$ mono- and dicotyledonous species at low and high nitrogen availibility. Physiologia Plantarum 95: 541–550.

Bassow, S.L. & Bazzaz, F.A. 1998. How environmental conditions affect canopy leaf-level photosynthesis in four deciduous tree species. Ecology 79: 2660–2675.

Bégin, C. & Filion, L. 1999. Black spruce (*Picea marianna*) architecture. Canadian Journal of Botany 77: 664–672.

Bell, C.J. & Rose, D.A. 1981. Light measurement and the terminology of flow. Plant, Cell and Environment 4: 89–96.

Bell, G.I. & Glasstone, S. 1970. Nuclear Reactor Theory. Robert E. Krieger Publishing Company, Malabar, Florida.

Bond, B.J., Farnsworth, B.T., Coulombe, R.A. & Winner, W.E. 1999. Foliage physiology and biochemistry in response to light gradients in conifers with varying shade tolerance. Oecologia 120: 183–192.

Brakke, T.W. 1994. Specular and diffuse components of radiation scattered by leaves. Agricultural and Forest Meteorology 71: 283–295.

Campbell, J.B. 1996. Introduction to Remote Sensing. 3 edn. Taylor & Francis, London.

Carter, G.A. & Smith, W.K. 1985. Influence of shoot structure on light interception and photosynthesis in conifers. Plant Physiology 79: 1038–1043.

Case, K.M. & Zweifel, P.F. 1967. Linear transport theory. Addison-Wesley, Reading, MA.

Cescatti, A. 1998. Modelling the radiative transfer in discontinuous canopies of asymmetric crowns I. Model structure and algorithms. Ecological Modelling 101: 263–274.

— & Zorer, R. 2003. Structural acclimation and radiation regime of silver fir (*Abies alba* Mill.) shoots along a light gradient. Plant, Cell and Environment 26: 429–442.

Chandrasekhar, S. 1950. Radiative Transfer. Clarendon Press, Oxford. Reprinted by Dover Publications, New York, 1960.

Charles-Edwards, D.A., Stutzel, H., Ferraris, R. & Beech, D.F. 1987. An analysis of spatial variation in the nitrogen content of leaves from different horizons within a canopy. Annals of Botany 60: 421–426.

Chen, J.M., Rich, P.M., Gower, S.T., Norman, J.M. & Plummer, S. 1997. Leaf area index of boreal forests: Theory, techniques and measurements. Journal of Geophysical Research D 102: 29 429–29 443.

Dang, L.D., Margolis, H.A., Sy, M., Coyea, M.R., Collatz, G.J. & Walthall, C.L. 1997. Profiles of photosynthetically active radiation, nitrogen and photosynthetic capacity in the boreal forest: Implications for scaling from leaf to canopy. Journal of Geophysical

Research D 102: 28 845–28 859.

Daughtry, C.S.T., Biehl, L.L. & Ranson, K.J. 1989. A new technique to measure the spectral properties of conifer needles. Remote Sensing of Environment 27: 81–91.

DeJong, T.M. & Doyle, J.F. 1985. Seasonal relationships between leaf nitrogen content (photosynthetic capacity) and leaf canopy light exposure in peach (*Prunus persica*). Plant, Cell and Environment 8: 701–706.

Disney, M., Lewis, P. & North, P.R.J. 2000. Monte Carlo ray tracing in optical canopy reflectance modelling. Remote Sensing Reviews 18: 163–196.

— , Lewis, P. & Saich, P. 2006. 3D modelling of forest canopy structure for remote sensing simulations in the optical and microwave domains. Remote Sensing of Environment 100: 114–132.

Eichelmann, H., Oja, V., Rasulov, B., Padu, E., Bichele, I., Petta, H., Kull, O. & Laisk, A. 2005. Adjustment of leaf photosynthesis to shade in a natural canopy: reallocation of nitrogen. Plant, Cell and Environment 28: 389–401.

Ellsworth, D.S. & Reich, P.B. 1993. Canopy structure and vertical patterns of photosynthesis and related leaf traits in a deciduous forest. Oecologia 96: 169–178.

Evans, J.R. 1989. Photosynthesis and nitrogen relationships in leaves of $C_3$ plants. Oecologia 78: 9–19.

— 1993. Photosynthetic acclimation and nitrogen partitioning within a lucerne canopy. I. Canopy charasteristics. Australian Jounal of Plant Physiology 20: 55–67.

— & Seeman, J.R. 1989. The allocation of protein nitrogen in the photosynthetic apparatus: costs, consequences and control. In: W.R. Briggs (ed.) Photosynthesis. Alan R. Liss, New York, pp. 183–205.

Farquhar, G.D. 1989. Models of integrated photosynthesis of cells and leaves. Philosophical transactions of the Royal Society of London, Series B 323: 357–367.

Field, C. 1983. Allocating leaf nitrogen for the maximization of carbon gain: Leaf age as a control on the allocation program. Oecologia 56: 341 – 347.

— & Mooney, H.A. 1986. The photosynthesis-nitrogen relations in wild plants. In: T. Givnish (ed.) On the Economy of Plant Form and Function. Cambridge University Press, Cambridge, pp. 25–55.

Foley, J.D., van Dam, A., Feiner, S.K. & Hughes, J.F. 1990. Computer Graphics: Principles and Practice. 2 edn. Addison-Wesley, Reading, Massachusetts.

Friend, A.D. 2001. Modelling canopy $CO_2$ fluxes: are 'big-leaf' simplifications justified? Global Ecology & Biography 10: 603–619.

Gates, D.M. & Benedict, C.M. 1963. Convection phenomena from plants in still air. American Journal of Botany 50: 536–573.

Gelderen, D.M.V. & Van Hoey Smith, J.R.P. 1996. Conifers: The Illustrated Encyclopedia. Timber Press, Oregon.

Glassner, A.S. 1995. Principles of Digital Image Synthesis. Morgan Kaufmann, San Francisco.

Gobron, N., Pinty, B., Verstraete, M. & Govaerts, Y. 1999. The MERIS Global Vegetation Index (MGVI): description and pleriminary application. International Journal of Remote Sensing 20: 1917–1927.

Gutschick, V.P. 1991. Joining leaf photosynthesis models and canopy photon-transport models. In: R. Myneni & J. Ross (eds.) Photon-Vegetation Interactions. Springer-Verlag,

Berlin, pp. 501–535.

Han, Q.M., Kawasaki, T., Nakano, T. & Chiba, Y. 2004. Spatial and seasonal variability of temperature responses of biochemical photosynthesis parameters and leaf nitrogen content within a *Pinus densiflora* crown. Tree Physiology 24: 737–744.

Hirosaka, K. & Terashima, I. 1996. Nitrogen partitioning among photosynthetic components and its consequence in sun and shade plants. Functional Ecology 10: 335–343.

Hirose, T. 2005. Development of the Monsi–Saeki theory on canopy structure and function. Annals of Botany 95: 483–494.

— & Werger, M.J.A. 1987a. Maximizing daily canopy photosynthesis with respect to the leaf nitrogen allocation pattern in the canopy. Oecologia 72: 520–526.

— & Werger, M.J.A. 1987b. Nitrogen use efficiency in instantaneous and daily photosynthesis of leaves in the canopy of a *Solidaga altissima* stand. Physiologia plantarum 70: 215–222.

— , Werger, M.J.A. & van Rheenen, J.W.A. 1989. Canopy development and leaf nitrogen distribution in a stand of *Carex acutiformis*. Ecology 70: 1610–1618.

Hollinger, D.Y. 1989. Canopy organization and foliage photosynthetic capacity in a broad leaved evergreen montane forest. Functional Ecology 3: 53–62.

— 1996. Optimality and nitrogen allocation in a tree canopy. Tree Physiology 16: 627–634.

Holman, J.P. 1986. Heat Transfer. 6 edn. McGraw-Hill, New York.

Ishii, H. & Ford, E.D. 2001. The role of epicormic shoot production in maintaining foliage in old *Pseudotsuga menziesii* (Douglas-fir) trees. Canadian Journal of Botany 79: 251–264.

Ishimaru, A. 1999. Wave Propagation and Scattering in Random Media. Wiley-IEEE Press, New York.

Jensen, H.W. 2001. Realistic Image Synthesis Using Photon Mapping. AK Peters, Wellesley, Massachusetts.

Kellomäki, S. & Oker-Blom, P. 1981. Specific needle area of Scots pine and its dependence on light conditions inside the canopy. Silva Fennica 15: 190–198.

Kirkham, M.B. 2005. Principles of Soil and Plant Water Relations. Elsevier Academic Press, San Diego, California.

Knyazikhin, Y., Mießen, G., Panfyorov, O. & Gravenhorst, G. 1997. Small-scale study of three-dimensional distribution of photosynthetically active radiation in a forest. Agricultural and Forest Meteorology 88: 215–239.

— , Kranigk, J., Myneni, R.B., Panfyorov, O. & Gravenhorst, G. 1998a. Influence of small-scale structure on radiative transfer and photosynthesis in vegetation canopies. Journal of Geophysical Research D 103: 6133–6144.

— , Martonchik, J.V., Myneni, R.B., Diner, D. & Running, S.W. 1998b. Synergistic algorithm for estimating vegetation canopy leaf area index and fraction of absorbed photosynthetically active radiation from MODIS and MISR data. Journal of Geophysical Research D 103: 32 257–32 276.

— , Glassy, J., Privette, J.L., Tian, Y., Lotsch, A., Zhang, Y., Wang, Y., Morisette, J.T., Votava, P., Myneni, R.B., Nemani, R.R. & Running, S.W. 1999. MODIS Leaf Area Index (LAI) and Fraction of Photosynthetically Active Radiation Absorbed by Vegetation (FPAR) Product (MOD15) Algorithm Theoretical Basis Document. Tech. rep., NASA Goddard Space Flight Center, Greenbeld, Maryland.

Kotchenova, S.Y., Shabanov, N.V., Knyazikhin, Y., Davis, A.B., Dubayah, R. & Myneni,

R.B. 2003. Modeling lidar waveforms with time-dependent stochastic radiative transfer theory for remote estimation of forest structure. Journal of Geophysical Research D 108: 4484–4496.

Kramer, P.J. 1995. Water Relations of Plants and Soil. Academic Press, San Diego, California.

Kull, O. 2002. Acclimation of photosynthesis in canopies: models and limitations. Oecologia 2002: 267–279.

— & Niinemets, Ü. 1993. Variations in leaf morphometry and nitrogen concentration in *Betula pendula, Corylus avellana* and *Lonicera xylosteum*. Tree Physiology 12: 311–318.

— & Tulva, I. 2002. Shoot structure and growth among a vertical profile within a *Populus-Tilia* canopy. Tree Physiology 22: 1167–1175.

Kuusk, A. & Nilson, T. 2000. A directional multispectral forest reflectance model. Remote Sensing of Environment 72: 244–252.

— & Nilson, T. 2001. Testing directional properties of a forest reflectance model. Journal of Geophysical Research D 106: 12 011–12 021.

— , Nilson, T. & Paas, M. 2002. Angular distribution of radiation beneath forest canopies using a CCD-radiometer. Agricultural and Forest Meteorology 110: 259–273.

Laisk, A., Eichelmann, H., Oja, V., Rasulov, B., Padu, E., Bichele, I., Petta, H. & Kull, O. 2005. Adjustment of leaf photosynthesis to shade in a natural canopy: rate parameters. Plant, Cell and Environment 28: 375–388.

Lappi, J. & Smolander, H. 1984. Integration of the hyperbolic radiation-response function of photosynthesis. Photosynthetica 18: 402–410.

Larcher, W. 2003. Physiological Plant Ecology. 4 edn. Springer, Berlin.

Leuning, R., Cromer, R.N. & Rance, S. 1991. Spatial distributions of foliar nitrogen and phosphorus in crowns of *Eucalyptus grandis*. Oecologia 88: 504–510.

Leverenz, J.W. & Hinckley, T.M. 1990. Shoot structure, leaf area index, and productivity of evergreen conifer stands. Tree Physiology 6: 135–149.

— & Jarvis, P.G. 1980. Photosynthesis in Sitka spruce (*Picea sitchensis* (Bong.) Carr.). IX. the relative contribution made by needles at various positions in the shoot. Journal of Applied Ecology 17: 59–68.

Mandelbrot, B.B. 1983. The Fractal Geometry of Nature. Freeman, New York.

Marek, M., Masarovicová, E., Kratochvíla, I., Eliás, P. & Janous, D. 1989. Stand microclimate and physiological activity of tree leaves in an oak-hornbeam forest. II. Leaf photosynthetic activity. Trees 4: 234–240.

Medlyn, B., Barrett, D., Landsberg, J. & Clement, P.S.R. 2003. Conversion of canopy intercepted radiation to photosynthate: a review of modelling approaches for regional scales. Functional Plant Biology 30: 153–169.

Meir, P., Kruijt, B., Broadmeadow, M., Barbosa, E., Kull, O., Carswell, F., Nobre, A. & Jarvis, P.G. 2002. Acclimation of photosynthetic capacity to irradiance in tree canopies in relation to leaf nitrogen concentration and leaf mass per unit area. Plant, Cell and Environment 25: 343–357.

Mesarch, M.A., Walter-Shea, E.A., Asner, G.P., Middleton, E.M. & Chan, S.S. 1999. A revised measurement methodology for conifer needles spectral optical properties: Evaluating the influence of gaps between elements. Remote Sensing of Environment 68: 177–192.

Metropolis, N. 1987. The beginning of the Monte Carlo method. Los Alamos Science 15: 125–130.

— & Ulam, S. 1949. The Monte Carlo method. Journal of American Statistical Association 44: 335–341.

Michaelis, L. & Menten, M.L. 1913. Die Kinetik der Invertinwirkung. Biochemische Zeitschrift 49: 334–336.

Middleton, E.M., Chan, S.S., Rusin, R.J. & Mitchell, S.K. 1997. Optical properties of black spruce and jack pine needles at BOREAS sites in Saskatchewan, Canada. Canadian Journal of Remote Sensing 23: 108–119.

Monsi, M. & Saeki, T. 1953. Über den Lichtfaktor in den Pflanzengesellschaften und seine Bedeutung für die Stoffproduktion. Japanese Journal of Botany 14: 22–55. English translation, On the factor of light in plant communities and its importance for matter production, published in Annals of Botany (2005) 95: 549-567.

Mooney, H.A. & Gulmon, S.L. 1979. Environmental and evolutionary constraints on the photosynthetic characteristics of higher plants. In: O.T. Solbrig, S. Jain, G.B. Johnson & P.H. Raven (eds.) Topics in plant population ecology. Columbia University Press, New York, pp. 316–337.

Myneni, R.B. & Ross, J. (eds.) 1991. Photon-Vegetation Interactions. Springer-Verlag, Berlin.

— , Ross, J. & Asrar, G. 1989. A review on the theory of photon transport in leaf canopies. Agricultural and Forest Meteorology 45: 1–153.

Niinemets, Ü. & Kull, O. 1995. Effects of light availibility and tree shape on the architecture of assimilative surface in the canopy of *Picea abies*: variation in shoot structure. Tree Physiology 15: 791–798.

Niklas, K.J. 1992. Plant Biomechanics: An Engineering Approach to Plant Form and Function. University of Chicago Press, Chicago.

Nilson, T. 1992. Radiative transfer in nonhomogeneous plant canopies. In: G. Stanhill (ed.) Advances in Bioclimatology 1. Springer Verlag, Berlin, pp. 59–88.

— 1999. Inversion of gap frequency data in forest stands. Agricultural and forest meteorology 98-99: 437–448.

— & Ross, J. 1997. Modeling radiative transfer through forest canopies: Implications for canopy photosynthesis and remote sensing. In: H.L. Gholz, K. Nakane & H. Shimoda (eds.) The use of remote sensing in the modeling of forest productivity. Kluwer Academic Publishers, Dordrecht, The Netherlands, pp. 23–60.

— , Anniste, J., Lang, M. & Praks, J. 1999. Detemination of needle area indices of coniferous forests canopies in the NOPEX region by ground-based optical measurements and satellite images. Agricultural and Forest Meteorology 98-99: 449–462.

Norman, J.M. & Jarvis, P.G. 1974. Photosynthesis in Sitka spruce (*Picea sitchensis* (Bong.) Carr.). III. Measurements of canopy structure and interception of radiation. Journal of Applied Ecology 11: 375–398.

Oker-Blom, P. 1985. Photosynthesis of a Scots pine shoot: Simulation of the irradiance distribution and photosynthesis of a shoot in different radiation fields. Agricultural and Forest Meteorology 34: 31–40.

— 1986. Photosynthetic radiation regime and canopy structure in modelled forest stands. Acta Forestalia Fennica 197: 1–44.

— & Kellomäki, S. 1983. Effect of grouping of foliage on the within-stand and within-

crown light regime: Comparison of random and grouping canopy models. Agricultural Meteorology 28: 143–155.

— & Smolander, H. 1988. The ratio of shoot sihouette area to total needle area in Scots pine. Forest Science 34: 894–906.

— , Lahti, T. & Smolander, H. 1992. Photosynthesis of a Scots pine shoot: A comparison of two models of shoot photosynthesis in direct and diffuse radiation fields. Tree Physiology 10: 111–125.

— , Lappi, J. & Smolander, H. 1991. Radiation regime and photosynthesis of coniferous stands. In: R. Myneni & J. Ross (eds.) Photon-Vegetation Interactions. Springer-Verlag, Berlin, pp. 469–499.

Panferov, O., Knyazikhin, Y., Myneni, R.B., Szarzynski, J., Engwald, S., Schnitzler, K.G. & Gravenhorst, G. 2001. The role of canopy structure in the spectral variation of transmission and absorption of solar radiation in vegetation canopies. IEEE Transaction on Geosciences and Remote Sensing 39: 241–253.

Pons, T.L., Schieving, F., Hirose, T. & Werger, M.J.A. 1990. Optimization of leaf nitrogen allocation for canopy photosynthesis in *Lysimachia vulgaris*. In: H. Lambers, M.L. Cambridge, H. Konings & T.L. Pons (eds.) Causes and consequences of variation in growth rate and productivity of higher plants. SPB Academic Publishing, Hague, pp. 175–186.

Rautiainen, M., Stenberg, P., Nilson, T. & Kuusk, A. 2004. The effect of crown shape on the reflectance of coniferous stands. Remote Sensing of Environment 89: 41–52.

Roberts, D., Ustin, S., Ogunyemiyo, S., Greenberg, J., Dobrowski, S., Chen, J. & Hinckley, T. 2004. Spectral and structural measures of northwest forest vegetation at leaf to landscape scales. Ecosystems 7: 545–562.

Rock, B.N., Williams, D.L., Moss, D.M., Lauten, G.N. & Kim, M. 1994. High-spectral resolution field and laboratory optical reflectance measurements of red spruce and eastern hemlock needles and branches. Remote Sensing of Environment 47: 176–189.

Ross, J. 1981. The Radiation Regime and Architecture of Plant Stands. Kluwer, Hague.

Schieving, F. & Poorter, H. 1999. Carbon gain in a multispecies canopy: the role of specific leaf area and photosynthetic nitrogen use efficiency in the tragedy of the commons. New Phytologist 143: 201–211.

— , Pons, T.L., Werger, M.J.A. & Hirose, T. 1992. Vertical distribution of nitrogen and photosynthetic activity at different plant densities in *Carex acutiformis*. Plant and Soil 142: 9–17.

Schoettle, A.W. & Smith, W.K. 1991. Interaction between shoot characteristics and solar irradiance in the crown of *Pinus contorta* ssp. *latifolia*. Tree Physiology 9: 245–254.

Shabanov, N.V., Wang, Y., Buermann, W., Dong, J., Hoffman, S., Smith, G., Tian, Y., Knyazikhin, Y. & Myneni, R.B. 2003. The effect of spatial heterogeneity in validation of the MODIS LAI and FPAR algorithm over broadleaf forests. Remote Sensing of Environment 85: 410–423.

Simpson, G.C. 1928. Some studies in terrestrial radiation. Memoirs of the Royal Meteorological Society 2: 69–95.

Smith, W.K. & Carter, G.A. 1988. Shoot structural effects on needle temperatures and photosynthesis in conifers. American Journal of Botany 75: 496–500.

Smolander, H. 1984. Measurement of fluctuating irradiance in field studies of photosynthesis. Acta Forestalia Fennica 187: 1–56.

— & Oker-Blom, P. 1989. The effect of nitrogen content on the photosynthesis of Scots pine

needles and shoots. In: E. Dreyer et al (eds.) Annales des Sciences Forestieres 46 suppl. Forest Tree Physiology. pp. 473–475.

— , Stenberg, P. & Linder, S. 1994. Dependence of light interception efficiency of Scots pine shoots on structural parameters. Tree Physiology 14: 971–980.

— , Oker-Blom, P., Ross, J., Kellomäki, S. & Lahti, T. 1987. Photosynthesis of a Scots pine shoot: Test of a shoot photosynthesis model in a direct radiation field. Agricultural and Forest Meteorology 39: 67–80.

Sobolev, V.V. 1970. Light Scattering by Planetary Atmospheres. Pergamon Press, New York.

Sprugel, D. 1989. The relationship of evergreennes, crown architecture, and leaf size. American Naturalist 133: 465–479.

— , Brooks, J.R. & Hinckley, T.M. 1996. Effects of light on shoot geometry and needle morphology in *Abies amabilis*. Tree Physiology 16: 99–108.

Stenberg, P. 1995. Penumbra in within-shoot and between-shoot shading in conifers and its significance for photosynthesis. Ecological Modelling 77: 215–231.

— 1996a. Correcting LAI-2000 estimates for the clumping of needles in shoots of conifers. Agricultural and Forest Meteorology 79: 1–8.

— 1996b. Simulations on the effects of shoot structure and orientation on vertical gradients in intercepted light by conifer canopies. Tree Physiology 16: 99–108.

— , Linder, S. & Smolander, H. 1995a. Variation in the ratio of shoot silhouette area to needle area in fertilized Norway spruce trees. Tree Physiology 1995: 705–712.

— , Smolander, H. & Kellomäki, S. 1993. Description of crown structure for light interception models: Angular and spatial distribution of shoots in young Scots pine. Studia Forestalia Suecica 191: 843–50.

— , DeLucia, E.H., Schoettle, A.W. & Smolander, H. 1995b. Photosynthetic light capture and processing from cell to canopy. In: W.K. Smith & T.M. Hinckley (eds.) Resource Physiology of Conifers: Acquisition, Allocation, and Utilization. Academic Press, San Diego, California, pp. 3–38.

— , Kangas, T., Smolander, H. & Linder, S. 1999. Shoot structure, canopy openness, and light interception in Norway spruce. Plant, Cell and Environment 22: 1133–1142.

— , Palmroth, S., Bond, B.J., Sprugel, D.G. & Smolander, H. 2001. Shoot structure and photosynthetic efficiency along the light gradient in a Scots pine canopy. Tree Physiology 21: 805–814.

Thomas, G.E. & Stamnes, K. 1999. Radiative Transfer in the Atmosphere and Ocean. Cambridge University Press, Cambrigde.

Thornley, J.H.M. 1976. Mathematical Models in Plant Physiology. Academic Press.

— 2002. Instantaneous canopy photosynthesis: Analytical expressions for sun and shade leaves based on exponential light decay down the canopy and an acclimated non-rectangular hyperbola for leaf photosynthesis. Annals of Botany 89: 451–458.

Walter-Shea, E.A. & Norman, J.M. 1991. Leaf optical properties. In: R. Myneni & J. Ross (eds.) Photon-Vegetation Interactions. Springer-Verlag, Berlin, pp. 229–251.

Werger, M.J.A. & Hirose, T. 1991. Leaf nitrogen distribution and whole canopy photosynthetic carbon gain in herbaceous stands. Vegetatio 97: 11–20.

Williams, D. 1991. A comparison of spectral reflectance properties at the needle, branch, and canopy level for selected conifer species. Remote Sensing of Environment 35: 79–93.

Wilson, K.B., Baldocchi, D.D. & Hanson, P.J. 2000. Spatial and seasonal variability of photosynthesis parameters and their relationship to leaf nitrogen in a deciduous forest. Tree Physiology 20: 565–587.

Zhang, Y., Tian, Y., Myneni, R.B., Knyazikhin, Y. & Woodcock, C.E. 2002. Assessing the information content of multiangle satellite data for mapping biomes I: Statistical analysis. Remote Sensing of Environment 80: 418–434.

Zimmerman, M.H. & Brown, C.L. 1971. Trees: Structure and Function. Springer-Verlag, New York.

# I

**Tree Physiology** 21, 797–803


# A method for estimating light interception by a conifer shoot

SAMPO SMOLANDER[1] and PAULINE STENBERG[2]

[1] *Rolf Nevanlinna Institute, P.O. Box 4, FI-00014 University of Helsinki, Finland*

[2] *Department of Forest Ecology, P.O. Box 27, FI-00014 University of Helsinki, Finland*

Received August 18, 2000

**Summary** We present an operational method for estimating the amount of PAR intercepted by a coniferous shoot. Interception of PAR by a shoot is divided into three components: the amount of radiation coming from the sky, the transmission of radiation through the surrounding vegetation, and the shoot's silhouette area facing the direction of the incoming radiation. All three components usually vary with direction. Radiation incident from the sky consists of direct and diffuse radiation. The well-known equation of motion for the sun and Beer's Law for atmospheric transmittance are used to simulate the directional distribution of direct sunlight for any given period of time. The diffuse component is assumed to be uniform. Meteorological field measurements are used to calibrate the absolute amounts of the direct and diffuse components. The gap fraction (proportion of visible sky) in different directions around a shoot is measured by analyzing a hemispherical fish-eye photograph, taken at the location of the shoot, with an image processing program. Similarly, the shoot silhouette area (SSA) is measured by photographing the shoot from many different directions. The measurements of SSA are interpolated by a method called trigonometric interpolation to obtain the directional distribution of SSA over the entire hemisphere. This distribution is then rotated according to the shoot's position in the canopy. Multiplying incoming PAR, canopy gap fraction and SSA in different directions, and summing over all directions, gives an estimate of PAR intercepted by the shoot during the chosen period of time. The method is described step by step, and applied, as an example, to a shoot from a Scots pine (*Pinus sylvestris* L.) stand in central Finland. Differences in radiation interception properties between sun and shade shoots and their relevance to canopy-scale models are discussed.

*Keywords: gap fraction, light interception, shoot silhouette area, SPAR, STAR, trigonometric interpolation.*

## Introduction

Characterization of the photosynthetic radiation regime of coniferous forests has proved problematic because of their heterogeneous canopy architecture caused by the grouping of foliage at different levels of hierarchy (Norman and Jarvis 1975, Oker-Blom 1986, Nilson 1992). Many arguments support consideration of the shoot as the basic element of photosynthetic light capture in conifers (Stenberg et al. 1995). However, the complex geometrical arrangement of needles on shoots requires a different conceptual and methodological approach to quantitatively characterize the amount of photosynthetically active radiation (PAR) absorbed by the shoot.

We note that the PAR intercepted by leaves or shoots in a canopy cannot be directly measured, e.g., by the traditional method of placing horizontal sensors in some fixed arrangement within the canopy. Improved accuracy has been obtained by increasing the number of sensors and the period of measurement; however, the limitation is not related to spatial and temporal resolution but to lack of correspondence. As formulated by Anderson (1966), radiation measurements are invalid because radiation is measured with artificial surfaces that differ from the photosynthetically active elements with respect to size, structure, arrangement and directional distribution.

We have developed a method for estimating the amount of PAR intercepted by a coniferous shoot during a specified period of time. The directional distribution of incoming radiation is modeled, based on the well-known equation of motion for the sun, Beer's Law for atmospheric transmittance, and semi-empirical relationships for the proportion of direct and diffuse radiation. The absolute amount of incoming radiation during the specified time period is calibrated from meteorological field measurements. No measurements of irradiance within the canopy are required, because conifer needles scatter only a minor part of the photosynthetically active radiation (i.e., absorption is close to unity) (Williams 1991). The fraction of above-canopy PAR entering a shoot can thus be estimated based on the canopy gap fraction in different directions of the upper hemisphere. Similarly, for a given direction of radiation, the PAR intercepted by the shoot is proportional to the shoot's silhouette area in that direction. The directional distribution of gaps in the canopy is provided by hemispherical photographs taken at the shoot's location. The directional distribution of shoot silhouette area (SSA), rotated according to the shoot's original position in the canopy, is obtained by trigonometric interpolation based on photographical measurements of the silhouette area in several specified directions. Multiplying incoming PAR, canopy gap fraction and SSA in different directions, and summing over all directions, gives an estimate of the PAR intercepted by the shoot during the chosen time period.

## Methods

### *Theoretical background*

Let $q(\omega)$ denote the seasonal amount of radiant energy (from solid angle to unit area; J $sr^{-1}$ $m^{-2}$) incident from the direc - tion $\omega$ of the hemisphere $\Omega$. The function $gf(\omega)$ denotes the gap fraction (proportion of visible sky) of the surrounding vegetation, as seen from the location of a shoot in the direc - tion $\omega$. The function gf has values from 0 to 1. The term $SSA(\omega)$ denotes the shoot silhouette area on a plane normal to the direction $\omega$. A shoot's seasonal light interception ($SLI_s$; intercepted radiation per unit needle area) can be expressed as:

$$SLI_s = \frac{1}{NA}\int_{\Omega} q(\omega)gf(\omega)SSA(\omega)d\omega, \quad (1)$$

where the integral is the total amount of energy intercepted by the shoot. The ratio of the integral to the needle area (NA) of the shoot yields the mean amount of intercepted energy per unit needle area. The ratio of SSA to NA is known as STAR (silhouette to total area ratio), when NA refers to the total (all sides) needle area. The spherically averaged STAR ($\overline{STAR}$) is defined as:

$$\overline{STAR} = \frac{1}{NA}\frac{1}{2\pi}\int_{\Omega} SSA(\omega)d\omega. \quad (2)$$

If NA is expressed on a projected area basis, the corresponding ratios are denoted SPAR and $\overline{SPAR}$ (Stenberg et al. 1995). Seasonal light interceptance ($SLI_s$; Equation 1) is obtained as an integral of the directional values of STAR (SPAR) weighted by the radiant energy incident from these directions.

For comparison, the intercepted radiation per unit area of a flat horizontal surface (e.g., a flat sensor) at the shoot's location would be:

$$SLI_h = \int_{\Omega} q(\omega)gf(\omega)\sin(a_\omega)d\omega, \quad (3)$$

where $a_\omega$ is altitude angle of the direction $\omega$. The intercepted radiation per unit cross-sectional area of a spherical surface (e.g., a spherical sensor) would be:

$$SLI_O = \int_{\Omega} q(\omega)gf(\omega)d\omega. \quad (4)$$

This quantity is also known as radiant field strength (Bell and Rose 1981). Note that throughout the paper, radiation is assumed to be incident from the upper hemisphere only.

### *Above-canopy radiation regime*

In the simulations, the amount of PAR above the atmosphere, or the PAR component of the solar constant, is assumed to be $S_0 = 600$ W $m^{-2}$ (Weiss and Norman 1985). The instantaneous location of the sun in the sky is given by the solar altitude $a_s$ and azimuth $\phi_s$ angles. These can be solved from the formulas:

$$\sin a_s = \cos h\cos\delta\cos\Phi + \sin\delta\sin\Phi \quad (5)$$

and

$$\begin{cases} \sin\phi_s = \dfrac{\sin h\cos\delta}{\cos a_s} \\ \cos\phi_s = \dfrac{\cos h\cos\delta\sin\Phi - \sin\delta\cos\Phi}{\cos a_s}, \end{cases} \quad (6)$$

where $h$ denotes hour angle, $\delta$ is declination and $\Phi$ is latitude (Karttunen et al. 1996).

Atmospheric transmittance of direct sunlight from the zenith direction is denoted by $\tau$ and air mass by $m$. Air mass is the relative path length through the atmosphere from solar altitude angle $a_s$ and is approximated by $m = \min(1/\sin a_s, 35)$ (List 1984). Assuming clear sky conditions, the instantaneous irradiance of direct sunlight on a surface perpendicular to the radiation is given by Beer's Law as $S_0\tau^m$. Gates (1980) suggests values between 0.6 and 0.7 for $\tau$. A value of $\tau = 0.7$ is used in the example.

The sky is divided into sections by altitude and azimuth angles (see Figure 1). Resolutions of 5° by 30°, or higher, are recommended in the computation. In Figures 1–4, a resolution of 15° by 45° ($6 \times 8 = 48$ sections) is used. The method is conceptually easy to adjust for uneven divisions in relation to altitude or azimuth angle—for example, so that the solid angles of the sections are equal. The trajectory of the sun is followed throughout the growing season. At every time step (e.g., 1 min), Equations 5 and 6 are used to locate the sun in one of the sections, and the energy input, obtained as $S_0\tau^m$ multiplied by the length of the time step, is added to the account of the section. These values are arranged in a matrix $S$ so that each row corresponds to a class of altitude angles and each column to a class of azimuth angles. For example, at a resolution of 15° by 45°, $S_{32}$ would indicate the sky section of 30–45° by altitude and 22.5–67.5° by azimuth. The values $S_{ij}$ give the directional distribution of direct radiation during the growing

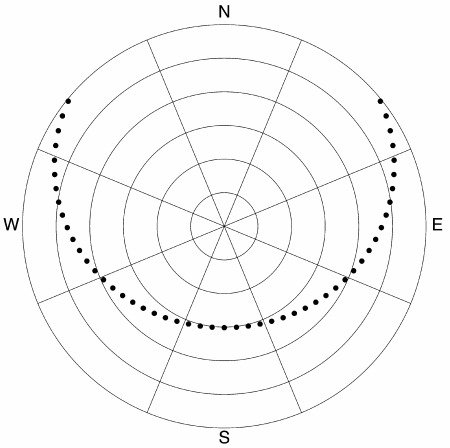


Figure 1. Division of the sky into $6 \times 8$ (15° by 45°) sections and the location of the sun every 20 minutes on August 1, 1998 in Suonenjoki (62°39′ N, 27°05′ E). In practice, a higher resolution is recommended.

season, assuming that every day was clear. The radiation energy from $S$ to a unit horizontal surface is given by:

$$E(S) = \sum_i \sum_j S_{ij} \sin_{ij}, \quad (7)$$

where $\sin_{ij}$ is the sine of the altitude angle of the midpoint of the section $i, j$. The summation is carried over all altitude and azimuth angle classes.

We used material from a Scots pine (*Pinus sylvestris* L.) stand at Suonenjoki Research Station (62°39′ N) as an example (Stenberg et al. 2001, this issue). The time period considered in the computations of the seasonal estimates (Equations 1, 3 and 4) was August 1998, because this was when the measurements were made. Performing the computation for August 1998 in Suonenjoki gives an irradiance of 188 MJ $m^{-2}$ for direct PAR (400–700 nm) to the horizontal plane. Meteorological field measurements give an irradiance of 136 MJ $m^{-2}$ of total (300–4000 nm) direct radiation to the horizontal plane in August 1998 (Finnish Meteorological Institute). The proportion of PAR in total radiation is approximately 45% (Larcher 1995), giving a value of 61.2 MJ $m^{-2}$ PAR in the meteorological observation. (We note that the proportion of PAR in direct and diffuse radiation depends on many factors—see Ross and Sulev 2000—but for simplicity we used 45% in both cases.) Thus, multiplying every entry in the matrix $S$ by the factor:

$$k = \frac{61.2 \text{ kJ m}^{-2}}{188 \text{ kJ m}^{-2}} = 0.326, \quad (8)$$

or simply writing $kS$, gives a calibrated estimate of the directional distribution of direct PAR radiation above Suonenjoki in August 1998. We note that this estimate is based on the assumption that, on average, the reduction in direct radiation by cloud cover is similar in all directions. If there were only thick clouds, the value for $k$ would represent the fraction of time when the sun was unobscured by clouds.

The meteorological field measurements give an irradiance of 187 KJ $m^{-2}$ for total diffuse radiation to the horizontal plane during August 1998. Again, 45%, or 84.2 KJ $m^{-2}$, is assumed to be PAR. A matrix $D$ is constructed by:

$$D_{ij} = \text{sa}_{ij} \times \frac{84.2 \text{ kJ m}^{-2}}{\pi}, \quad (9)$$

where $\text{sa}_{ij}$ is the solid angle of the section $i, j$ in steradians. The matrix $D$ describes a uniform distribution of diffuse PAR radiation. Note that $D$ represents the sum of all diffuse PAR during the time period considered. Usually, in clear sky conditions, diffuse radiation is higher near the horizon, whereas during overcast conditions it is higher near the zenith (Robinson 1966).

Finally, the matrix $T = kS + D$ describes the directional distribution of PAR radiation above Suonenjoki for August 1998. The values of $T_{ij}$ serve as estimates of the function $q(\omega)$ (cf. Equations 1, 3 and 4) integrated over the respective sky sections $i, j$ (see Figure 2).

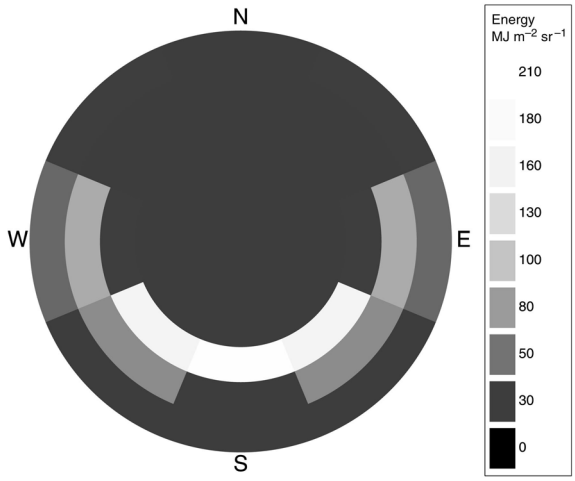


Figure 2. Simulated distribution of above-canopy PAR in Suonenjoki for August 1998. The value assigned to each section is the radiant energy per unit area incident from a unit solid angle of that section.

*Within-canopy radiation regime*

The shading effect of the surrounding vegetation can be analyzed from a hemispherical photograph taken at the location of a shoot. The orientation of the photograph must be known, and the camera should be leveled carefully. By means of hemispherical image analysis software, the photograph is divided into sections $i, j$ as in Figure 1, and the mean proportion of visible sky within each section is determined as the fraction of white pixels (see Figure 3; for details, see Stenberg et al. 2001, this issue). These values are represented by a matrix $G$, where $G_{ij}$ is the estimate of the function gf in the corresponding sky section (cf. Equations 1, 3 and 4). Multiplying the incoming energy, $T_{ij}$, from the direction $i, j$, by $G_{ij}$ yields an estimate of incoming energy from that particular direction to the location of the shoot (see Figure 4).

The seasonal radiation to a unit horizontal surface at the location of the shoot can be estimated as:

$$\text{SLI}_\text{h} = \sum_i \sum_j T_{ij} G_{ij} \sin_{ij}. \quad (10)$$

This estimate corresponds to the reading of a flat sensor measuring continuously during August 1998 at the location of the shoot. The estimate of seasonal radiation per unit cross-sectional area of a sphere is:

$$\text{SLI}_\text{O} = \sum_i \sum_j T_{ij} G_{ij}, \quad (11)$$

which is what a spherical sensor at the shoot's location would detect.

*Light interception by a shoot*

To utilize the directional distribution of incoming energy at a shoot's location to estimate light interception by the shoot, the directional distribution of the shoot silhouette area (SSA) must be known. Before detaching the shoot from the tree for measurements of SSA, the inclination and azimuth of the shoot

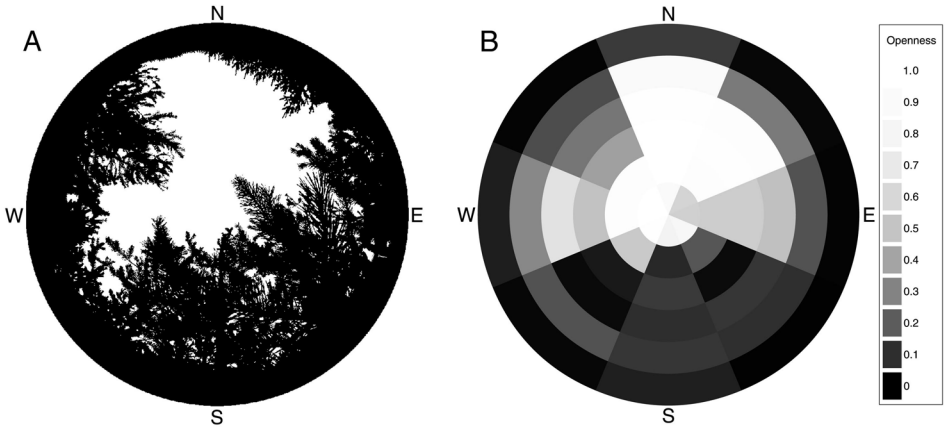


Figure 3. (A) A hemispherical photograph taken at the location of a shoot. Total openness is 0.33. (B) The same photograph after discretizing into sections (see Figure 1) and calculating the mean gap fraction for each section.

axis and the shoot's rotation angle to the vertical are measured. To define the rotation angle, picture a hypothetical plane dividing the shoot into dorsal and ventral sides, and a vector normal to this plane. The rotation angle is the angle between this vector and a vertical plane through the axis of the shoot. When the tip of the shoot is pointing toward the viewer, the positive opening direction of the rotation angle is clockwise. For the example shoot, azimuth was 160°, inclination was 45° and rotation was 0°.

The SSA of the shoot is measured photographically in different view directions ($\phi,\gamma$). We used a resolution of 30° in the $\phi$ direction and 90° in the $\gamma$ direction. The time to take and process the 11 photographs in this example was about 30 min per shoot (for further description of the measurement process see Stenberg et al. 2001, this issue).

The measured values were interpolated by two-dimensional generalization of trigonometric interpolation to give SSA($\phi,\gamma$) for all values of $\phi$ and $\gamma$ (Figure 5) (Smolander 1999; see Stoer and Bulirsch 1980, pp 76–84, for trigonometric interpolation, and Press et al. 1992, pp 95–97, for two dimensional interpolation). For the present application, trigonometric interpolation was used, because SSA is a periodic function of the angles. The value of $\overline{\text{STAR}}$ was calculated by Equation 2 based on the interpolated SSA($\phi,\gamma$) values, and $\Omega = (-\pi/2,\pi/2) \times (-\pi/2,\pi/2)$, $\omega = (\phi,\gamma)$ and $d\omega = \cos\phi d\phi d\gamma$.

Shoot silhouette area as seen from direction $\omega$ of the sky, SSA ($\omega$), is determined from the interpolation function SSA($\phi,\gamma$) (see Figure 5). The recorded information on the shoot's natural orientation in the canopy defines the coordinate transformation required to solve $\phi = \phi_\omega$ and $\gamma = \gamma_\omega$ for every $\omega$. A matrix of SSA is constructed such that $SSA_{ij}$ is the shoot silhouette area $SSA(\phi_\omega,\gamma_\omega)$ as seen from the centerpoint of the sky section $i, j$. Now $SLI_s$ can be estimated as:

$$SLI_s = \frac{1}{NA}\sum_{i,j} T_{ij} G_{ij} SSA_{ij}. \quad (12)$$

## Results

The example shoot intercepted 85.6 kJ of PAR during August 1998. In terms of $SLI_s$ (Equation 1), this amounted to 3.11 kJ $cm^{-2}$ per unit projected needle area (measured photographi-

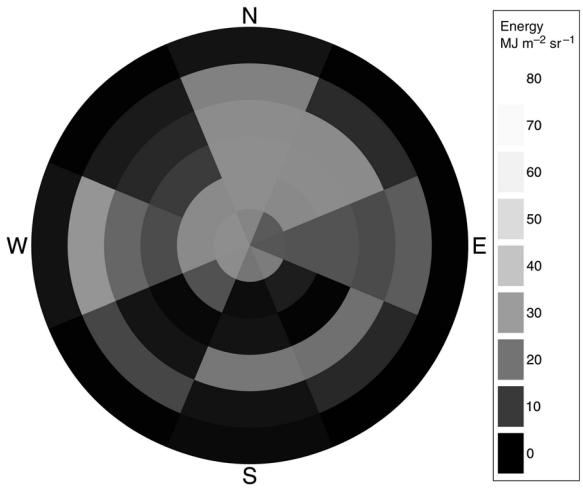


Figure 4. Hemispherical distribution of PAR at the location of a shoot. This image can be thought of as Figure 2 as seen through Figure 3B. Note the different scale.

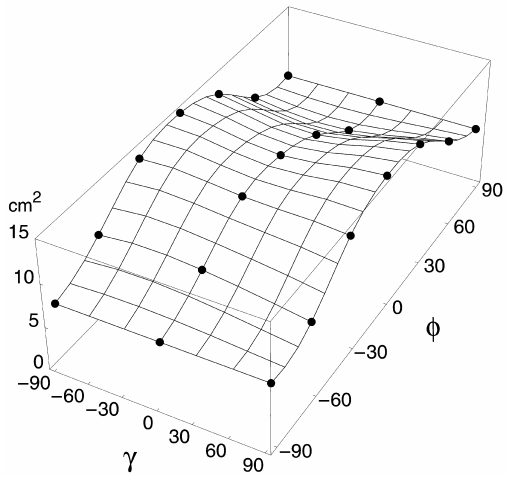


Figure 5. Directional distribution of SSA for the sample shoot. The solid circles denote measured values.

cally to be 27.5 $cm^2$) or 0.991 kJ $cm^{-2}$ per unit (all-sided) needle area (estimated as $\pi$ times the projected area). By comparison, the energy of PAR received on a horizontal plane ($SLI_h$) at the shoot's location during the same period was 4.48 kJ $cm^{-2}$, and $SLI_O$ was 7.02 kJ $cm^{-2}$. The numbers correspond to the readings that would have been given by a flat and a spherical sensor, respectively, placed at the location of the shoot. Values of $SLI_h$, or preferably $SLI_O$, which is unbiased insofar as it does not discriminate among directions, are appropriate measures of available PAR, and can be used to characterize the light environment at the location of the shoot. However, they are insufficient for estimating PAR intercepted by the shoot, because interception is a function of both the radiation field surrounding the shoot (the receiving object), and the structure and orientation of the shoot (object) itself.

We give an example to illustrate this point. Consider a collection (layer) of randomly distributed and spherically oriented needles situated at the same location (i.e., depth in the canopy) as our experimental shoot. These commonly used model assumptions imply that PAR interception per unit total needle area equals that of a spherical surface at the given location. Thus, in our example, the intercepted PAR per unit total needle area of the layer is estimated as $SLI_O$ divided by 4, i.e., 7.02 kJ $cm^{-2}/4$ = 1.76 kJ $cm^{-2}$. (Notice that the factor 1/4, which is the ratio of cross-sectional to total area of a sphere, enters because the reading of a spherical sensor is per unit cross-sectional area.) The value obtained (1.76 kJ $cm^{-2}$) is considerably higher than the calculated PAR interception per total needle area of our shoot (0.991 kJ $cm^{-2}$). The relative difference between the estimates $(1.76 - 0.991)/1.76 = 44\%$ indicates the degree to which the mutual shading of needles on the shoot decreased PAR interception during the time period considered.

The spherically averaged ratio of shoot silhouette area (intercepting area) to total needle area ($\overline{STAR}$, Equation 2) of the shoot was 0.141. We note that $SLI_O$ multiplied by $\overline{STAR}$ (7.02 kJ $cm^{-2}$ × 0.141 = 0.990 kJ $cm^{-2}$) almost exactly matched the calculated $SLI_s$ of the shoot, reflecting that the directional variation in SSA (Figure 5) was not extreme. This simplified method of estimating PAR interception by a shoot may be used as a first approximation, but is theoretically correct only when SSA does not vary with direction, or in the (unrealistic) case when the shoot receives the same amount of PAR from all directions of the upper hemisphere ($q$ × gf constant in Equation 1). In a study on *Abies amabilis* Dougl. *ex* J. Forbes (Stenberg et al. 1998), the simplified method was found to yield a conservative estimate, i.e., it underestimated $SLI_s$ by 15% on average, probably because shoots tend to be oriented so as to increase their PAR interception. This is possible in a nonisotropic radiation field. Comparison between the calculated, true $SLI_s$ and the value estimated by the simplified method gives a measure of the gain in PAR interception as a result of a favorable shoot angle.

## Discussion

Assessment of photosynthetic productivity and resource-use efficiency in plant canopies requires accurate estimates of the distribution of intercepted PAR by the foliage elements. Technical difficulties in measuring this distribution arise because of the large temporal and spatial variations in irradiance that occur within a canopy. Moreover, and more importantly, measurements are of transmitted rather than intercepted PAR. Because coniferous shoots in general are not structurally similar throughout the canopy (e.g., sun shoots and shade shoots), the efficiency with which they intercept the available (transmitted) PAR varies. As a result, the amount of PAR intercepted by shoots along the light gradient in the canopy is not directly proportional to the available PAR at the same locations. This realization has led to a deeper understanding of the role of structural adjustment as a mechanism for enhanced photosynthetic performance of shade foliage (shade acclimation) in conifers (Stenberg 1996, Sprugel et al. 1996). For example, in recent studies on *Picea abies* (L.) Karst and *Abies amabilis* (Stenberg et al. 1998, 1999; see also Sprugel et al. 1996) it was found that the increase in STAR (SPAR) with shading allowed shade shoots to intercept about twice as much PAR per unit needle area as sun shoots would intercept in similar radiation conditions.

Based on model terminology, the observed pattern means that the extinction coefficient increases as transmitted PAR decreases. This pattern is not captured by the classical canopy radiation models, which are built on the assumption of statistically independent leaf locations, described by a probability density function (e.g., the Poisson distribution) (Ross 1970, Mann et al. 1977, Norman 1980). In these models, the extinction coefficient is equivalent to the mean projection of unit leaf area, and varies only with leaf orientation and direction of radiation. Statistical dependency (nonrandomness) in leaf dispersion, e.g., deviations toward clumped or regular distributions, is a classical issue in radiation models (cf. Nilson 1971). For example, in many models, leaves are clumped into tree crowns, which may be regularly spaced, and the classical random theory is applied to individual crowns (e.g., Norman and Welles 1983). However, the clumping of needles on shoots cannot be treated by this approach because a statistical probability density function is not relevant for describing the spatial distribution of needles within the small region occupied by a shoot. The whole concept of leaf area density starts to collapse when smaller and smaller regions are considered (see an analog in Mandelbrot 1983, p. 8). This creates the well known problem in radiative transfer theory of how to handle small-scale structures (e.g., Knyazikhin et al. 1998).

In our model approach, we define the shoot as the basic unit, and describe crown structure in terms of shoot structure, and the angular and spatial distribution of shoots (Stenberg et al. 1993). The extinction coefficient then corresponds to mean STAR, averaged with respect to the directional distribution of PAR at the considered location. In addition to the effect of needle angles, it includes a factor (< 1) accounting for self-shading of shoots. Similar approaches have been used by, e.g., Smith et al. (1993), Cescatti (1998), and Nilson (1999). However, because of a lack of data, the extinction coefficient has

commonly been assumed to be constant throughout the canopy (spatially invariant). We emphasize that a vital part of shoot-level models is that they allow inclusion of the dynamic interaction among shoot structure, within-canopy PAR regime, and leaf area development. To this end, information is needed on how differences in shoot structure modify the gradients of PAR within the canopy and, conversely, how the availability of light influences shoot structure.

The methodology described in this paper forms part of our long-term goal to develop a proper characterization of the PAR regime within coniferous canopies. The method offers an operational means to estimate the PAR intercepted by shoots during any specified time period. Calculation of intercepted PAR is not by itself sufficient for predicting canopy photosynthesis without consideration of other environmental variables. For example, a detailed analysis of shoot photosynthesis requires estimates of the temporal distributions of irradiance on the needle area of the shoots (Stenberg et al. 2001, this issue). However, the method provides the necessary data for shoot-level models, which we believe are best suited to capture the effect of small-scale structure on the spatial distribution of PAR. Moreover, the method can be used to derive quantitative relationships among available PAR, shoot structure, and intercepted PAR, thus providing a tool for including structural acclimation as an active feedback mechanism in long-term simulations.

At present, accuracy in the measurement of canopy gap fractions (transmission) and shoot silhouette area (SSA) is ensured by high-resolution digital cameras. Also, the estimates of SSA in unmeasured directions, obtained by trigonometric interpolation, are believed to be accurate. Uncertainty remains regarding a realistic description of the above-canopy radiation field. The simulated directional distribution of above-canopy radiation was based on two assumptions: first, that cloud cover reduces direct radiation similarly in all directions; and second, that the directional distribution of incoming diffuse radiation is uniform. We believe that these assumptions are good for longer (month-scale) time periods, when the random effects of clouds average out. Producing the distribution for a short time period (e.g., a single day), would require knowledge or assumptions about the nature of cloudiness during the time period considered.

## References


Anderson, M.C. 1966. Some problems of simple characterization of the light climate in plant communities. *In* Light as an Ecological Factor. Eds. R. Bainbridge, G.C. Evans and O. Rackham. Blackwell Science Publishers, Oxford, pp 77–90.

Bell, C.J. and D.A. Rose. 1981. Light measurement and the terminology of flow. Plant Cell Environ. 4:89–96.

Cescatti, A. 1998. Effects of needle clumping in shoots and crowns on the radiative regime of a Norway spruce canopy. Ann. Sci. For. 22:89–102.

Gates, D.M. 1980. Biophysical ecology. Springer-Verlag, New York, 611 p.

Karttunen, H., P. Kröger, H. Oja, M. Poutanen and K.J. Donner. 1996. Fundamental astronomy, 3rd Edn. Springer-Verlag, Heidelberg, 532 p.

Knyazikhin, Y., J. Kranigk, R. Myneni, O. Panfyorov and G. Gravenhorst. 1998. Influence of small-scale structure on radiative transfer and photosynthesis in vegetation cover. J. Geophys. Res. 103: 6133–6144.

Larcher, W. 1995. Physiological plant ecology, 3rd Edn. Springer-Verlag, Heidelberg, 506 p.

List, R.J. 1984. Smithsonian meteorological tables, 6th Edn. Smithsonian Institute, Washington, D.C., 572 p.

Mandelbrot, B.B. 1983. The fractal geometry of nature. Freeman, New York, 468 p.

Mann, J.E., G.L. Curry, D.J. Hartfield and D.W. Demichele. 1977. A general law for direct sunlight penetration. Math. Biosci. 34: 63–78.

Nilson, T. 1971. A theoretical analysis of the frequency of gaps in plant stands. Agric. Meteorol. 8:25–38.

Nilson, T. 1992. Radiative transfer in non-homogeneous plant canopies. *In* Advances in Bioclimatology, Vol. 1. Ed. G. Stanhill. Springer-Verlag, Berlin, pp 59–88.

Nilson, T. 1999. Inversion of gap frequency data in forest stands. Agric. For. Meteorol. 98:437–448.

Norman, J.M. 1980. Interfacing leaf and canopy light interception models. *In* Predicting Photosynthesis for Ecosystem Models, Vol. 2. Eds. J.D. Hesketh and J.W. Jones. CRC Press, Boca Raton, FL, pp 49–67.

Norman, J.M. and P.G. Jarvis. 1975. Photosynthesis in Sitka spruce (*Picea sitchensis* (Bong.) Carr.). V. Radiation penetration theory and a test case. J. Appl. Ecol. 12:839–877.

Norman, J.M. and J.M. Welles. 1983. Radiative transfer in an array of canopies. Agron. J. 75:481–488.

Oker-Blom, P. 1986. Photosynthetic radiation regime and canopy structure in modeled forest stands. Acta For. Fenn. 197:1–44.

Press, W.H., S.A. Teukolsky, W.T. Vetterling and B.F. Flannery. 1992. Numerical Recipes in FORTRAN, 2nd Edn. Cambridge Univ. Press, Cambridge, 963 p.

Robinson, N. 1966. Solar radiation, 1st Edn. Elsevier, Amsterdam, 347 p.

Ross, J. 1970. Mathematical models of photosynthesis in a plant stand. *In* Prediction and Measurement of Photosynthetic Productivity. Ed. I. Setlik. Centre for Agricultural Publishing and Documentation, Wageningen, pp 29–45.

Ross, J. and M. Sulev. 2000. Sources of errors in measurements of PAR. Agric. For. Meteorol. 100:103–125.

Smith, N.J., J.M. Chen and T.A. Black. 1993. Effects of clumping on estimates of stand leaf area index using the Li-Cor LAI-2000. Can. J. For. Res. 23:1940–1943.

Smolander, S. 1999. Sunray and forest. Master's thesis, Univ. of Helsinki, 46 p. In Finnish.

Sprugel, D., J.R. Brooks and T.M. Hinckley. 1996. Effects of light on shoot geometry and needle morphology in *Abies amabilis*. Tree Physiol. 16:91–98.

Stenberg, P. 1996. Simulations of the effects of shoot structure and orientation on vertical gradients in intercepted light by conifer canopies. Tree Physiol. 16:99–108.

Stenberg, P., E.H. DeLucia, A.W. Schoettle and H. Smolander. 1995. Photosynthetic light capture and processing from cell to canopy. *In* Resource Physiology of Conifers. Eds. W.K. Smith and T.M. Hinckley. Academic Press, New York, pp 3–38.

Stenberg, P., T. Kangas, H. Smolander and S. Linder. 1999. Shoot structure, canopy openness, and light interception in Norway spruce. Plant Cell Environ. 22:1133–1142.

Stenberg, P., S. Palmroth, B.J. Bond, D.G. Sprugel and H. Smolander. 2001. Shoot structure and photosynthetic efficiency along the light gradient in a Scots pine canopy. Tree Physiol. 21:805–814.

Stenberg, P., H. Smolander and S. Kellomäki. 1993. Description of crown structure for light interception models: Angular and spatial distribution of shoots in young Scots pine. Stud. For. Suec. 191: 43–50.

Stenberg, P., H. Smolander, D. Sprugel and S. Smolander. 1998. Shoot structure, light interception, and distribution of nitrogen in an *Abies amabilis* canopy. Tree Physiol. 18:759–767.

Stoer, J. and R. Bulirsh. 1980. Introduction to numerical analysis, 1st Edn. Springer-Verlag, New York, 609 p.

Weiss, A. and J.M. Norman. 1985. Partitioning solar radiation into direct and diffuse, visible and near-infrared components. Agric. For. Meteorol. 34:205–213.

Williams, D.L. 1991. A comparison of spectral reflectance properties at the needle, branch, and canopy level for selected conifer species. Remote Sens. Environ. 35:79–93.

# II

**Tree Physiology** 18, 759–767


# Shoot structure, light interception, and distribution of nitrogen in an *Abies amabilis* canopy

PAULINE STENBERG,[1] HEIKKI SMOLANDER,[2] DOUGLAS SPRUGEL[3] and SAMPO SMOLANDER[4]

[1] *Department of Forest Ecology, P.O. Box 24, FI-00014 University of Helsinki, Finland*

[2] *The Finnish Forest Research Institute, Suonenjoki Research Station, FI-77600 Suonenjoki, Finland*

[3] *College of Forest Resources, AR-10, University of Washington, Seattle, WA 98195, USA*

[4] *Department of Biosciences, Division of Genetics, P.O. Box 56, FI-00014 University of Helsinki, Finland*

Received January 5, 1998

**Summary** We studied the effects of variation in shoot structure and needle morphology on the distributions of light and nitrogen within a Pacific silver fir (*Abies amabilis* (Dougl.) Forbes) canopy. Specifically, we investigated the role of morphological shade acclimation in the determination of resource use efficiency, which is claimed to be optimal when the distribution of nitrogen within the canopy is directly proportional to the distribution of intercepted photosynthetically active radiation (PAR). Shoots were collected from different heights in the crowns of trees representing four different size classes. A new method was developed to estimate seasonal light interceptance (SLI, intercepted PAR per unit needle area) of the shoots using a model for the directional distribution of above-canopy PAR, measurements of shoot silhouette area and canopy gap fraction in different directions. The ratio $SLI/SLI_o$, where the reference value $SLI_o$ represents the seasonal light interceptance of a spherical surface at the shoot location, was used to quantify the efficiency of light capture by a shoot. The ratio $SLI/SLI_o$ doubled from the top to the bottom of the canopy, mainly as a result of smaller internal shading in shade shoots than in sun shoots. Increased light-capturing efficiency of shade shoots implies that the difference in intercepted light by sun shoots versus shade shoots is much less than the decrease in available light from the upper to the lower canopy. For example, SLI of the five most sunlit shoots was only about 20 times greater than the SLI of the five most shaded shoots, whereas $SLI_o$ was 40 times greater for sun shoots than for shade shoots. Nitrogen content per unit needle area was about three times higher in sun needles than in shade needles. This variation, however, was not enough to produce proportionality between the amounts of nitrogen and intercepted PAR throughout the canopy.

*Keywords: morphological acclimation, Pacific silver fir, resource use efficiency.*

## Introduction

Several theories exist on how structure and function in plant canopies should be organized to optimize the utilization of resources such as light, water, and nutrients (Verhagen et al. 1963, Kuroiwa 1970, Horn 1971, Mooney and Gulmon 1979, Field 1983, Bloom et al. 1985, Evans 1989, Farquhar 1989, Chen et al. 1993). These theories produce different solutions depending on the assumptions and constraints the optimization is based on.

Early theories showed that if the parameters of the light response curve do not vary with position in the canopy, photosynthesis is optimized if light interception per unit leaf area is constant throughout the canopy (Verhagen et al. 1963). This optimization is generally unachievable because upper leaves inevitably shade lower leaves, although it can be counteracted to some extent by differences in leaf angle (Miller 1967, Kuroiwa 1970, Horn 1971) and shoot structure (Sprugel 1989, Leverenz and Hinckley 1990, Sprugel et al. 1996, Stenberg 1996).

Other theories are based on the observation that the photosynthetic capacity of leaves (expressed as maximum $CO_2$ uptake per unit mass) is often proportional to their nitrogen concentration (Field and Mooney 1986). Given this, it can be shown that resource use is optimized when the distribution of nitrogen within the canopy is directly proportional to the distribution of intercepted PAR, when both are expressed on an area basis (e.g., Farquhar 1989). Many plant canopies have now been studied from this perspective (Field 1983, Hirose et al. 1989, Hollinger 1989, Ellsworth and Reich 1993, Evans 1993, Kull and Niinemets 1993), and in nearly all cases, it has been found that nitrogen per unit leaf area varies in parallel with light availability, although it rarely decreases sharply enough to remain proportional to light at lower levels of the canopy. However, these theories do not specify the physiological or morphological mechanism by which an optimal distribution is obtained, and structural variations above the level of the leaf have rarely been considered. Many common morphological and physiological adaptations to shade are in general agreement with an efficient use of resources, but quantitative estimates of their combined effects on, for example, canopy photosynthesis, are largely missing.

Acclimation responses causing variation in the physiology and morphology of leaves in different light environments greatly increase the complexity, but also the flexibility, of resource use optimization. Morphological adaptations in conifers include increases in specific needle area (SNA) and the ratio of shoot silhouette area to needle area with shading (e.g., Leverenz and Hinckley 1990, Niinemets and Kull 1995, Stenberg et al. 1995, Sprugel et al. 1996). The ratio of shoot silhouette area to needle area is referred to as STAR or SPAR, depending on whether total needle surface area or projected needle area is used in the denominator, respectively. The increase in STAR (SPAR) at lower irradiances reduces the variation in intercepted light per unit needle area of shoots in different parts of the canopy (Stenberg 1996). The simultaneous increase in SNA further diminishes the differences in light interception per unit needle mass or unit nitrogen.

These adaptations are in qualitative agreement with the theory by Farquhar (1989) stating that resource use is optimized when the distribution of photosynthetic capacity and nitrogen is proportional to the distribution of intercepted light (see Sprugel et al. 1996). However, to estimate the effects of acclimation in a canopy it is necessary to quantify the degree to which changes in SNA and SPAR modify the distribution of light and nitrogen. To do this, variations in nitrogen concentration, SNA and SPAR along the entire light gradient in the canopy must be described. The effects of variations in SPAR and SNA on the distribution of intercepted light within a canopy must also be quantified. It is a complicated problem because leaf and shoot morphology do not solely affect the photosynthetic properties of the leaf (shoot) itself, but change the whole profile of light in the canopy. In addition, because the shoot silhouette area varies with the direction of radiation (sun angle), it is not obvious how best to quantify light interception by a coniferous shoot.

We examined changes in SNA, SPAR and nitrogen concentration in Pacific silver fir (*Abies amabilis* (Dougl.) Forbes) with shading, and analyzed the implications of these changes on the distribution and utilization of light and nitrogen within the canopy. Special efforts were made to produce accurate estimates of seasonal light interception by the shoots, based on measurements of canopy transmittance and shoot silhouette area from many different angles.

## Material and methods

### *In situ measurements*

Measurements were made in a 37-year-old *A. amabilis* stand at 1200 m elevation in the Findley Lake research area about 65 km southeast of Seattle, WA (47°20′ N, 121°35′ W). We collected 47 current-year shoots (30 in 1994 and 17 in 1995) from the tips of branches at different heights in the crowns of eight trees. Tree height ranged from 2.4 to 8.6 m, and shoots were collected from two trees of each of the size classes: suppressed (< 4 m), intermediate (4–6 m), codominant (6–8 m), and dominant (≥ 8 m). Data were split into two categories, one comprising shoots from codominant and dominant trees (29 shoots), and the other comprising shoots from suppressed and intermediate trees (18 shoots).

Shoot position and orientation were recorded before removing the shoots. The orientation of a shoot was determined by the inclination and azimuth of the shoot axis, and the shoot's rotation angle to the vertical. To define the rotation angle, we picture a vector ($r$) perpendicular to the hypothetical plane dividing the shoot into upper and lower sides, and pointing toward the shoot's upper side. We measured the angle of $r$ to the vertical plane through the shoot axis, and attached to it a positive or negative sign depending on the opening direction. The positive opening direction of $r$ is clockwise when the tip of the shoot is pointing toward the viewer.

After the sample was collected, we took a hemispherical photograph at each shoot location with a Nikon 8-mm lens and Kodachrome 200 film. These photographs were analyzed with the CANOPY hemispherical photo analysis program (Rich 1989). The program provided the fraction of gaps separately for 18 inclination bands (width 5°) and eight azimuths (width 45°) (144 different sky sections) as well as total canopy openness, defined as the unweighted fraction of open sky (indirect site factor according to Anderson (1964) and Rich (1989)).

Mathematically, canopy openness is defined as:

$$\text{OPENNESS} = \frac{1}{2\pi}\int_{\Omega} gf(\omega)d\omega, \quad (1)$$

where $\Omega$ represents the upper hemisphere and $gf(\omega)$ the gap fraction in the direction $\omega$ of the sky.

### *Measurement of shoot morphology and silhouette area*

The directional distribution of shoot silhouette area (SSA) was produced by measuring SSA photographically in different view directions ($\phi$, $\gamma$) and constructing spline functions to interpolate smoothly between the measured values (bicubic spline interpolation; see Press et al. 1992). The silhouette areas were measured with a digital camera attached to an image analysis system (OPTIMAS, BioScan Inc., Edmonds, WA). The focal length of the lens (AF Nikkor) was 180 mm, and the distance between shoot and camera was 7.0 m for long shoots and 4.2 m for small shoots. The maximum view angle of the shoot was 1.5°. The system was calibrated according to the manufacturer's specifications for each measurement distance.

Following earlier practice (Oker-Blom and Smolander 1988), we define the inclination angle ($\phi$) as the angle of the shoot axis to the plane of projection. Thus, for $\phi = 0°$, the shoot axis is perpendicular to the direction of view (camera), and for $\phi = \pm 90°$, the shoot axis is parallel to the direction of view. The value of $\phi$ is positive when the branch tip is pointing toward the viewer, and negative when the branch tip is pointing away from the viewer. The rotation angle ($\gamma$) is defined as the angle between the vector ($r$) and the plane going through the shoot axis and the view direction. Thus, when $\gamma = 0°$, the shoot's upper side is facing the viewer, and when $\gamma = \pm 90°$, the shoot is viewed from the side (see Figure 1).

A set of measurements was made where the rotation angle ($\gamma$) was held fixed and the inclination angle ($\phi$) was changed in

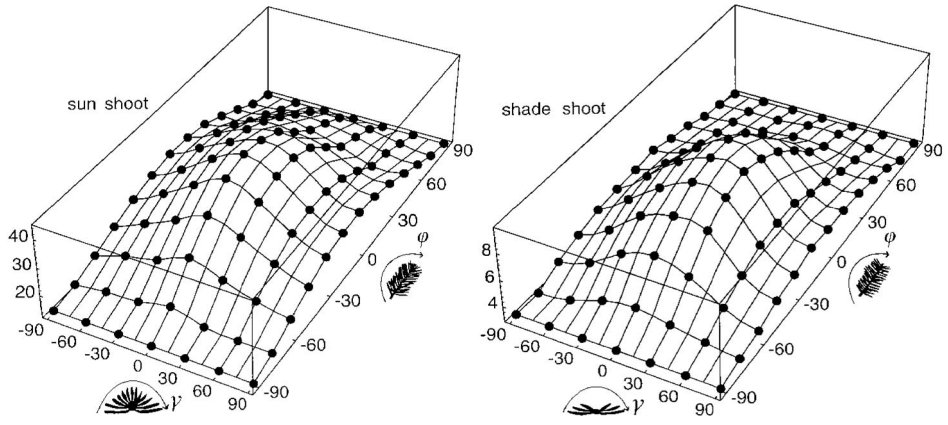


Figure 1. Directional distribution of SSA ($cm^2$) of a sun shoot and a shade shoot. The shoot is assumed to lie on its flat side, and the branch tip points to the positive ϕ-axis. The ● denotes a measured value. Note the different scales on the vertical axes for the sun (left) and shade shoots.

equal steps. This procedure was then repeated after changing the rotating angle in equal steps. In the 1994 measurements, the inclination and rotation angles were both changed in steps of 45°, giving a total of 16 silhouette areas measured per shoot. In 1995, the inclination angle was changed in steps of 15°, and the rotation angle was changed in steps of 30°, giving 72 silhouette areas measured per shoot. Interpolation surfaces for SSA of a "sun" shoot (canopy openness = 0.746) and a "shade" shoot (canopy openness = 0.130) are shown in Figure 1.

After measurement of shoot silhouette area, needles were detached from the shoot and the projected area of all needles on the shoot ($PNA_s$) was measured photographically with the OPTIMAS-system, equipped with a lens with a focal length of 50 mm (see Kershaw and Larsen 1992). The silhouette to projected leaf area ratio (SPAR) was obtained by dividing SSA by $PNA_s$. The ratio of SSA(0,0) to $PNA_s$ is referred to as $SPAR_{max}$, although SSA does not necessarily attain its maximum value at $\phi = \gamma = 0$ (Figure 1). The mean of SSA taken over all directions of the sphere ($\overline{SSA}$) was obtained by calculating the mean of the spline function constructed to describe SSA in all directions. The value of $\overline{SSA}$ divided by $PNA_s$ yields the spherically averaged silhouette area ratio ($\overline{SPAR}$).

We also measured shoot length, number of needles per shoot, mean needle length and thickness, and needle dry weight (48 h at 70 °C). The nitrogen content of needles was measured with a LECO CHN-900 analyzer (LECO Co., St. Joseph, MI) (Table 1).

### *Simulation of above-canopy and within-canopy distributions of PAR*

Incoming PAR was simulated by a method similar to that described by Stenberg (1996), but taking into account the azimuthal direction of the sun also. The period from June 1 to October 1 was chosen to represent the growing season at the study site. Input assumptions and parameters for the simulation model were as follows: (1) the amount of PAR available at the top of the atmosphere (the PAR equivalent of the solar constant) was assigned the value of 600 W $m^{-2}$ (Weiss and Norman 1985); (2) it was assumed that 61% of the PAR incident on a horizontal surface at the top of the atmosphere is received at the ground (Western Solar Utilization Network 1980); (3) of the penetrated PAR, 55% entered as direct radiation, and 45% as diffuse sky radiation (Fritschen and Hsia 1979) (Assumptions 1–3 fixed the seasonal amount of incoming PAR per unit horizontal surface ($Q_h$) at 1203 MJ $m^{-2}$, of which the direct and diffuse components were 662 MJ $m^{-2}$ and 541 MJ $m^{-2}$, respectively); (4) the directional distribution of sunlight was produced by assuming that clear sky conditions prevailed throughout the season, and transmittance of the atmosphere to direct radiation was set to 0.73 in the zenith direction, and was corrected for atmospheric path length. The distribution obtained in this way was then multiplied by a factor (< 1) to give the "known" amount of direct PAR; and (5) the directional distribution of diffuse radiation was assumed to be isotropic.

The simulated distribution of PAR incident from different sections of the sky is shown in Figure 2. Total incoming PAR, expressed as the energy received per unit cross-sectional area of a spherical surface ($Q_o$), was 2109 MJ $m^{-2}$. The directional distribution of PAR around a shoot (Figure 3A) was obtained by multiplying each entry in the sky energy matrix (Figure 2A) by the corresponding entry in the hemispherical matrix (Figure 3B), containing the gap fractions in the 144 different sections of the sky.

Table 1. Structural characteristics and estimates of the light environment of the sample shoots.

| Characteristic | Range | Mean |
|---|---|---|
| Shoot length (cm) | 2.2–15.7 | 7.7 |
| Needle density ($cm^{-1}$) | 8.5–28 | 18.1 |
| Needle area per shoot ($cm^2$) | 3.4–111.6 | 40.3 |
| Needle thickness (mm) | 0.25–0.88 | 0.54 |
| Needle length (mm) | 8–26 | 17.9 |
| SNA ($cm^2\ g^{-1}$) | 33.2–122.5 | 62.3 |
| N concentration (%) | 0.56–1.4 | 0.95 |
| N content (mg $cm^{-2}$) | 0.084–0.354 | 0.174 |
| $\overline{SPAR}$ | 0.262–0.561 | 0.359 |
| $SPAR_{max}$ | 0.337–0.993 | 0.556 |
| $\overline{SSA}$/needle dry weight ($cm^2\ g^{-1}$) | 9.05–51.75 | 23.96 |
| Openness | 0.006–0.82 | 0.313 |
| SLI (kJ $cm^{-2}$) | 0.94–59.5 | 23.7 |
| $SLI_o$ (kJ $cm^{-2}$) | 1.88–187 | 68.8 |
| $SLI/SLI_o$ | 0.252–0.764 | 0.414 |

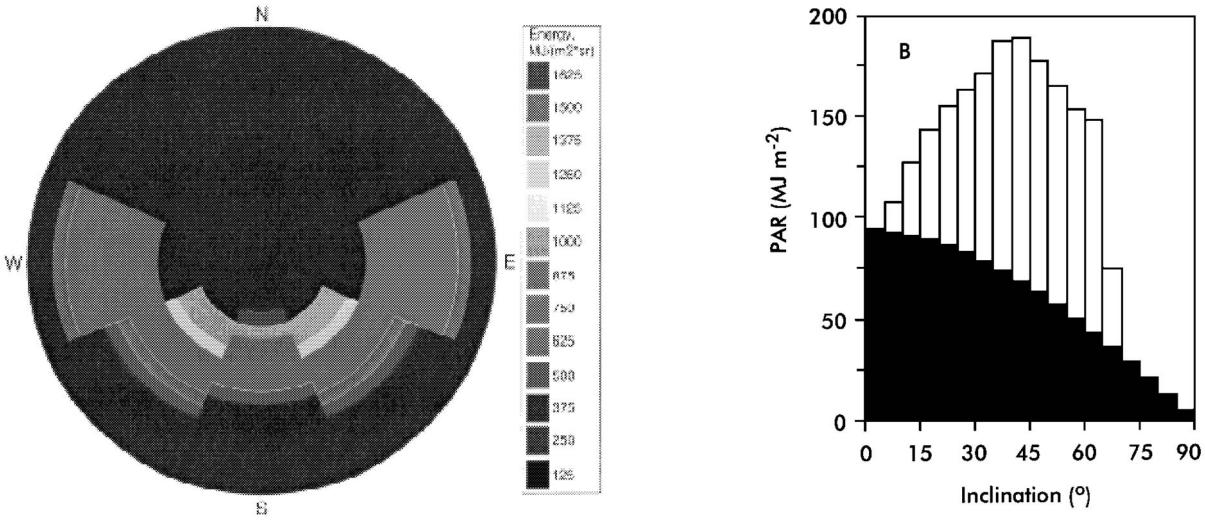


Figure 2. Simulated distributions of above-canopy PAR at the study site during the growing season. A. Sky energy matrix—the hemisphere is divided in 144 (18 × 8) sections, and the value (color) assigned to each section is the radiant energy per unit area incident from unit solid angle around that direction of the sky. Values shown on the scale correspond to the upper limits of the intervals. B. Division of direct (□) and diffuse (■) PAR into inclination bands.

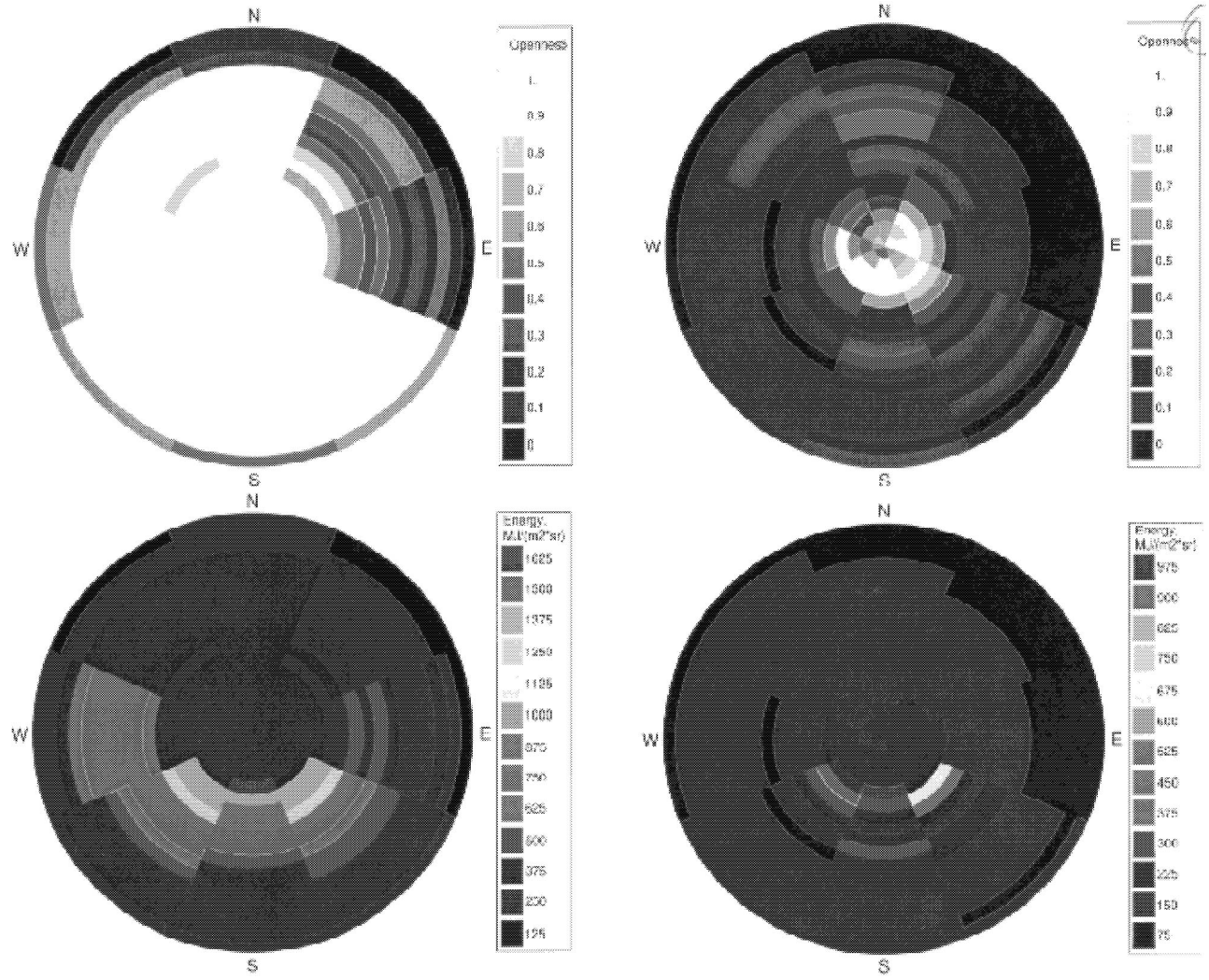


Figure 3. A. Canopy openness (digitized photographs), presented as a hemispherical matrix, at the location of a sun shoot (top left panel) and a shade shoot (top right panel). B. Hemispherical distribution of PAR at the shoot locations. Note the different scales for the top and bottom panels.

*Estimation of light interception by the shoots*

We define the seasonal light interceptance (SLI) of a shoot as the amount of PAR intercepted per unit projected leaf area of the shoot ($PNA_s$) during the growing season. Formally:

$$SLI = \int_{\Omega} q(\omega)gf(\omega)SPAR(\phi_\omega, \gamma_\omega)d\omega, \quad (2)$$

where $q(\omega)$ is the seasonal amount of radiant energy (per unit area and solid angle) incident from the direction ω of the sky (see Figure 2A). The inclination angle ($\phi_\omega$) and rotation angle ($\gamma_\omega$) (Equation 2) with respect to a given view direction (ω) vary with shoot orientation.

Equation 2 was numerically integrated by summation over the sky sections ($i = 1, ..., 144$). The inclination ($\phi_i$) and rotation ($\gamma_i$) angles corresponding to the direction from the midpoint of each section ($i$) were calculated based on the recorded information of the shoot's natural orientation in the canopy. Technically, this was done by transformation of the coordinate system (see Figure 1). The (interpolated) value of $SSA(\phi_i, \gamma_i)$ was then assigned to section ($i$).

The efficiency of light capture by a shoot was quantified by comparing SLI to the amount of PAR received per unit cross-sectional area of a spherical surface at the same location ($SLI_o$):

$$SLI_o = \int_{\Omega} q(\omega)gf(\omega)d\omega. \quad (3)$$

The $SLI_o$ can be interpreted as a measure of the amount of available PAR at the shoot location, whereas SLI is the actual PAR intercepted by the shoot. We used the ratio of SLI to $SLI_o$ to compare the relative efficiency of light capture by shoots in different parts of the canopy.

From Equations 2 and 3, it follows that if there is no directional variation in SSA (i.e., SPAR equals $\overline{SPAR}$ in all directions), or if the shoot is surrounded by an isotropic radiation field ($q(\omega)gf(\omega)$ is constant), then $SLI/SLI_o = \overline{SPAR}$.

## Results

*The radiation regime*

Because the directional distribution of diffuse sky radiation was assumed to be isotropic, differences in the amount of radiant energy from different sections of the sky result from the direct solar component (Figure 2A). The highest value (brightest spot) is found in the section containing the position of the sun at its maximal elevation (≈ 67° at the given latitude). Only diffuse radiation is incident from inclination angles above 67°. The direct component causes a shift in the distribution toward higher inclination angles (Figure 2B). The median angle, defined so that equal parts (50%) of the total radiation are received from smaller and larger inclination angles, respectively, was 37.6°. For comparison, the median angle of isotropic radiation is 30°.

The angular distribution of PAR becomes narrower and its center (the median angle) moves closer to the zenith with depth in the canopy (Figure 4), because near-horizontal angles get rapidly blocked (see Figure 3A). However, even in the lower canopy, the radiation was incident from many different directions (Figures 3B and 4A).

*Shoot and needle structure versus canopy openness*

Interpolation surfaces for SSA were fairly symmetrical with respect to the γ-axis but somewhat skewed in the ϕ-direction (Figure 1). In sun shoots, where needles point upward, the shoot silhouette area is significantly larger when the shoot is viewed from the base toward the tip (i.e., for negative values of ϕ). Accordingly, maximum SSA was generally not obtained at $\phi = 0°$, but at slightly negative ϕ-values. Shade shoots are flatter than sun shoots, which implies a larger variation in SSA along the γ-axis. The sun shoot depicted in Figure 1 had $SPAR_{max} = 0.422$ and $\overline{SPAR} = 0.292$. Values for the shade shoot were $SPAR_{max} = 0.644$ and $\overline{SPAR} = 0.412$.

Both $\overline{SPAR}$ and $SPAR_{max}$ decreased with canopy openness, which ranged from 0.006 to 0.82 (Figure 5, Table 1). Moderate shading had only a small effect on SPAR, whereas a sharp increase occurred in deeper shade (openness ≈ 0–25%). There

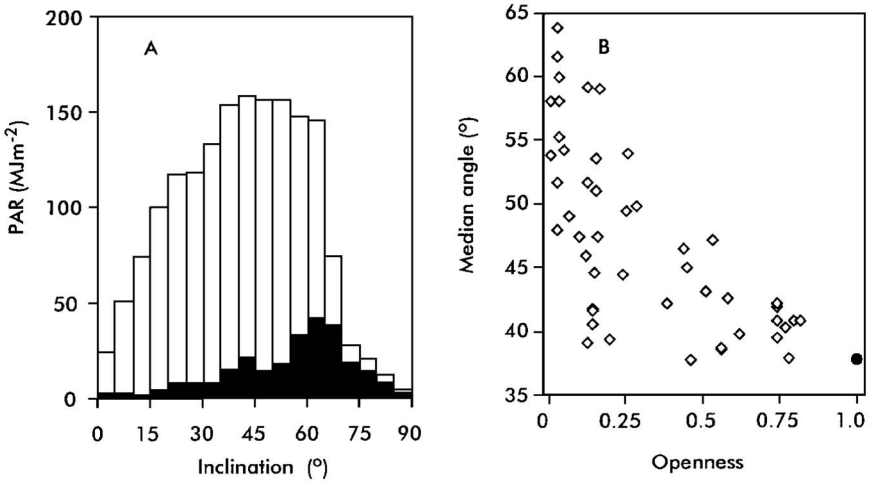


Figure 4. A. Energy of PAR during growing season incident from different inclination angles at the locations of the sun shoot (□) and shade shoot (■). B. The median angle of incident radiation for all sample shoots plotted against canopy openness. The ● denotes the median angle (36.6°) of above-canopy radiation (canopy openness = 1).

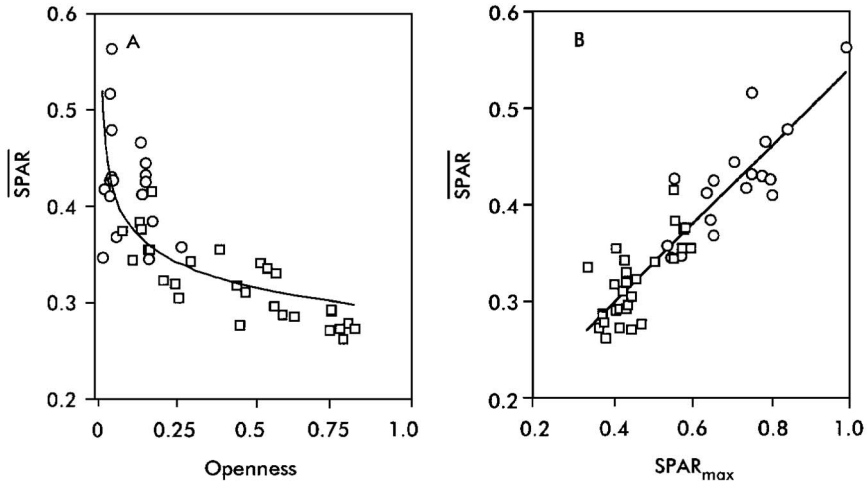


Figure 5. A. Relationship between $\overline{SPAR}$ and canopy openness. B. Relationship between $SPAR_{max}$ and $\overline{SPAR}$. Symbols: dominant and codominant trees (tree height > 6 m) are represented by □; intermediate and suppressed trees (tree height < 6 m) by ○. Regressions fitted to whole data: A. $r^2 = 0.59$ and B. $r^2 = 0.83$.

was a strong linear correlation ($r^2 = 0.83$) between $SPAR_{max}$ and $\overline{SPAR}$ (Figure 5B); however, $SPAR_{max}$ increased relatively more with shading than did $\overline{SPAR}$. Mean $SPAR_{max}$ for the five most sunlit shoots (mean openness = 0.784) was 0.395, and for the five most shaded shoots (mean openness = 0.020), it was 0.737, i.e., 1.86 times greater. The corresponding values for $\overline{SPAR}$ were 0.275 and 0.424, giving a ratio of 1.54.

Needle thickness increased and specific needle area (SNA) decreased with canopy openness (Figure 6). As a result of changes in $\overline{SPAR}$ (Figure 5) and SNA, mean shoot silhouette area per unit needle mass dry weight (ndw) $\overline{SSA}$/ndw (= the product of $\overline{SPAR}$ and SNA) was up to five times higher for shade shoots than for sun shoots (Figure 6C).

Needle nitrogen concentration increased with canopy openness in the dominant and codominant trees, but in the suppressed and intermediate trees, this relationship broke down (Figure 7A). The highest nitrogen concentrations were found in needles from suppressed trees. As a result, there was no correlation between nitrogen concentration and canopy openness for the data as a whole (all trees). A strong positive correlation, on the other hand, existed between nitrogen content per unit projected needle area and canopy openness (Figure 7B).

*Efficiency of light capture*

The $SLI/SLI_o$ ratio varied between 0.25 to 0.76, and showed a strong negative nonlinear correlation ($r^2 = 0.67$) with canopy openness (Figure 8). The lower curve depicted in Figure 8 shows the corresponding value of $\overline{SPAR}$. There was a strong linear correlation ($r^2 = 0.99$) between $SLI/SLI_o$ and $\overline{SPAR}$, but $SLI/SLI_o$ was, on average, 15% higher. If there was no directional variation in either SPAR or in the radiation field surrounding the shoot, $SLI/SLI_o$ would be equal to $\overline{SPAR}$. The difference may be interpreted as the increase in SLI caused by a favorable orientation of the shoot in relation to the actual radiation field at its location.

*Distribution of light and nitrogen*

Nitrogen content was linearly related to SLI (Figure 9), but the regression line had a positive intercept because the ratio of nitrogen to intercepted PAR increased toward the bottom of the canopy. Although (as a result of the changes in shoot geometry) the total range of variation in SLI (0.94 to 59.5 kJ $cm^{-2}$) was considerably less than the total range in canopy openness, it remained many times greater than the variation in nitrogen content (0.084 to 0.354 mg $cm^{-2}$). Consequently, proportionality between these two variables could not be expected. For the whole data, there was a more than twentyfold variation (38.8 to 980.8 mg $kJ^{-1}$) in the ratio of nitrogen to intercepted PAR. The largest ratios and most of the variation occurred in the lower canopy. For shoots situated at a canopy openness above 30%, the range of variation in the amount of nitrogen per unit of intercepted PAR was reduced to between 38.8 and

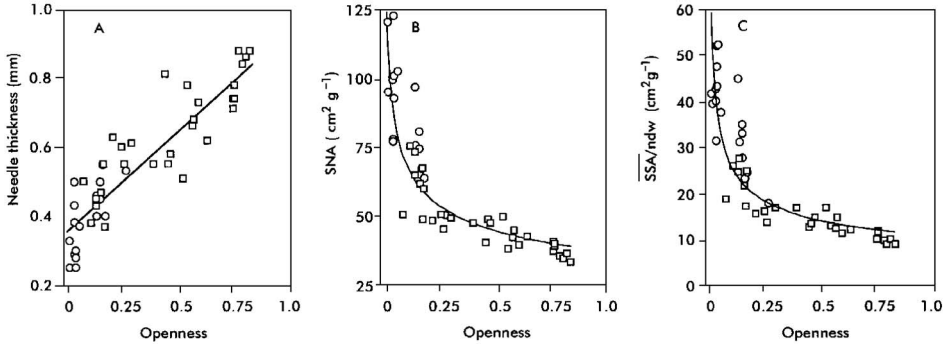


Figure 6. Needle thickness, SNA, and $\overline{SSA}$/ndw as a function of canopy openness (symbols are as in Figure 5). Regressions: A. $r^2 = 0.81$; B. $r^2 = 0.82$; and C. $r^2 = 0.82$.

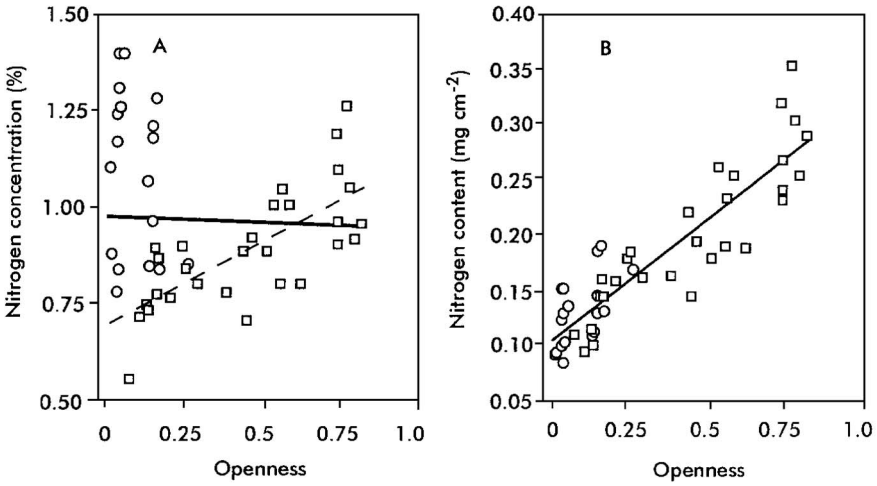


Figure 7. A. Relationship between nitrogen concentration and canopy openness. Thick line = all trees ($r^2$ = 0.002); thin line = dominant and codominant trees ($r^2$ = 0.52). B. Relationship between nitrogen content and canopy openness ($r^2$ = 0.80). Symbols: dominant and codominant trees (tree height > 6 m) are represented by □; intermediate and suppressed trees (tree height < 6 m) by ○.

72.0 mg $kJ^{-1}$, and no correlation ($r^2$ = 0.004) of the ratio with canopy openness remained.

## Discussion

### *Shade acclimation and light interception efficiency*

The ratio $SLI/SLI_o$, which was used to quantify the efficiency of light capture by shoots in the prevailing light conditions, was more than twice as high in shade shoots as in sun shoots (Figure 8). The increase in $SLI/SLI_o$ with shading is consistent with an efficient utilization of light by the canopy as a whole. Efficient light capture is not necessarily useful at the top of the canopy, where there is more than enough light available to maintain high rates of photosynthesis. On the contrary, low light-capturing efficiency of sun shoots may be advantageous because it implies a reduced risk of light saturation and smaller transpiration demand (because the intercepted light is distributed over a large leaf area). Moreover, it enables more light to penetrate to deeper canopy layers, thus improving the light conditions of shade shoots. This, in combination with the high light-capturing efficiency of shade shoots, considerably evens out the vertical gradient in intercepted light (Stenberg 1996).

The increase in $SLI/SLI_o$ with shading was mainly achieved by smaller within-shoot shading (larger $\overline{SPAR}$) in shade shoots than in sun shoots (Figure 5). In addition, the combined effects of shoot orientation and variation in SSA acted to increase SLI of a shoot in its prevailing (non-isotropic) light conditions. The SLI was, on average, about 15% higher than would be predicted simply by the increase in $\overline{SPAR}$ (Figure 8), indicating a tendency of the shoots to be oriented so as to increase their light interception. However, the increase in SLI caused by a favorable shoot orientation was modest and not appreciably higher for shade shoots than for sun shoots. This is because

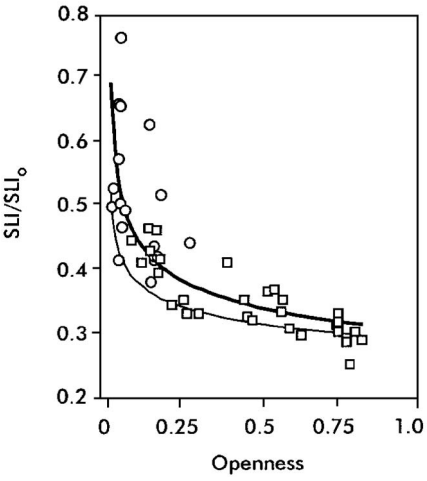


Figure 8. Ratio of SLI to $SLI_o$ as a function of canopy openness. The lower curve (thin line) shows the value of $\overline{SPAR}$ (Figure 5A). Symbols: dominant and codominant trees (tree height > 6 m) are represented by □; intermediate and suppressed trees (tree height < 6 m) by ○.

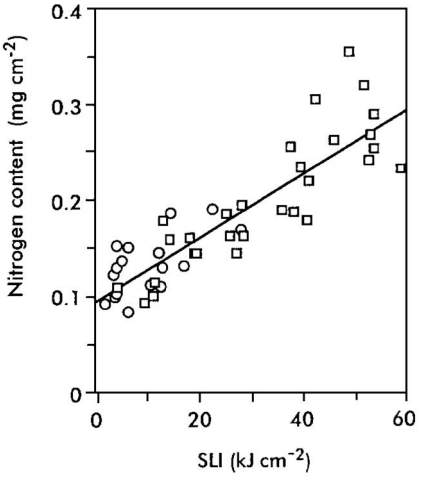


Figure 9. Relationship between nitrogen content and SLI. The regression line is: $y = 0.0032x + 0.097$; $r^2$ = 0.78. Symbols: dominant and codominant trees (tree height > 6 m) are represented by □; intermediate and suppressed trees (tree height < 6 m) by ○.

even in the lower canopy, the angular distribution of PAR is not concentrated around one particular direction (Figures 3 and 4). Thus, the "optimal solution," represented by a flat shoot turning its maximal silhouette area perpendicular to the (one) direction of radiation, cannot be realized.

Differences in needle shape cause some ambiguity in the interpretation of SLI, when SLI is defined on a projected needle area basis. Because sun needles are thicker than shade needles (Figure 6), they have a larger ratio of total to projected area. Consequently, the difference in $SLI/SLI_o$ between sun and shade shoots would have been larger if SLI had been expressed on a total needle area basis. The same is true, only to a much larger extent, when the efficiency of light interception is expressed on a needle mass basis. Because of the increase in SNA with shading, mean silhouette area per unit needle dry weight ($\overline{SSA}$/ndw) was up to five times higher in shade shoots than in sun shoots (Figure 6).

*Relation between nitrogen and intercepted light*

Changes in shoot geometry brought about a considerable flattening of the vertical gradient of light interception per unit needle area (SLI). The increase in specific needle area (SNA) with shading (Figure 6) further decreased the differences in light interception by sun and shade shoots, when expressed per unit needle mass. However, because mean nitrogen concentration was similar in shade needles and sun needles (Figure 7), the amount of nitrogen per unit intercepted PAR was much higher at the bottom of the canopy than at the top of the canopy (Figure 9).

## Conclusions

To develop and test theories on the optimal use of resources, we need accurate estimates of how these resources are allocated in real canopies. It has proved particularly problematic to measure the amount of intercepted PAR by leaves at different positions in the canopy. Technical difficulties arise from the great temporal and spatial variation of irradiance that occurs in the canopy. A far more serious problem, however, is the lack of correspondence between PAR measured with artificial surfaces (e.g., flat horizontally lying sensors) and the distribution of PAR on the actual needle surface. As shown in this study, within-shoot shading and variation in leaf angle and shoot shape greatly modify the gradient of light interception within the canopy.

To estimate quantitatively light interception by a shoot, the directional distributions of SSA and PAR incident on the shoot must be known. The directional distribution of above-canopy PAR at any given location can be produced in a straightforward manner. It can then be combined with hemispherical photographs (or measurements with the LAI-2000 plant canopy analyzer; Li-Cor, Inc., Lincoln, NE) to give the directional distribution of PAR and an estimate of $SLI_o$ at any desired (shoot) location in the canopy.

The method applied here to produce the directional distribution of shoot silhouette area is too cumbersome for standard use. However, the interpolation surfaces (Figure 1) constructed in this exercise indicate that there is a high degree of regularity in the shoot shape, which was also supported by the strong correlation between $\overline{SPAR}$ and $SPAR_{max}$ (Figure 5B). It seems reasonable to believe, therefore, that the directional distribution of shoot silhouette area could be estimated fairly accurately using a shape function based on measurements in a few specified directions only (Stenberg 1996). This would offer an operational method for the determination of seasonal light interception by shoots at different positions in the canopy, not involving any measurements of irradiance.

A close correlation was found between $\overline{SPAR}$ and the light-capturing efficiency ($SLI/SLI_o$). The $SLI/SLI_o$ was higher than predicted by $\overline{SPAR}$ alone (Figure 8), but the gradients were similar. Thus, if actual values of SLI are not needed, $\overline{SPAR}$ combined with the radiation regime may provide a good estimate of the gradient of light interception (relative difference at top and bottom of the canopy). To simplify further, the close dependency between $\overline{SPAR}$ and $SPAR_{max}$ makes it possible to estimate $\overline{SPAR}$ based on measurements of $SPAR_{max}$.

**Acknowledgments**

This work was supported by a grant from the Finnish Academy of Science to H. Smolander. The authors express sincere thanks to Thomas M. Hinckley and Timothy A. Martin for help in field measurements and use of the OPTIMAS-system, and to Pekka Voipio for assistance with data processing and figures.

**References**

Anderson, M.C. 1964. Studies of the woodland light climate. I. The photographic computation of light conditions. J. Ecol. 52:27–41.

Bloom, A.J., F.S. Chapin and H.A. Mooney. 1985. Resource limitation in plants—an economic analogy. Annu. Rev. Ecol. Syst. 16:363–392.

Chen, J.-L., J.F. Reynolds, P.C. Harley and J.D. Tenhunen. 1993. Coordination theory of leaf nitrogen distribution in a canopy. Oecologia 93:63–69.

Ellsworth, D.S. and P.B. Reich. 1993. Canopy structure and vertical patterns of photosynthesis and related leaf traits in a deciduous forest. Oecologia 96:169–178.

Evans, J.R. 1989. Photosynthesis and nitrogen relationships in leaves of $C_3$ plants. Oecologia 78:9–19.

Evans, J.R. 1993. Photosynthetic acclimation and nitrogen partitioning within a lucerne canopy. I. Canopy characteristics. Aust. J. Plant Physiol. 20:55–67.

Farquhar, G.D. 1989. Models of integrated photosynthesis of cells and leaves. Phil. Trans. R. Soc. Lond. 323:357–367.

Field, C.B. 1983. Allocating leaf nitrogen for the maximization of carbon gain: leaf age as a control on the allocation program. Oecologia 56:341–347.

Field, C.B. and H.A. Mooney. 1986. The photosynthesis–nitrogen relationship in wild plants. *In* On the Economy of Plant Form and Function. Ed. T. Givnish. Cambridge Univ. Press, Cambridge, pp 25–55.

Fritschen, L.J. and J. Hsia. 1979. Estimation of hourly direct beam and diffuse solar radiation from global solar radiation measurements. *In* Proc. Solar '79 Northwest. Eds. S. King and S. Killen. Solar 1979 Northwest, Seattle, WA, pp 193–194.

Hirose, T., M.J.A. Werger and J.W.A. van Rheenen. 1989. Canopy development and leaf nitrogen distribution in a stand of *Carex acutiformis*. Ecology 70:1610–1618.

Hollinger, D.Y. 1989. Canopy organization and foliage photosynthetic capacity in a broad-leaved evergreen montane forest. Func. Ecol. 3:53–62.

Horn, H. 1971. The adaptive geometry of trees. Princeton Univ. Press, Princeton, NJ, 144 p.

Kershaw, J.A. and D.R. Larsen. 1992. A rapid technique for recording and measuring the leaf area conifer needle samples. Tree Physiol. 11:411–417.

Kull, O. and Ü. Niinemets. 1993. Variations in leaf morphometry and nitrogen concentration in *Betula pendula*, *Corylus avellana*, and *Lonicera xylosteum*. Tree Physiol. 12:311–318.

Kuroiwa, S. 1970. Total photosynthesis of a foliage in relation to inclination of leaves. *In* Prediction and Measurement of Photosynthetic Productivity. Ed. I. Setlik. Proc. IBP/PP Tech. Meeting, Trebon. Ctr. for Agric. Publishing and Documentation, Wageningen, The Netherlands, pp 79–89.

Leverenz, J.W. and T.M. Hinckley. 1990. Shoot structure, leaf area index, and productivity of evergreen conifer stands. Tree Physiol. 6:135–149.

Miller, P.C. 1967. Leaf temperature, leaf orientation, and energy exchange in quaking aspen (*Populus tremuloides*) and Gambell's oak (*Quercus gambellii*) in central Colorado. Oecol. Plant. 2:241–270.

Mooney, H.A. and S.L. Gulmon. 1979. Environmental and evolutionary constraints on the photosynthetic characteristics of higher plants. *In* Topics in Plant Population Biology. Eds. O.T. Solbrig, S. Jain, G.B. Johnson and P. Raven. Cambridge Univ. Press, NY, pp 316–337.

Niinemets, Ü. and O. Kull. 1995. Effects of light availability and tree size on the architecture of assimilative surface in the canopy of *Picea abies*: variation in needle morphology. Tree Physiol. 15:307–315.

Oker-Blom, P. and H. Smolander. 1988. The ratio of shoot silhouette area to total needle area in Scots pine. For. Sci. 34:894–906.

Press, W.H., S.A. Teukolsky, W.T. Vetterling and B.P. Flannery. 1992. Numerical recipes in FORTRAN, 2nd Edn. Cambridge Univ. Press, 963 p.

Rich, P.M. 1989. A manual for analysis of hemispherical canopy photography. Los Alamos National Laboratory, LA-11733-M. Los Alamos, NM, 80 p.

Sprugel, D.G. 1989. The relationship of evergreenness, crown architecture, and leaf size. Am. Nat. 133:465–479.

Sprugel, D.G., J.R. Brooks and T.M. Hinckley. 1996. Effect of light on shoot geometry and needle morphology in *Abies amabilis*. Tree Physiol. 16:91–98.

Stenberg, P. 1996. Simulations of the effect of shoot structure and orientation on vertical gradients in intercepted light by conifers. Tree Physiol. 16:99–108.

Stenberg, P., S. Linder and H. Smolander. 1995. Variation in the ratio of shoot silhouette area to needle area in fertilized and non-fertilized trees of Norway spruce. Tree Physiol. 15:705–712.

Verhagen, A.M.W., J.H. Wilson and E.J. Britten. 1963. Plant production in relation to foliage illumination. Ann. Bot. 27:627–640.

Weiss, A. and J.M. Norman. 1985. Partitioning solar radiation into direct and diffuse, visible and near-infrared components. Agric. For. Meteorol. 34:205–213.

Western Solar Utilization Network. 1980. Washington solar and weather information: one in a series of thirteen climate data manuals for the states of the Western Region. Western SUN, Portland, OR, 43 p.

Images on page 762 were originally in color. Here are grayscale versions:

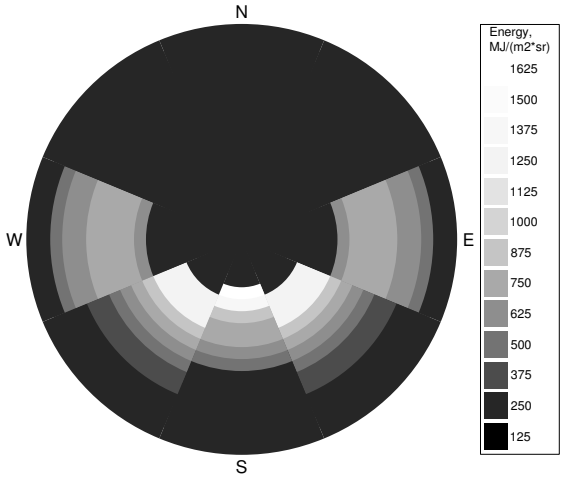


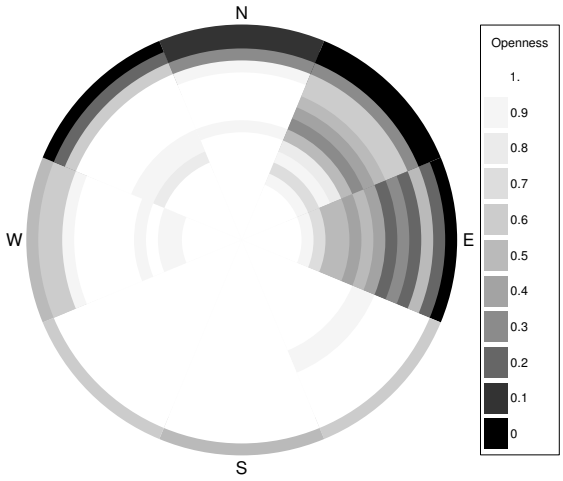


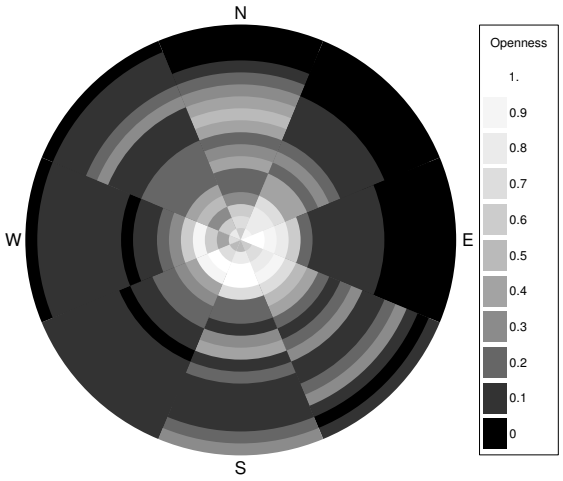


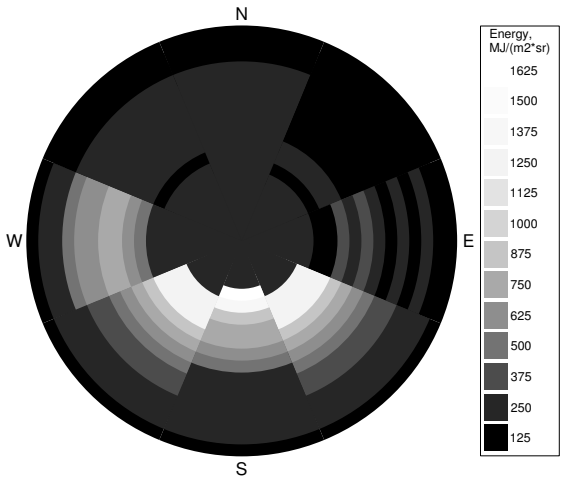


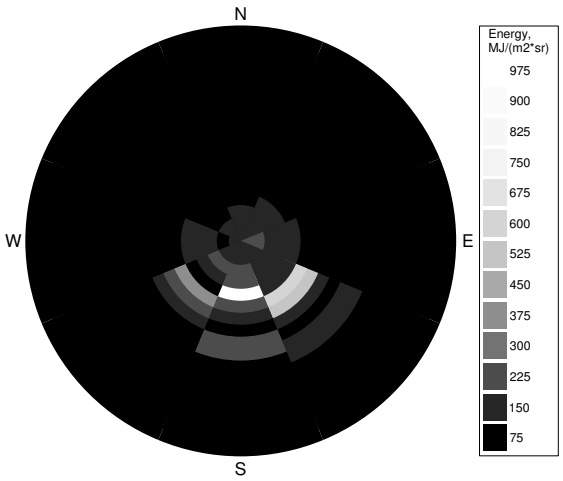

# III

**Tree Physiology** 22, 1185–1192


# Fertilization has little effect on light-interception efficiency of *Picea abies* shoots

SARI PALMROTH,[1–3] PAULINE STENBERG,[4] SAMPO SMOLANDER,[5] PEKKA VOIPIO[6] and HEIKKI SMOLANDER[6]

[1] *Department of Limnology and Environmental Protection, P.O. Box 62, FIN-00014, University of Helsinki, Finland*

[2] *Author to whom correspondence should be addressed (sari.palmroth@duke.edu)*

[3] *Nicholas School of the Environment and Earth Sciences, Box 90328, Duke University, Durham, NC 27708, USA*

[4] *Department of Forest Ecology, P.O. Box 27, FIN-00014, University of Helsinki, Finland*

[5] *Rolf Nevanlinna Institute, P.O. Box 4, FIN-00014, University of Helsinki, Finland*

[6] *Finnish Forest Research Institute, Suonenjoki Research Station, FIN-77600 Suonenjoki, Finland*

Received December 3, 2001; accepted April 13, 2002; published online October 1, 2002

**Summary** We investigated effects of nutrient availability on shoot structure and light-interception efficiency based on data from control (C) and irrigated + fertilized (IL) trees of Norway spruce (*Picea abies* (L.) Karst.). The sampling of 1-year-old shoots was designed to cover the variation in canopy exposure within the live crown zone, where current-year shoots were still found. Canopy openness was used as a measure of light availability at the shoot's position. Openness values for the sample shoots ranged from 0.02 to 0.77 on the IL plot, and from 0.10 to 0.96 on the C plot.

Among needle dimensions, needle width increased most with canopy openness. At fixed canopy openness, needle width was larger, and the ratio of needle thickness to width was smaller in IL trees than in C trees. Specific needle area (SNA) and the ratio of shoot silhouette area to total needle area (STAR) decreased with canopy openness, so that the combined effect was a threefold decrease in the ratio of shoot silhouette area to unit dry mass (SMR = STAR × SNA) along the studied range of openness values. This means that the light-interception efficiency of shoots per unit needle dry mass was three times higher for the most shaded shoots than for sun shoots. A test of the effect of fertilization on the relationships of SNA, STAR and SMR indicated statistically significant differences in both slope and intercept for SNA and STAR, and in the intercept for SMR. However, the differences partly cancelled each other so that, at medium values of canopy openness, differences between treatments in predicted SNA, STAR and SMR were small. At 0.5 canopy openness, predicted STAR of IL shoots was 6.1% larger than STAR of C shoots, but SMR of IL shoots was 10% smaller than that of C shoots. The results suggest that light-interception efficiency per unit needle area or mass of the shoots is not greatly affected by fertilization.

*Keywords: LAI, nitrogen, Norway spruce, structural acclimation.*

## Introduction

The increase in stand productivity in response to fertilization can be attributed to an increase in photosynthetic performance and faster accumulation of leaf area index (LAI) (e.g., McMurtrie and Wolf 1983, Linder and Rook 1984). These factors can be analyzed separately, although they are in dynamic interaction, because the production of new foliage is part of the total canopy photosynthetic production. Leaf area can increase only as long as carbon uptake in photosynthesis is sufficient to meet the maintenance and construction costs of new leaves and associated woody structures and the export of carbon to developing buds (Givnish 1988, Schoettle and Fahey 1994). Net photosynthetic rate of a leaf in a given light environment is determined by its efficiency in capturing available photosynthetically active radiation (PAR, light-interception efficiency) and converting it to photosynthates (conversion efficiency) (Stenberg et al. 2001). Structural adjustment that changes leaf area display is the only available mechanism to allocate the incoming photons in some desired fashion onto leaf surfaces, and plasticity limits the extent to which different characteristics may be adjusted. It is known that morphological characteristics of needles and shoots change in response to shading (Del Rio and Berg 1979, Hager and Sterba 1985, Leverenz and Hinckley 1990, Schoettle and Smith 1991, Niinemets and Kull 1995*a*, 1995*b*, Sprugel et al. 1996), but the role of nutrients in these responses is not well understood. To assess the effect of nutrient availability on structural shade acclimation, we need to quantify and compare light-interception efficiencies along the naturally occurring light gradient within stands of different fertility.

Interception of PAR per unit needle area of a shoot situated in a given light environment is directly proportional to its shoot silhouette to total needle area ratio (STAR) (Stenberg et al. 2001). Because mean STAR ($\overline{\text{STAR}}$; Oker-Blom and Smolander 1988) is closely related to the light extinction coeffi-

cient, $\overline{STAR}$ modifies the vertical gradient of PAR, thus providing a useful tool for analyzing the dynamic interaction between canopy structure and radiation regime. As a complement to STAR, we used the ratio of shoot silhouette area to needle dry mass (SMR) to quantify light-interception efficiency per unit dry mass invested in foliage. We determined the relationships of STAR and SMR with canopy openness in Norway spruce (*Picea abies* (L.) Karst.), and studied the effects of fertilization on these relationships.

## Materials and methods

Measurements were made in the Norway spruce experimental stand situated at the Flakaliden research area (64°07′ N, 19°27′ E, 310 m a.s.l.) in Sweden. The stand was planted with 4-year-old seedlings in 1963, and the nutrient optimization experiment was established in 1987. The treatments are applied to plots of 50 × 50 m. Two treatments were used in this study: (1) a control (C) plot, and (2) an irrigated + fertilized (IL) plot, in which a complete nutrient solution has been injected into the irrigation water daily during the growing season constantly since 1987 (see Linder (1995) for further details on the experimental design). The development of the two canopies, since the start of the fertilization regime, has resulted in remarkable differences in tree size and LAI (see Table 1; S. Linder, Swedish University of Agricultural Sciences, personal communication), providing a setup for quantifying changes in needle and shoot structure with shading and for comparing those responses between fertilized and unfertilized trees.

### *In situ measurements*

The data consisted of structural measurements taken in mid-July of 1995, 1996, 1997 and 1998. Results from 1997 have been reported previously by Stenberg et al. (1999). One-year-old shoots were selected from different canopy positions within the two experimental plots, representing two regimes of nitrogen availability. Sampling was designed to cover the range in canopy openness values within the crown zone, where current-year shoots could still be found. In practice, each year, two to four healthy trees from each of the two plots were selected and six to 16 shoots were sampled from different heights along the length of the living crown. This strategy ensured that the sampling (exposure) range was as wide as possible even without a priori knowledge about the distribution of openness values within the canopies and at the specific locations of the shoots. Nevertheless, maximum values of canopy openness for the sample shoots were somewhat lower on the IL plot, because the tops of the crowns were inaccessible with the ladder that was available. Minimum openness values were consistently lower on the IL plot than on the C plot.

Table 1. Diameter at breast height (DBH), mean height (Height), basal area (BA), stand volume ($V$), growth (CAI), and leaf area index (LAI) of trees in the irrigated + fertilized (IL) and control (C) plots used in this study. The estimates are from years 1995 and 1998.

| Plot | Year | DBH (cm) | Height (cm) | BA ($m^2$ $ha^{-1}$) | $V$ ($m^3$ $ha^{-1}$) | CAI ($m^3$ $ha^{-1}$ $year^{-1}$) | LAI |
|---|---|---|---|---|---|---|---|
| IL | 1995 | 10.8 | 701 | 23.4 | 97.6 | 12.9 | 5.9 |
| | 1998 | 12.8 | 845 | 32.6 | 143 | 17.4 | 8.4 |
| C | 1995 | 6.4 | 459 | 7.7 | 25.4 | 3.2 | 2.3 |
| | 1998 | 7.2 | 520 | 9.1 | 34.9 | 4.8 | 2.9 |

Canopy openness, defined as the unweighted fraction of unobscured sky (Sprugel et al. 1996), was used as a measure of light availability at the shoot's position. A measurement with the LAI-2000 Plant Canopy Analyzer (Li-Cor, Lincoln, NE) was taken at the location of each shoot applying no field of view restrictor. Above-canopy reference measurements were taken every 15 s by a second instrument placed in open conditions. To prevent direct sunlight from reaching the sensors, all measurements were taken in the evening when the sun was less than 16° above the horizon. Canopy openness was computed based on the gap fraction values in different sections of the sky provided by the LAI-2000. Canopy openness is mathematically defined as:

$$\text{openness} = \frac{1}{2\pi}\int_{\Omega} g_f(\omega)\,d\omega, \quad (1)$$

where $g_f(\omega)$ denotes the gap fraction in the solid angle ($d\omega$) around the direction ($\omega$) of the upper hemisphere ($\Omega$).

### *Shoot and needle silhouette area measurements*

Shoot silhouette areas (SSA) in different directions were measured photographically (see Table 2 for instrumentation). In our set-up design, the shoot was attached with a pin (at the mid-point of the twig) to a graduated dial that was fixed to a metal stand. Thus, the shoot's position with respect to the view direction of the camera could be adjusted by (1) changing the angle between shoot axis (twig) and the optical axis of the camera, and (2) reattaching the shoot to the pin so that different sides of the shoot were facing the camera. The camera was fixed at a distance of 160–300 cm from the shoot depending on the size of the shoot and the properties of the lens used, such that the maximum field of view obtained was 4°. The silhouette image was taken against the light table in an otherwise dark room. Excess light was minimized by covering the light table with 50% neutral dark film and the unused area of the light table was covered by curtains. The distance between the shoot and the light table was 15 cm.

In our coordinate system, the optical axis of the camera (or view direction) was horizontal, and the shoot inclination angle ($\phi$) refers to the angle of the shoot axis (twig) to the vertical. Thus, for $\phi = 0°$, the twig was perpendicular to the direction of view, and for $\phi = 90°$ the twig was parallel to it (a view along the axis corresponding to the minimum shoot silhouette area). The rotation angle ($\gamma$) was defined such that $\gamma = 0°$ when the shoot's upper side was facing the viewer (camera). Thus, rotating the shoot 90° (along the shoot axis) from that gave the "side view" ($\gamma = 90°$). For Norway spruce shoots, the silhouette area commonly attains its maximum value at about $\phi = 0°$

Table 2. Equipment used in the photo analyses. Images were analyzed with a video band image analysis program (1995–1996) (Helsinki University of Technology, Espoo, Finland) and with Colan Colorimetric Image Analysis Software (1997–1998) (ColorSoft, Keminmaa, Finland).

| Year | Field of view (°) | Film/camera | Lens | Pixel size (mm) | Pixels ($cm^{-2}$) |
|---|---|---|---|---|---|
| 1995 | 4 | Film Tmax 100 | Nikon 180 mm, Micro Nikkor 55 mm (needles) | 0.4–0.6 | 280–625 |
| 1996 | 3 | Film Tmax 100 | Nikon 180 mm, Micro Nikkor 55 mm (needles) | 0.08–0.13 | 5,900–15,600 |
| 1997 | 4 | Kodak DCS-420 | Nikon 180 mm | 0.08–0.13 | 5,900–15,600 |
| 1998 | 2 | Kodak DCS-460 | Sigma 400, Micro Nikkor 60 mm (needles) | 0.04 | 62,500 |

and $\gamma = 0°$, i.e., when the shoot axis and shoot's upper side are perpendicular to the view direction. Therefore, SSA (0,0) is commonly (although not quite accurately) referred to as the maximum silhouette area.

In 1995, 1997 and 1998, the measurement procedure was as follows. A set of measurements was taken where the inclination angle ($\phi$) was changed in steps of 30° ($\phi = 0°$, 30°, 60°, 90°, 120°, 150°). The rotation angle ($\gamma$) was 0° in the first set of measurements, and the procedure was repeated four times changing $\gamma$ in steps of 45° ($\gamma = 0°$, 45°, 90°, 135°, 180°) or six times changing $\gamma$ in steps of 30° (only in 1997). When changing $\gamma$, the previous view direction was marked before the shoot was detached. The shoot was then reattached to the stand at the desired rotation angle. In 1996, measurements were taken only at four rotation angles at a shoot inclination of $\phi = 0°$.

After completing the shoot silhouette area and structural measurements (see below), the projected area (silhouette area) of all needles on the shoot was measured photographically. For this purpose, needles were laid out (not overlapping) on an acrylic plate as they fell. The acrylic plate, which was used to prevent the halo effect from burning the needle edges, was placed 35 mm above the horizontal light table. The silhouette area measuring system was calibrated with watch spindles or with precision wires with diameters from 0.8 to 2.0 mm that matched mean needle diameter.

The spherically averaged shoot silhouette area ($\overline{SSA}$) was calculated by the method of Smolander and Stenberg (2001). In computing the spherically averaged shoot silhouette to total needle area ratio ($\overline{STAR}$), the correction for the twig area was made as described by Stenberg et al. (1999). In addition to $\overline{STAR}$, maximum shoot silhouette to total needle area ratio ($STAR_{max}$) was calculated by using SSA(0,0) instead of $\overline{SSA}$. We used $STAR_{max}$ as a complement to $\overline{STAR}$ mainly because measurements in 1996 did not allow computation of $\overline{SSA}$. The spherically averaged ratio of shoot silhouette area to needle dry mass ($\overline{SMR}$) was calculated by multiplying $\overline{STAR}$ by the specific needle area (SNA).

*Structural measurements*

All needles of the shoot were detached and counted, and the length and diameter of the twig were measured. We estimated mean needle length by measuring the lengths of 10–30 sample needles with a ruler. In addition, three to six needles were picked from different sides of the central part of the shoot for determination of needle thickness and width. Needle dry mass (48 h at 60–70 °C) of the remaining needles of the shoot was determined and, in 1996 and 1997, foliar nitrogen concentration was determined with a LECO CHN-900 analyzer (LECO, St. Joseph, MI).

Anatomical leaf thickness ($t_n$) and width ($w_n$) were measured from needle cross sections (Figure 1) (see Stenberg et al. (1999) for details of the method). In 1995–1997, the cross sections were photographed on slide film, and needle thickness and width were measured by projecting the slides on the screen. In 1998, the dimensions were measured with a digital camera and the Colan Image Analysis Program (ColorSoft, Keminmaa, Finland).

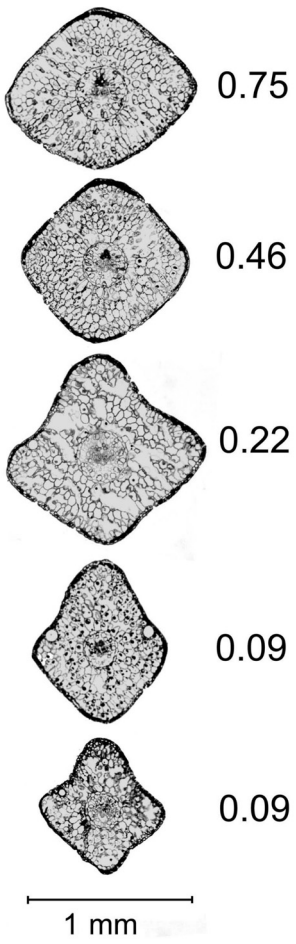


Figure 1. Cross sections of needles at different canopy openness values between 0.09 and 0.75. Data are from the IL plot in 1997.

*Geometric needle area estimates*

Total needle area ($A_t$) was estimated from mean needle length ($l_n$), $t_n$ and $w_n$ as:

$$A_t = 2l_n\sqrt{t_n^2 + w_n^2}. \quad (2)$$

Equation 1 applies to a rhomboidal prism, which was chosen to best approximate the shape of our Norway spruce needles (see Figure 1). Total needle area of a shoot (TNA) was estimated as $A_t$ multiplied by the number of needles on the shoot.

A geometric estimate of projected needle area ($A_p$) was computed based on the rhomboid model (Niinemets and Kull 1995*a*) as:

$$A_p = l_n \frac{(\max(t_n, w_n))^2}{\sqrt{t_n^2 + w_n^2}}, \quad (3)$$

where $A_p$ is the projected area of a needle lying on its side so that the angle to the horizontal is less for the larger diagonal. In our material, needle thickness was not consistently larger than needle width. Consequently, as indicated in the formula, we always used the larger dimension in the numerator in calculating $A_p$. The geometric estimate ($A_p$) agreed fairly well with the photographically measured projected needle area (Figure 2). On average, $A_p$ calculated by the rhomboid model exceeded the photographically measured projected area by 2%.

*Statistical analysis*

Relationships of $\overline{STAR}$, $STAR_{max}$, SNA and $\overline{SMR}$ with canopy openness (data from all years pooled) were described by a simple regression (reduced model): $y = \beta_0 + \beta_1 X_1$, where $X_1$ denotes the logarithm (ln) of canopy openness, ln(openness), which linearized the response function. The difference between treatments in the relationships was studied by using an indicator ("dummy") variable to account for the effect of fertilization. Multiple linear regression models of the type (full model): $y = \beta_0 + \beta_1 X_1 + \beta_2 X_2 + \beta_3 X_1 X_2$ were thus fitted to the whole data, where $X_1$ is ln(openness) and $X_2$ is the dummy variable, which was assigned the value 1 for IL shoots and 0 for C shoots (Neter et al. 1983, SYSTAT statistical software package, SYSTAT, Evanston, IL). The full model structure allows both the intercept and the slope of the regression to vary between the groups (indicated by 0 and 1). Testing for differences in intercept ($\beta_2 \neq 0$) and slope ($\beta_3 \neq 0$) was done by calculating partial $F$ statistics for the coefficients of the full model.

## Results

In trees on both the C and IL plots, there was a slightly increasing trend in needle nitrogen concentration ($N_m$) from the bottom to the top of the canopy (Figure 3), and $N_m$ was lower in 1996 than in 1997. The ratio of needle thickness to width ($t_n/w_n$) ranged from 0.75 to 2.1 in IL trees, and from 0.79 to 1.9 in C trees. The ratio decreased with increasing canopy openness (Figure 4a) mainly because of an increase in needle width. For 88% of the needles $t_n/w_n$ was between 0.75 and 1.25. The ratio of total to projected needle area ($A_t/A_p$) varied between 2.5 and 4.0 (Figure 4b). The value 4 is obtained when the needle cross section is a square ($t_n = w_n$ in Equations 2 and 3). The structural measurements of needle and shoot characteristics are summarized in Table 3.

Shoot size, quantified by twig length ($l_t$) and total needle area (TNA), was positively correlated with canopy openness (Table 4). There were decreases in STAR, SNA and SMR with increasing canopy openness in both control and fertilized trees (Figures 5–7). The combined effect of the changes in SNA

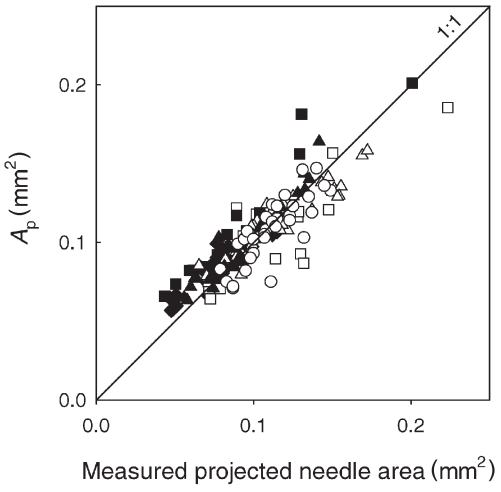


Figure 2. Projected needle area calculated with the rhomboid model ($A_p$) plotted against photographically measured projected needle area. Data are from 1995 (◇, ◆), 1996 (□, ■), 1997 (△, ▲) and 1998 (○, ●). Closed symbols refer to the IL plot and open symbols to the C plot.

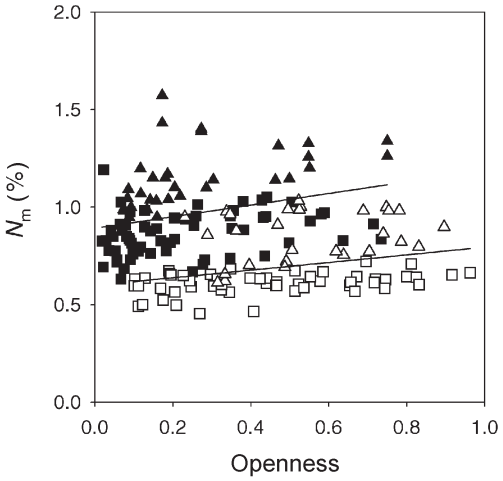


Figure 3. Foliar nitrogen concentration ($N_m$) as a function of canopy openness. Data are from 1996 (□, ■) and 1997 (△, ▲). Closed symbols refer to the IL plot and open symbols to the C plot. The $P$-values of the regressions are 0.006 (IL) and 0.012 (C).

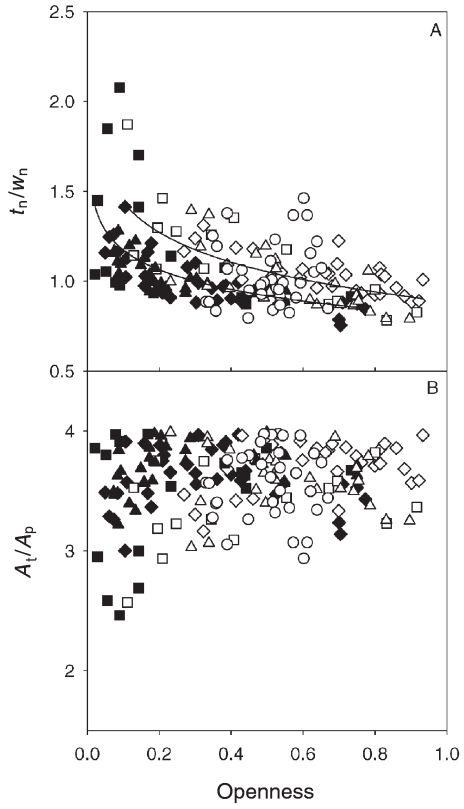


Figure 4. Ratio of needle thickness to needle width ($t_n/w_n$) (A) and total needle area to projected needle area ($A_t/A_p$) (B) as a function of canopy openness. Symbols as in Figure 2.

(Figure 5) and $\overline{\text{STAR}}$ (Figure 6) was a more than threefold change in $\overline{\text{SMR}}$ along the range of openness values in the study (Figure 7). The effects of fertilization on the relationships of $\overline{\text{STAR}}$, $\text{STAR}_{max}$, SNA and $\overline{\text{SMR}}$ with canopy openness are summarized in Table 5. The difference in intercept (values of the dependent variables at full canopy openness) was statistically significant for SNA ($P < 0.001$), $\overline{\text{STAR}}$ ($P < 0.01$) and $\overline{\text{SMR}}$ ($P < 0.01$). At full canopy openness, IL shoots had 21% smaller predicted SNA and 14% larger predicted $\overline{\text{STAR}}$ than C shoots. However, the slopes of the relationships were larger for SNA ($P < 0.05$) and smaller for $\overline{\text{STAR}}$ ($P < 0.05$) in the IL shoots than in the C shoots, implying that the predicted differences in SNA and $\overline{\text{STAR}}$ between C and IL shoots decreased at lower values of canopy openness. At an openness value of 0.5, predicted SNA of IL shoots was 12% smaller and predicted $\overline{\text{STAR}}$ was 6.1% larger than those of C shoots. No statistically significant differences ($P > 0.05$) between treatments were found in the relationships between $\text{STAR}_{max}$ and canopy openness. For the relationships between $\overline{\text{SMR}}$ and canopy openness, the intercept (predicted value of $\overline{\text{SMR}}$ in unshaded conditions) was 26% smaller for IL shoots ($P < 0.01$) than for C shoots. However, because the rate of change in $\overline{\text{SMR}}$ with increased shading was smaller in C shoots than in IL shoots (although not statistically significant), at 0.5 canopy openness the predicted $\overline{\text{SMR}}$ was only 10% smaller for IL shoots than for C shoots.

## Discussion

Fertilization increased foliage nitrogen concentration ($N_m$), but $N_m$ varied only slightly with canopy openness (Figure 2). In both IL and C trees, needle width ($w_n$) increased more with canopy openness than needle thickness ($t_n$). At similar openness values, there was no clear effect of fertilization on $t_n$, but $w_n$ was larger in IL trees than in C trees. As a result, IL trees had smaller $t_n/w_n$ at a fixed canopy openness (see Figure 4a).

Table 3. Sampling protocol and the ranges of needle length ($l_n$), needle thickness ($t_n$), needle width ($w_n$), thickness to width ratio ($t_n/w_n$), total needle area to projected area ratio ($A_t/A_p$), specific needle area (SNA), foliar nitrogen concentration ($N_m$), twig length ($l_t$), total needle area (TNA), needle number density ($N_n/l_t$), needle area packing (TNA/$l_t$), spherically averaged shoot silhouette to total area ratio ($\overline{\text{STAR}}$), maximum STAR ($\text{STAR}_{max}$) and shoot silhouette to foliage dry mass ratio ($\overline{\text{SMR}}$).

| | IL 1995 | C 1995 | IL 1996 | C 1996 | IL 1997 | C 1997 | C 1998 |
|---|---|---|---|---|---|---|---|
| No. shoots/no. trees | 35/3 | 30/3 | 62/4 | 55/4 | 32/2 | 28/2 | 48/8 |
| Shoot order | 1st | 1st | 1st | 1st | Varying | Varying | 1st |
| Openness | 0.05–0.77 | 0.27–0.93 | 0.02–0.74 | 0.10–0.96 | 0.07–0.75 | 0.23–0.90 | 0.26–0.69 |
| $l_n$ (mm) | 9.1–16.3 | 7.6–13.4 | 7.0–17.6 | 5.6–20.8 | 9.6–15.9 | 6.7–12.5 | 8.9–13.6 |
| $t_n$ (mm) | 0.86–1.4 | 0.85–1.2 | 0.82–1.5 | 1.0–1.4 | 0.86–1.3 | 1.1–1.5 | 0.81–1.5 |
| $w_n$ (mm) | 0.69–1.7 | 0.72–1.2 | 0.57–1.5 | 0.65–1.6 | 0.81–1.4 | 0.83–1.9 | 0.81–1.5 |
| $t_n/w_n$ | 0.75–1.4 | 0.88–1.3 | 0.87–2.1 | 0.78–1.9 | 0.88–1.28 | 0.79–1.4 | 0.79–1.5 |
| $A_t/A_p$ | 3.0–4.0 | 3.2–4.0 | 2.5–4.0 | 2.7–4.0 | 3.2–4.0 | 3.0–4.0 | 2.9–4.0 |
| SNA ($cm^2\ g^{-1}$) | 74–199 | 89–147 | 74–195 | 56–153 | 85–190 | 75–127 | 67–129 |
| $N_m$ (%) | | | 0.63–1.2 | 0.45–0.72 | 0.96–1.6 | 0.65–1.1 | |
| $l_t$ (cm) | 3.3–22 | 2.9–8.9 | 3.0–22 | 1.5–23 | 3.0–20 | 1.6–9.2 | 2.2–9.0 |
| TNA ($cm^2$) | 18.5–150 | 10.2–64.0 | 8.7–205 | 6.8–157 | 13.1–137 | 7.4–82.6 | 22.8–86.2 |
| $N_n/l_t$ ($cm^{-1}$) | 10–20 | 17–26 | 9–21 | 11–33 | 12–22 | 13–23 | 15–27 |
| TNA/$l_t$ ($cm^2\ cm^{-1}$) | 3.6–7.8 | 4.5–11.4 | 2.9–9.2 | 3.1–12.7 | 4.0–11.6 | 3.4–9.7 | 4.5–11.4 |
| $\overline{\text{STAR}}$ | 0.121–0.209 | 0.105–0.169 | | | 0.122–0.188 | 0.103–0.166 | 0.103–0.173 |
| $\text{STAR}_{max}$ | 0.153–0.310 | 0.133–0.224 | 0.127–0.364 | 0.122–0.240 | 0.143–0.246 | 0.115–0.234 | 0.116–0.251 |
| $\overline{\text{SMR}}$ | 10.5–41.7 | 10.0–21.9 | | | 12.1–29.6 | 8.5–21.8 | 9.8–16.4 |

Table 4. A Spearman correlation matrix for canopy openness, and needle and shoot characteristics. Symbols as in Table 3. Asterisks indicate statistical significance (* = $P < 0.05$, ** = $P < 0.01$ and *** = $P < 0.001$) of the correlations.

| | Treatment | Openness | $l_n$ | $t_n$ | $w_n$ | $t_n/w_n$ | SNA | $l_t$ | TNA | $N_n/l_t$ | $\overline{STAR}$ |
|---|---|---|---|---|---|---|---|---|---|---|---|
| $l_n$ | IL | 0.32 ** | | | | | | | | | |
| | C | 0.28 ** | | | | | | | | | |
| $t_n$ | IL | 0.51 *** | –0.16 | | | | | | | | |
| | C | –0.04 | 0.03 | | | | | | | | |
| $w_n$ | IL | 0.83 *** | 0.13 | 0.82 *** | | | | | | | |
| | C | 0.24 * | 0.15 | 0.65 *** | | | | | | | |
| $t_n/w_n$ | IL | –0.85 *** | –0.35 ** | –0.31 ** | –0.76 *** | | | | | | |
| | C | –0.34 *** | –0.09 | –0.06 | –0.75 *** | | | | | | |
| SNA | IL | –0.88 *** | –0.19 | –0.57 *** | –0.77 *** | 0.70 *** | | | | | |
| | C | –0.52 *** | –0.36 *** | –0.27 ** | –0.52 *** | 0.54 *** | | | | | |
| $l_t$ | IL | 0.69 *** | 0.21 | 0.48 *** | 0.72 *** | –0.67 *** | –0.70 *** | | | | |
| | C | 0.42 *** | 0.35 *** | –0.00 | 0.35 *** | –0.53 *** | –0.60 *** | | | | |
| TNA | IL | 0.81 *** | 0.46 *** | 0.51 *** | 0.82 *** | –0.78 *** | –0.72 *** | 0.88 *** | | | |
| | C | 0.45 *** | 0.61 *** | 0.20 * | 0.51 *** | –0.51 *** | –0.61 *** | 0.87 *** | | | |
| $N_n/l_t$ | IL | –0.02 | 0.22 * | –0.30 ** | –0.19 | 0.00 | 0.21 | –0.39 *** | –0.13 | | |
| | C | 0.16 | 0.12 | –0.29 ** | –0.21 * | 0.14 | 0.18 | –0.16 | –0.05 | | |
| $\overline{STAR}$ | IL | –0.58 *** | –0.32 ** | –0.25 * | –0.58 *** | 0.70 *** | 0.28 * | –0.44 *** | –0.66 *** | –0.30 * | |
| | C | –0.50 *** | –0.25 * | –0.07 | –0.39 *** | 0.44 *** | 0.19 | –0.45 *** | –0.62 *** | –0.49 *** | |
| $\overline{SMR}$ | IL | –0.96 *** | –0.26 * | –0.56 *** | –0.85 *** | 0.80 *** | 0.93 *** | –0.75 *** | –0.84 *** | 0.07 | 0.58 *** |
| | C | –0.63 *** | –0.43 *** | –0.22 * | –0.60 *** | 0.62 *** | 0.77 *** | –0.70 *** | –0.82 *** | –0.14 | 0.70 *** |

On both plots, $t_n/w_n$ decreased with increasing openness, from values of > 1 to values of < 1, but the value of canopy openness at which the shift occurred was smaller in fertilized trees than in control trees. Ranges in the ratio of total to projected needle area ($A_t/A_p$) were also similar on both plots (2.5 to 4.0 in IL trees and 2.7 to 4.0 in C trees). Because $A_t/A_p$ attains its maximum value (= 4) when $t_n = w_n$ (Equations 2 and 3), there was no monotonically increasing trend in $A_t/A_p$ with light availability (Figure 4b). This is in contrast to results obtained in central European Norway spruce provenances (Niinemets and Kull 1995*a*, Sellin 2000).

Specific needle area is a function of needle dimensions and density. Needle flatness can be characterized by the ratio of the larger of $t_n$ and $w_n$ to the smaller of these dimensions (Sellin 2000). The smaller and flatter the needle, the larger the ratios of needle surface area to volume ($V_n$) ($A_t/V_n = 4\sqrt{(D_1^2 + D_2^2/D_1 D_2)}$) and SNA (assuming constant density). The increase in SNA with shading in our material (Figure 5) was more closely associated with decreasing needle size than with increasing needle flatness, which did not show any clear trend over the common range of openness values. Needle width alone explained ~50% of the variation in SNA in IL

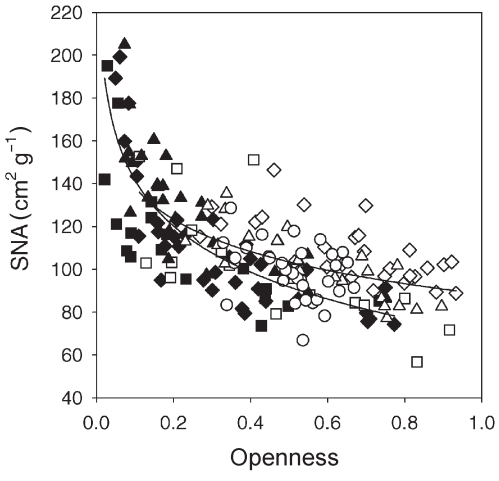


Figure 5. Specific needle area (SNA) as a function of canopy openness. See Table 5 for parameters of the fitted curves.

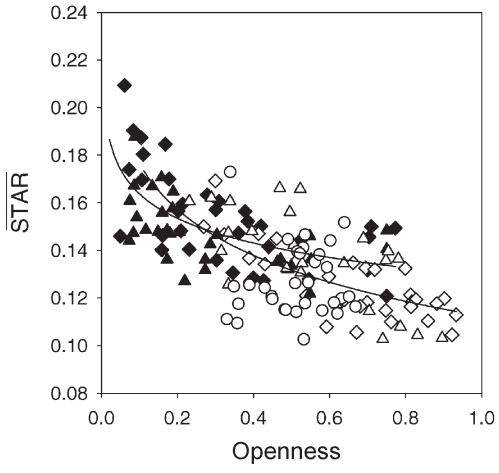


Figure 6. Mean shoot silhouette to total needle area ratio ($\overline{STAR}$) as a function of canopy openness. See Table 5 for parameters of the fitted curves.

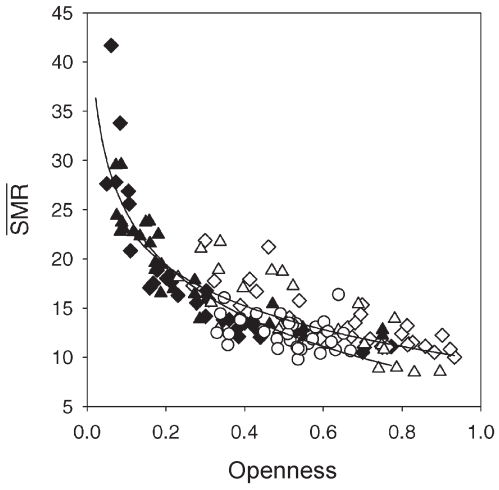


Figure 7. Mean shoot silhouette area per unit needle dry mass ($\overline{SMR}$) as a function of canopy openness. See Table 5 for parameters of the fitted curves.

trees, and ~75% in C trees (data from 1995–1997). Needle density (needle dry mass/geometrically calculated $V_n$) changed little within the common range of observed openness values on the C and IL plots, but IL needles were somewhat denser than C needles. Thus, the higher SNA for C shoots than for IL shoots within this range was related to both smaller needles and lower needle density.

Statistically significant differences between treatments were found in the intercepts of the relationships of $\overline{STAR}$ and $\overline{SMR}$ with canopy openness (Figures 6 and 7). In open conditions, IL trees produced shoots that had somewhat higher STAR (less mutual shading within shoot) than C trees, but they had lower SMR (SMR = STAR × SNA) because of their smaller SNA. However, the differences in intercepts were offset by opposite differences in the rate of change with shading (slopes of the relationships) (Table 5). As a result, the differences between treatments in predicted $\overline{STAR}$ and $\overline{SMR}$ had different signs at high openness and low openness values, respectively, and were relatively minor at medium openness (e.g., 0.5, a value well within the common range of observed openness values on the C and IL plots). For $STAR_{max}$, which showed a strong positive correlation with $\overline{STAR}$ ($r^2 = 0.88$), no significant effect of fertilization on either slope or intercept was found. This test covered a larger data set (including data from 1996, see Table 3), and the range of canopy openness values was wider.

Although total canopy PAR interception is a saturating function of LAI, mean canopy openness (available light) and mean light interception per unit leaf area or mass decrease with increasing LAI. The ability of trees to adjust shoot structure to increase light-interception efficiency of shade foliage is an important determinant of the amount of LAI that can be maintained. We looked at the light-interception efficiency of individual shoots along an openness gradient in two canopies differing in LAI. We found a twofold increase in STAR and a threefold increase in SMR with shading. The C and IL shoots were similar in terms of light-interception efficiency per unit area or mass within the overlapping range of canopy openness values. However, there were no current-year shoots below 10% canopy openness on the C plot, whereas on the IL plot current-year shoots were still found at 2% openness. This suggests that the higher capacity of fertilized trees to produce and maintain foliage at lower irradiances does not result from in-

Table 5. Reduced models ($y = \beta_0 + \beta_1 \ln(\text{openness})$), where a single line was fitted to the whole data (IL + C) (upper section of table) together with individual regression models for SNA, $\overline{STAR}$, $STAR_{max}$ and $\overline{SMR}$ for fertilized (IL) and control (C) plots (lower section of table). Root mean square errors (RMSE) are given for the reduced model and the full model ($y = \beta_0 + \beta_1 \ln(\text{openness}) + \beta_2 X_2 + \beta_3 \ln(\text{openness}) X_2$), where $X_2$ is an indicator variable. Asterisks indicate statistical significance (* = $P < 0.05$, ** = $P < 0.01$ and *** = $P < 0.001$) of the between-treatment differences in the intercept ($\beta_0$) and slope ($\beta_1$). Predicted values of the dependent variables are calculated at a canopy openness of 0.5.

| | | $\beta_0$ | $\beta_1$ | $r^2$ | $N$ | RMSE | $y$ (0.5) |
|---|---|---|---|---|---|---|---|
| SNA | Reduced | 83.3 | –25.0 | 0.56 | 188 | 16.9 | |
| | Full | | | | | 16.3 | |
| $\overline{STAR}$ | Reduced | 0.118 | –0.021 | 0.47 | 153 | 0.015 | |
| | Full | | | | | 0.014 | |
| $STAR_{max}$ | Reduced | 0.144 | –0.036 | 0.49 | 188 | 0.028 | |
| | Full | | | | | 0.028 | |
| $\overline{SMR}$ | Reduced | 9.01 | –6.68 | 0.76 | 153 | 2.53 | |
| | Full | | | | | 2.47 | |
| SNA | IL | 70.3 *** | –31.0 * | 0.66 | 83 | | 91.8 |
| | C | 88.5 | –21.7 | 0.28 | 105 | | 104 |
| $\overline{STAR}$ | IL | 0.129 ** | –0.015 * | 0.38 | 64 | | 0.140 |
| | C | 0.113 | –0.028 | 0.28 | 89 | | 0.132 |
| $STAR_{max}$ | IL | 0.154 | –0.032 | 0.41 | 83 | | 0.176 |
| | C | 0.140 | –0.039 | 0.30 | 105 | | 0.167 |
| $\overline{SMR}$ | IL | 7.22 ** | –7.60 | 0.81 | 64 | | 12.5 |
| | C | 9.78 | –5.95 | 0.42 | 89 | | 13.9 |

creased light-interception efficiency at the shoot level. Rather, it may reflect higher conversion efficiency of shade foliage or changes in allocation between shoots and roots and, thereby, lower construction costs per unit new leaf area in terms of supporting woody tissues (Givnish 1988). Aboveground biomass and growth were higher on the fertilized plot than on the control plot. The associated increase in photosynthetic production is likely to be a combined effect resulting from higher LAI, increasing the total canopy PAR interception, and higher conversion efficiency per unit of intercepted PAR. In contrast, the difference in potential PAR capture per unit leaf mass of shoots developed at similar light environments was small.

**Acknowledgments**

We thank Sune Linder for offering us excellent working facilities and for being such a great host during our long-term field measurements at Flakaliden. Contribution to this study by Marja-Leena Jalkanen, Taru Palosuo Raimo Pesonen, Sirkka Sutinen and Jouni Voipio is gratefully acknowledged. The work has been supported by Grants 52228 and 47615 from the Academy of Finland.

**References**

Del Rio, E. and A. Berg. 1979. Specific leaf area of Douglas-fir reproduction as affected by light and needle age. For. Sci. 25:183–186.

Givnish, T.J. 1988. Adaptation to sun and shade: a whole plant perspective. Aust. J. Plant Physiol. 15:63–92.

Hager, H. and H. Sterba. 1985. Specific leaf area and needle weight of Norway spruce (*Picea abies*) in stands of different densities. Can. J. For. Res. 15:389–392.

Leverenz, J.W. and T.M. Hinckley. 1990. Shoot structure, leaf area index and productivity of evergreen conifer stands. Tree Physiol. 6: 135–149.

Linder, S. 1995. Foliar analysis for detecting and correcting nutrient imbalances in Norway spruce. Ecol. Bull. 44:178–190.

Linder, S and D.A. Rook. 1984. Effects of mineral nutrition on carbon dioxide exchange and partitioning in trees. *In* Nutrition in Plantation Forests. Eds. G.D. Bowen and E.K.S. Nambiar. Academic Press, London, pp 212–236.

McMurtrie, R. and L. Wolf. 1983. Above- and below-ground growth of forest stands: a carbon budget model. Ann. Bot. 52:437–448.

Neter, J., W. Wasserman and M.H. Kutner. 1983. Applied linear regression models. Richard D. Irwin, Homewood, IL, 547 p.

Niinemets, Ü. and O. Kull. 1995*a*. Effects of light availability and tree size on the architecture of assimilative surface in the canopy of *Picea abies*: variation in needle morphology. Tree Physiol. 15: 307–315.

Niinemets, Ü. and O. Kull. 1995*b*. Effects of light availability and tree size on the architecture of assimilative surface in the canopy of *Picea abies*: variation in shoot structure. Tree Physiol. 15: 791–798.

Oker-Blom, P. and H. Smolander. 1988. The ratio of shoot silhouette area to total needle area in Scots pine. For. Sci. 34:894–906.

Schoettle, A.W. and T.J. Fahey. 1994. Foliage and fine root longevity of pines. Ecol. Bull. 43:136–153.

Schoettle, A.W. and W.K. Smith. 1991. Interrelation between shoot characteristics and solar irradiance in the crown of *Pinus contorta* ssp. *latifolia*. Tree Physiol. 9:245–254.

Sellin, A. 2000. Estimating the needle area from geometric measurements: application of different calculation methods to Norway spruce. Trees 14:215–222.

Smolander, S. and P. Stenberg. 2001. A method for estimating light interception by a conifer shoot. Tree Physiol. 21:797–804.

Sprugel, D.G., J.R. Brooks and T.M. Hinckley. 1996. Effect of light on shoot and needle morphology in *Abies amabilis*. Tree Physiol. 16:91–98.

Stenberg, P., T. Kangas, H. Smolander and S. Linder. 1999. Shoot structure, canopy openness, and light interception in Norway spruce. Plant Cell Environ. 22:1133–1142.

Stenberg, P., S. Palmroth, B.J. Bond, D.G. Sprugel and H. Smolander. 2001. Shoot structure and photosynthetic efficiency along the light gradient in a Scots pine canopy. Tree Physiol. 21:805–814.

# IV

Available online at www.sciencedirect.com
SCIENCE DIRECT®
Remote Sensing of Environment 88 (2003) 363–373
Remote Sensing of Environment
www.elsevier.com/locate/rse

# A method to account for shoot scale clumping in coniferous canopy reflectance models

Sampo Smolander[a,*], Pauline Stenberg[b]

[a] Division of Biometry, Rolf Nevanlinna Institute, University of Helsinki, P.O. Box 4, FIN-00014 Helsinki, Finland
[b] Department of Forest Ecology, P.O. Box 27, FIN-00014 University of Helsinki, Helsinki, Finland

Received 22 January 2003; received in revised form 3 June 2003; accepted 6 June 2003

**Abstract**

The three-dimensional structure of a coniferous shoot gives rise to multiple scattering of light between the needles of the shoot, causing the shoot spectral reflectance to differ from that of a flat leaf. Forest reflectance models based on the radiative transfer equation handle shoot level clumping by correcting the radiation attenuation coefficient with a clumping index. The clumping index causes a reduction in the interception of radiation by the canopy at a fixed leaf area index (LAI). In this study, we show how within-shoot multiple scattering is related to shoot scale clumping and derive a similar, but wavelength dependent, correction to the scattering coefficient. The results provide a method for integrating shoot structure into current radiative transfer equation based forest reflectance models. The method was applied to explore the effect of shoot scale clumping on canopy spectral reflectance using simple model canopies with a homogeneous higher level structure. The clumping of needles into shoots caused a wavelength dependent reduction in canopy reflectance, as compared to that of a leaf canopy with similar interception. This is proposed to be one reason why coniferous and broad-leaved canopies occupy different regions in the spectral space and exhibit different dependency of spectral vegetation indices on LAI.


*Keywords:* Leaf area index; Monte Carlo modelling; Radiative transfer models; Remote sensing; Vegetation canopy model

## 1. Introduction

A well known problem in the radiative transfer theory is how small-scale structures should be handled (Knyazikhin, Martonchik, Myneni, Diner, & Running, 1998; Ross, 1981; Shabanov, Knyazikhin, Baret, & Myneni, 2000). In coniferous canopies, the dense clumping of needles in the small region occupied by a shoot causes variation in needle area density at the shoot size scale (i.e. from centimeters to decimeters). It is not feasible to include such small-scale variation into any leaf area density distribution that is to be useful in formulating the radiative transfer problem for three-dimensional plant canopies. In other words, the "elementary volume", used in formulating radiative transfer problems, should be small enough that essentially no mutual shading between the elements exists but large enough for statistical laws, such as Beer's law, to apply (Ross, 1981). In coniferous canopies, there is already substantial mutual shading between the needles of a shoot (Oker-Blom & Smolander, 1988).

A possible way to overcome this problem is to use the shoot as the basic structural element in radiative transfer models for conifers (Nilson & Ross, 1997). The canopy structure is then described in terms of the spatial and angular distribution of shoots, and the geometrical and spectral properties of leaves are replaced with those of shoots. This approach, using the annual shoot as the basic structural unit, has long been applied in light interception models (Cescatti, 1998; Nilson, Anniste, Lang, & Praks, 1999; Oker-Blom & Kellomäki, 1983; Stenberg, Smolander, & Kellomäki, 1993) and LAI measurement techniques (Chen, Rich, Gower, Norman, & Plummer, 1997; Stenberg, 1996). A key parameter entering these models is the shoot silhouette to total area ratio (STAR) (Oker-Blom & Smolander, 1988), which is conceptually analogous to the *G*-function, or the mean projection of unit foliage area, defined for flat leaves (Nilson, 1971). These models have been designed specifically for the estimation of photosynthesis, and the spectral properties of

* Corresponding author. Tel.: +358-9-4111-0756; fax: +358-9-1912-2779.
*E-mail address:* Sampo.Smolander@Helsinki.Fi (S. Smolander).

0034-4257/$ - see front matter © 2003 Elsevier Inc. All rights reserved.
doi:10.1016/j.rse.2003.06.003

shoots have not been considered important because the scattering of photosynthetically active radiation (PAR) by conifer needles is known to be very small (Daughtry, Ranson, & Biehl, 1989). Some recent canopy reflectance models (Knyazikhin et al., 1998; Kuusk & Nilson, 2000; Shabanov et al., 2000) have accounted for the effect of small-scale clumping by modifying the *G*-function but in these approaches the shoot has not been explicitly used as the basic element in evaluating the area scattering phase function of the transport equation. The presence of within-shoot multiple scattering has long been recognized (Gates & Benedict, 1963; Norman & Jarvis, 1975), but in order to take it into account in radiative transfer models, it is necessary to derive quantitative relationships between the structure and the scattering properties of a shoot.

In this paper, we present a method by which the effect of needle clumping into shoots can be accounted for in canopy reflectance models. The approach was developed using empirical data on Scots pine (*Pinus sylvestris* L.) together with a previously developed geometrical model of Scots pine shoots. First, we simulated the scattering phase function of a Scots pine shoot for different wavelengths and for different directions of the incoming beam of photons. Secondly, we estimated the shoot-specific but wavelength independent parameter $p_{sh}$, corresponding to the probability that a photon scattered from the needle surface of the shoot will interact with the shoot again. The parameter $p_{sh}$ is conceptually similar to the canopy structural parameter ($p_i$, probability of interaction) defined by Knyazikhin et al. (1998), which links together canopy absorptance and scattering at any two different wavelengths (Panferov et al., 2001). In thermal engineering, a similar concept is known as view factor or shape factor, giving the proportion of radiation emitted from a body that hits the body again (e.g. Holman, 1986).

We show that the parameter $p_{sh}$ provides a similar link at the shoot level. That is, knowing $p_{sh}$ and the scattering coefficient of a needle, the scattering coefficient of a shoot for any given wavelength can be calculated by a simple equation. Third, we derive a theoretical relationship between $p_{sh}$ and the spherically averaged STAR ($\overline{\mathrm{STAR}}$), and present empirical verification using material on shoot structure and $\overline{\mathrm{STAR}}$ in Scots pine (Stenberg, Palmroth, Bond, Sprugel, & Smolander, 2001). Results from the shoot level simulations are used to construct a "shoot-like leaf" with similar *G*-value and scattering properties as the shoot.

Canopies composed of flat leaves, shoots, and "shoot-like leaves" were built, and simulations at the canopy level were performed to compare the spectral reflectance of the canopies for similar values of leaf area index (LAI). We used simple Poisson canopies, where the foliage elements (shoots or leaves) were randomly distributed and spherically oriented. Needle reflectance and transmittance were assumed to be similar to those of leaves, the difference between the canopy reflectances thus being caused solely by shoot structure. The main results from the simulations were that: (i) the clumping of needles into shoots produced a wavelength dependent reduction in canopy reflectance as compared to a leaf canopy with similar LAI, and that (ii) the reflectance behavior of the "real" shoot canopy was well approximated by using "shoot-like leaves", thus providing a means for integrating shoot structure into leaf-based reflectance models.

## 2. Materials and methods

### 2.1. Description of shoot structure

The three-dimensional structure of a coniferous shoot gives rise to multiple scattering within the shoot, causing the scattering from a shoot to differ from that of a flat leaf (Fig. 1). For description of shoot structure, we used a geometrical model for Scots pine shoots, and structural data from a previous investigation (Stenberg et al., 2001). The shoot depicted in Fig. 1A was generated from a model using the following assumptions: (i) needles were of the same size and cylindrical in shape, (ii) needle pairs were evenly positioned along the shoot axis, (iii) the angle between needle and shoot axis was constant, (iv) the orientation of

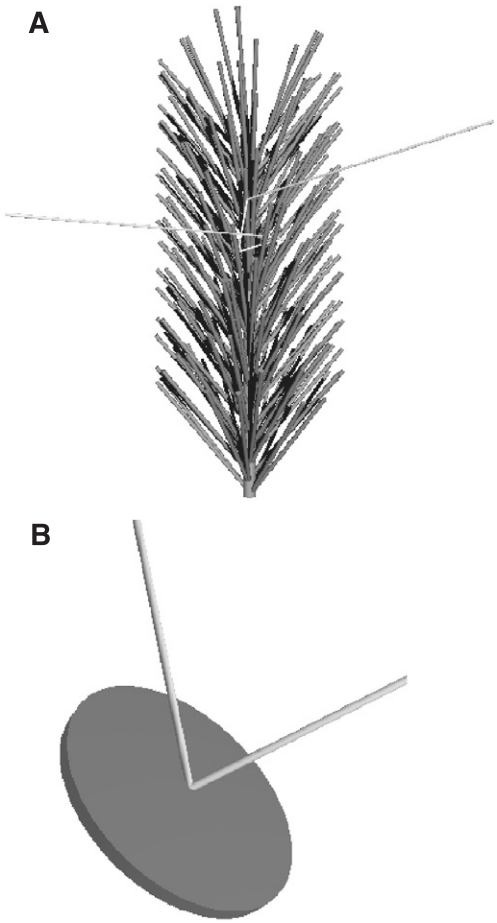


Fig. 1. Presentation of the problem: a photon reflected from a shoot may have interacted with the shoot several times (multiple scattering) (A), whereas with a flat leaf there is only one interaction (B).

needles around the shoot axis followed a Fibonacci phyllotactic arrangement with a divergence angle of $8/13 \times 2\pi$ between successive needle pairs (Cannell & Bowler, 1978), and (v) the fascicle angle, which is the opening angle between the two needles in a fascicle, was uniformly distributed between 0 and $2/13\pi$. The structural parameters of the "average" Scots pine shoot chosen for the simulation of scattering phase function are shown in Table 1.

$\overline{\text{STAR}}$ (Table 1) denotes the spherically averaged shoot silhouette to total area ratio, mathematically defined as:

$$\overline{\text{STAR}} = \frac{1}{\text{TNA}} \frac{1}{4\pi} \int_{4\pi} \text{SSA}(\Omega) \text{d}\Omega \quad (1)$$

where TNA denotes the total needle area of the shoot, and SSA($\Omega$) is the shoot silhouette area in direction $\Omega$. Integration over all directions of the sphere is denoted by $4\pi$. $\overline{\text{STAR}}$ was calculated based on photographically measured SSA in different directions, using the procedure described by Smolander and Stenberg (2001).

### 2.2. Simulation of the shoot scattering phase function

A beam of photons of specific wavelength was fired toward the shoot from different directions, and a ray-tracing procedure was used to follow the path of each photon (this method is called "ray tracing from the light sources" by Foley, van Dam, Feiner, & Hughes, 1990 to emphasize the fact that the paths of the photons are followed in the direction the photons actually move).

The simulation procedure was as follows. The beam direction was held fixed (entering parallel to the $x$-axis), and the shoot was placed so that its midpoint was in the origin and its axis was along a chosen direction, denoted by $\Omega$. A large number ($N$) of photons was fired from different ($y$, $z$) coordinates chosen randomly from an area ($S$). This area was defined so as to contain all the shoot silhouette area (SSA) (Fig. 2). From the total number of fired photons, the proportion ($N_i^{(\Omega)}$) that hit the shoot (first-order interaction) was followed by ray tracing, whereas the photons that did not hit the shoot were just counted. For a given direction, the fraction of fired photons hitting the shoot ($N_i^{(\Omega)}/N$) thus corresponds to SSA/$S$ in the considered direction.

Each photon intercepted by the shoot was followed until it was absorbed, or finally escaped the shoot. By

Table 1
Structural parameters of the model shoot

| | |
|---|---|
| Number of needles | 190 |
| Total needle area | 156.3 cm$^2$ |
| Needle length | 2.85 cm |
| Needle diameter | 0.092 cm |
| Needle angle (from twig) | 40.5° |
| Fascicle angle | 0–27.7° |
| Twig length | 7.7 cm |
| Twig diameter | 0.3 cm |
| $\overline{\text{STAR}}$ | 0.133 |

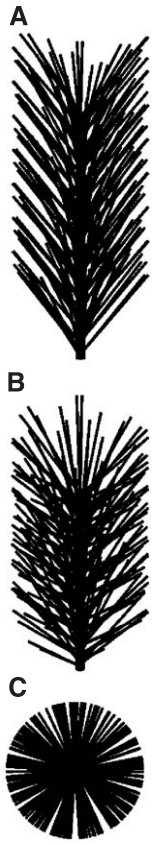


Fig. 2. Silhouettes of the model shoot as seen (A) from side, (B) at 45° angle, and (C) axially.

intercepted photons, we mean all the photons that originally hit the shoot, regardless of whether they finally were absorbed or scattered. At the points where a photon hit the needle surface, the photon was either absorbed, reflected, or transmitted through the needle. Needle reflectance ($\rho_L$) and transmittance ($\tau_L$) were assumed to have the same value. Reflection or transmission of a photon hitting a needle occurred with a probability equal to one half of the needle scattering coefficient ($\omega_L$) at the specified wavelength, and absorption occurred with probability $1-\omega_L$. The twig was assumed to have similar reflectance as the needles, but transmittance through the twig was set to zero. All surfaces were assumed to reflect as Lambertian surfaces, reradiating the intercepted photons following a cosine distribution around the normal to the surface at the point of reflection. The transmitted part of the radiation was assumed to emerge from a point on the opposite side of the needle, and to follow a cosine distribution around the normal to this opposite surface. (Sometimes in the lower part of a fascicle, the point on the opposite side of the needle was inside the other needle of the fascicle. In this case, the point of emergence was taken to be on the opposite side of that other needle.)

For a Lambertian surface, the fraction of photons reflected into a solid angle d$\Omega$ around ($\theta$, $\phi$) (=polar and azimuth

angle relative to the needle surface normal at the point of reflection) is given by:

$$f(\theta,\phi)\mathrm{d}\Omega = \frac{1}{\pi}\cos\theta\mathrm{d}\Omega = \frac{1}{\pi}\cos\theta\sin\theta\mathrm{d}\theta\mathrm{d}\phi. \quad (2)$$

A new direction for a reflected or transmitted photon was generated following this distribution and the ray-tracing procedure was repeated. The final fate of every photon was recorded in terms of: (i) whether it was absorbed or scattered (reflected or transmitted), (ii) its outgoing direction in case of scattering, and (iii) the total number of interactions within the shoot.

The scattering coefficient of a shoot, unlike that of a flat Lambertian surface, varies with the direction of incoming radiation. We define the mean shoot scattering coefficient ($\omega_{sh}$) as the fraction of scattered photons to photons intercepted by the shoot in an isotropic radiation field. Let $\Omega$=($\theta$, $\phi$) denote the orientation of the shoot in relation to beam direction, and SSA($\Omega$) and $\omega_{sh}(\Omega)$ the silhouette area and scattering coefficient, respectively, of the shoot in the considered orientation. The number of intercepted photons is proportional to SSA($\Omega$), and we have:

$$\omega_{sh} = \frac{1}{4\pi\overline{\mathrm{SSA}}}\int_{4\pi}\omega_{sh}(\Omega)\mathrm{SSA}(\Omega)\mathrm{d}\Omega, \quad (3)$$

where $\overline{\mathrm{SSA}}$ denotes the spherically averaged SSA.

Simulation of the scattering phase function of the shoot in an isotropic radiation field was carried out with the procedure described above, with the difference that before a new photon was fired, the orientation of the shoot axis was generated again according to the uniform spherical density function. Interaction between the shoot and a photon from the direction $\Omega$ in relation to the shoot occurred with probability SSA($\Omega$)/$S$, the total fraction of intercepted photons ($N_i/N$) being proportional to $\overline{\mathrm{SSA}}$. The shoot scattering coefficient ($\omega_{sh}$) was calculated as the ratio of photons finally escaping the shoot ($N_e$) to the total number of photons initially hitting the shoot ($N_i$), $\omega_{sh} = N_e/N_i$. Notice that the shoot scattering coefficient can also be interpreted as the scattering coefficient of a layer of spherically oriented shoots (not shading each other).

### 2.3. Estimation of the shoot structural parameter $p_{sh}$

Simulations of $\omega_{sh}$ were performed to estimate the shoot structural parameter $p_{sh}$, expressing the probability that a photon scattered from the needle surface of the shoot will interact within the shoot again. We use a heuristic approach to derive a relation linking the shoot scattering coefficient ($\omega_{sh}$) and absorptance ($A_{sh} = 1 - \omega_{sh}$) to the parameter $p_{sh}$. At every interaction between a photon of specific wavelength $\lambda$ and a needle on the shoot, absorption occurs with probability $1 - \omega_L(\lambda)$, where $\omega_L(\lambda)$ is the needle scattering coefficient at the considered wavelength. Otherwise, with probability $\omega_L(\lambda)$, the photon is scattered and may interact within the shoot again (see Fig. 1A). Assuming that the probability by which a scattered photon will interact again (parameter $p_{sh}$) remains constant in successive interactions, shoot absorptance (the eventually absorbed fraction of the photons that initially hit the shoot) is obtained as the sum

$$A_{sh}(\lambda) = [1-\omega_L(\lambda)] + [1-\omega_L(\lambda)]p_{sh}\omega_L(\lambda) + [1-\omega_L(\lambda)]p_{sh}^2\omega_L(\lambda)^2 + \ldots = \frac{1-\omega_L(\lambda)}{1-p_{sh}\omega_L(\lambda)}. \quad (4)$$

Shoot absorptance ($A_{sh}$) normalized by the needle absorptance ($1 - \omega_L$) equals the average number ($n$) of interactions between a photon and the shoot. From Eq. (4) follows that

$$n = \frac{1}{1-p_{sh}\omega_L(\lambda)} \quad (5)$$

where the denominator $1 - p_{sh}\omega_L(\lambda)$ is the fraction of intercepted photons interacting only once with the shoot. Notice that for $\omega_L = 0$, or if $p_{sh} = 0$ (no within-shoot shading), we always have $n = 1$ (see Fig. 1).

The shoot scattering coefficient is now obtained (from Eqs. (4) and (5)) as:

$$\omega_{sh}(\lambda) = 1 - A_{sh}(\lambda) = \omega_L(\lambda)\frac{1-p_{sh}}{1-p_{sh}\omega_L(\lambda)} = \omega_L(\lambda)n(1-p_{sh}). \quad (6)$$

We see that the shoot scattering coefficient normalized by the needle scattering coefficient ($\omega_{sh}/\omega_L$) equals the average number of interactions ($n$) multiplied by the probability of escape ($1 - p_{sh}$). The ratio decreases when the shoot self-shading ($p_{sh}$) increases, and the ratio increases when $\omega_L$ increases. (In case of $p_{sh} = 0$, no within-shoot shading, the scattering coefficients for shoot and needle, $\omega_{sh}$ and $\omega_L$, are equal.)

### 2.4. Relationship between $\overline{STAR}$ and $p_{sh}$

If there were no mutual shading between the (assumed convex) needles on a shoot, the spherically averaged shoot silhouette to total area ratio, $\overline{\mathrm{STAR}}$ (Eq. (1)), would be 1/4. (This follows from Cauchy's theorem, stating that the spherically averaged projected area of any convex body equals one fourth of its total surface area; see Lang, 1991). The ratio between $\overline{\mathrm{STAR}}$ and 1/4, i.e. the ratio of spherically projected shoot area to spherically projected needle area, is $4\overline{\mathrm{STAR}}$. This quantity was defined by Stenberg, Linder, Smolander, and Flower-Ellis (1994) as the shoot shading factor ($\beta$) (see also Stenberg, 1996), and corresponds to the needle clumping index in shoots ($\kappa$) used by Nilson et al. (1999).

We proceed to show that $4\overline{\mathrm{STAR}}$ can also be interpreted as the mean probability that a photon emitted from a random point on the needle surface of the shoot will not hit another needle of the shoot (“probability of no interaction”). Consider a Lambertian surface of area $A$ emitting radiation at level $E$ per unit area per unit time (see Bell & Rose, 1981). If $A$ is the surface of a non-self-shadowing (convex) body, an observer from a random direction would see, on average, a silhouette area $A/4$ at constant radiance $E/\pi$ (since the brightness of a Lambertian surface does not depend on the view angle). Integrating this over all directions ($4\pi$) gives a total emitted energy of $AE$ per unit time, as it should. Now, if the object were self-shadowing, its average silhouette area $\overline{A_s}$ would be smaller than $A/4$. The observer would nevertheless see all of the surface at the same radiance $E/\pi$ (assuming here, that the surface only emits radiation but does not reflect it). Integrating as before, the total emitted energy is $4\overline{A_s}E$ per unit time. This means, that a proportion of $1-4\overline{A_s}/A=1-4\overline{\mathrm{STAR}}$ of the emitted energy does not leave the body, because it hits it again.

We recall that the shoot structural parameter $p_{sh}$ is the mean probability that a photon reflected from the surface of the shoot will interact with the shoot again. As we assumed Lambertian reflectance, $4\overline{\mathrm{STAR}}$ can in turn be interpreted as the probability that a reflected photon will escape the shoot. Consequently, $p_{sh}$ should be closely related to $1-4\overline{\mathrm{STAR}}$. The only difference between the parameters comes from the spatial averaging: $1-4\overline{\mathrm{STAR}}$ represents the mean over points on the surface, $p_{sh}$ is spatially averaged over the points of interaction.

To test the proposed relationship between $p_{sh}$ and $\overline{\mathrm{STAR}}$, we estimated $p_{sh}$ for eight additional Scots pine shoots for which the $\overline{\mathrm{STAR}}$ and parameter values needed in the simulations were available from a previous investigation (Stenberg et al., 2001). The shoots originated from different heights within a tree crown (the same tree from which our model shoot was taken) and represented a wide range of $\overline{\mathrm{STAR}}$ values.

### 2.5. Simulation of canopy reflectance

Canopies with randomly distributed shoots and leaves (Poisson canopies) were generated for different values of LAI. In addition, we constructed a “shoot-like leaf canopy”, composed of leaves with the same $G$-value and similar scattering properties as the shoot. Simulations were performed to produce the reflectance of these canopies, assumed to be bounded below by an all-absorbing surface (“black soil”). A beam of photons of a specific wavelength was fired into the canopies from a given direction, and a ray-tracing procedure was applied to follow each photon until it was absorbed, or escaped the canopy.

First, for every fired photon, the length ($l$) of its path through the canopy before any interaction with leaves/shoots occurred was determined. It was calculated using the probability that a photon, while travelling a distance $x$ in a Poisson canopy, does not interact with leaves,

$$P(l \geq x) = \exp(-G(\theta)u_L x) \tag{7}$$

where $u_L$ is the leaf area density and $G(\theta)$ denotes the mean projection of unit leaf or shoot area in the path direction (with zenith angle $\theta$).

The leaf area index (LAI) equals leaf area density ($u_L$) multiplied by total canopy depth ($D$), $\mathrm{LAI}=u_L D$. The relationship between canopy interceptance ($i_0$, the fraction of fired photons interacting with the canopy), corresponding to the probability $1-P(l \geq D/\cos\theta)$, and LAI is given by (cf. Eq. (7))

$$i_0 = 1-\exp\left(\frac{-Gu_L D}{\cos\theta}\right) = 1-\exp\left(\frac{-G\ \mathrm{LAI}}{\cos\theta}\right). \tag{8}$$

In our model canopies, a spherical orientation of leaves and shoots was assumed. The $G$-value in this case is independent of $\theta$ and equals 0.5 for leaves when leaf area is defined on a half of total surface area basis (Chen & Black, 1992). For shoots, using half of total needle area as the basis, the $G$-value corresponds to $2\overline{\mathrm{STAR}}$ (Oker-Blom & Smolander, 1988). Whenever $l\cos\theta$ was greater than the total depth of the canopy ($D$), the photon escaped to the soil. Otherwise, the photon interacted with a leaf or a shoot that was assumed to be situated at the sampled depth in the canopy.

When a photon collided with a leaf, the divergence angle $\beta$ (the angle between the propagating direction of the photon before and after collision) and the rotation angle $\psi$ (the angle of rotation for the new direction of propagation, around the axis of the old direction) were sampled according to the probability density function

$$f(\beta,\psi) = \frac{2}{3\pi^2}(\sin\beta - \beta\cos\beta) + \frac{2}{3\pi}(\cos\beta)\frac{\tau_L}{\omega_L}, \tag{9}$$

where $\omega_L$ is the leaf reflectance, $\tau_L$ leaf transmittance and where $\beta\in[0,\ \pi]$, $\psi\in[0,\ 2\pi]$. This is the scattering phase function for spherically oriented leaves (and is uniform for $\psi$) as explained in formula (II.6.9) on p. 257 in Ross (1981), but here it is normalized so that its integral over all directions is 1.

In the shoot canopy, the probability of a photon hitting the shoot from a certain direction should be proportional to the shoot silhouette area on a plane normal to the propagating direction of the photon. This was handled so that, in applying the procedure for spherically oriented shoots, if the photon (fired from a randomly chosen point on the area $S$ of fixed size) did not hit the shoot at the first try, it was fired again from a new point after resampling the shoot orientation. In this way, the probability of interaction with the shoot was proportional to its silhouette area, and the simulated outcome of the photon (absorbed or scattered to a specified direction)

was representative for spherical shoot orientation. The length of the path of photons scattered from the leaf or the shoot, before new interaction occurred, was sampled again using Eq. (7). Scattered photons escaped the canopy whenever $l$ was greater than the distance out from the canopy in the specified direction.

### 2.6. Simulation scheme

Canopy reflectance was expressed relative to that of an ideal (100% reflecting) Lambertian surface placed at the top of the canopy. The bidirectional reflectance factor (BRF) is defined as the ratio of radiant flux reflected from a surface area into a particular direction to what would have been reflected in case of an ideal Lambertian surface of the same area (Martonchik, Bruegge, & Strahler, 2000). A Lambertian surface produces an equal radiance in all directions of the upper hemisphere ($N/(\pi A)$, number of photons per unit solid angle per unit of emitting area normal to the direction of propagation), whereas the total flux (number of photons) into a unit solid angle is proportional to $\cos\theta$ (see Eq. (2)). The number of photons reflected from the canopy to a fixed solid angle $d\Omega$ around the zenith angle $\theta$ divided by $N\cos\theta d\Omega/\pi$ gives the BRF. In the simulations, photons entered from a zenith angle of 45°, and BRF was calculated assuming the receiving sensor (with 10 angular radius for $d\Omega$) to be in the zenith ($\theta = 0°$).

Canopy BRF of the leaf and shoot canopies was compared for similar values of LAI. Leaf and needle scattering coefficients of 0.1 and 0.9 were chosen to represent wavelengths around the "red edge" in the leaf spectra, characterized by an absorption peak in red and an absorption minimum in near-infrared (NIR). We hereafter refer to the simulated wavelengths as "red" and "NIR".

## 3. Results

### 3.1. Shoot scattering phase function

Fig. 3 shows the directional distribution of photons scattered from the model shoot, for different angles between the directions of the beam and the shoot axis, and also the case for spherically oriented shoots. The photons scattered from the shoot that changed their direction more than 90° were considered reflected, and photons that changed their direction less than 90° were considered transmitted. For the NIR wavelength (that is, for $\omega_L = 0.9$), the shoot scattering coefficient was $\omega_{sh} = 0.81$, with reflectance $\rho_{sh} = 0.47$ and transmittance $\tau_{sh} = 0.34$ (Fig. 3). For the red wavelength ($\omega_L = 0.1$), the shoot scattering coefficient was $\omega_{sh} = 0.059$, with $\rho_{sh} = 0.034$ and $\tau_{sh} = 0.025$. The scattering phase function of the spherically oriented shoots was closely imitated by the scattering phase function of the shoot-like leaf, for which transmittance $\tau_L$ was 42% of $\omega_L$ at both wavelengths. Thus, the shoot scattering phase functions had more weight in the backscattering directions than the corresponding leaf scattering phase functions (Fig. 4). (It is to be noted that the shoot transmittance and reflectance, as defined above, are not directly comparable to leaf transmittance and reflectance. With the shoot, photons scattering less than 90° were always considered transmitted. With spherically oriented leaves, a photon may well scatter less than 90° also when it is technically reflected, not transmitted.)

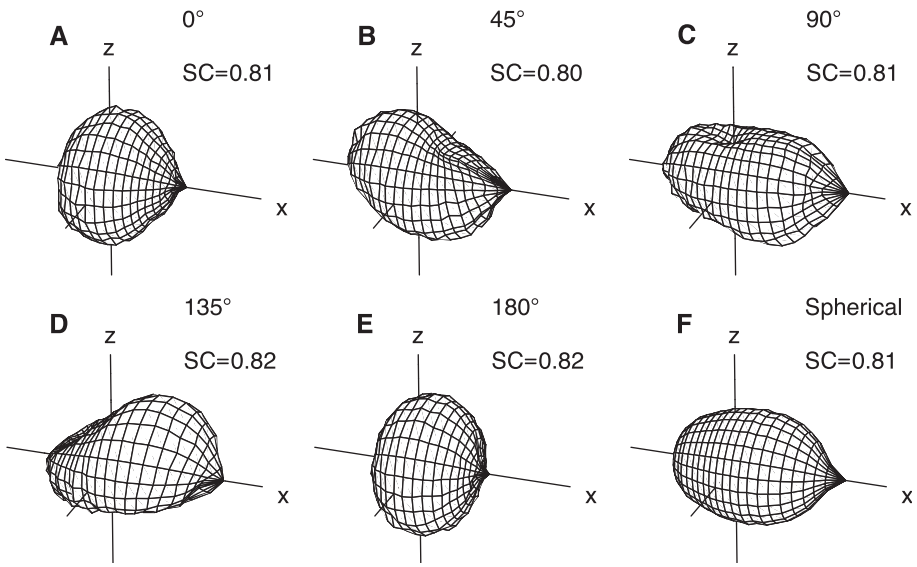


Fig. 3. Shoot scattering coefficient (SC) and the directional distribution of scattered photons for NIR wavelengths (needle SC = 0.9) for different directions of incoming radiation. The beam of radiation enters from the direction of the $x$-axis, and the shoot tip is directed to an angle of (A) 0° (B) 45° (C) 90°, (D) 135°, and (E) 180° opening from the $x$-axis towards the $z$-axis. In (F), the average directional distribution and scattering coefficient for scattering from randomly oriented shoots are presented.

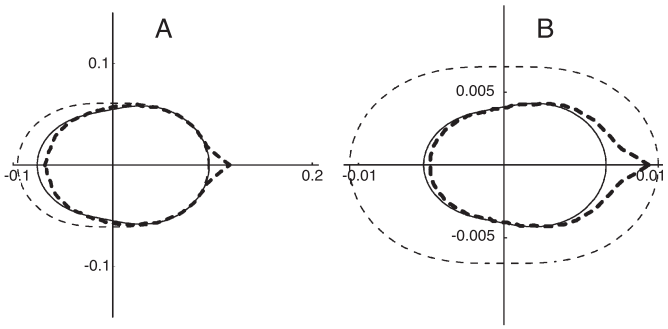


Fig. 4. Cross-sectional views of scattering phase functions for (A) leaf with $\rho_L = 0.45$, $\tau_L = 0.45$ (thin dashed line), shoot (thick dashed line) with values $\rho_L = 0.45$ and $\tau_L = 0.45$ for its needles, and leaf with $\rho_L = 0.47$ and $\tau_L = 0.34$ (thin line), (B) leaf with $\rho_L = 0.05$, $\tau_L = 0.05$ (thin dashed line), shoot (thick dashed line) with values $\rho_L = 0.05$ and $\tau_L = 0.05$ for its needes, and leaf with $\rho_L = 0.034$ and $\tau_L = 0.025$ (thin line). The radiation is assumed to come from the direction of positive $x$-axis and to meet the object in origo.

### 3.2. Shoot scattering coefficient as a function of the parameter $p_{sh}$

The shoot scattering coefficient $\omega_{sh}$ was simulated for a range of needle scattering coefficients $\omega_L = 0.1, 0.2, \ldots, 1$. The shoot structural parameter $p_{sh}$ was estimated based on the simulations performed for $\omega_L = 1$. It was calculated as the weighted mean of the ratios $n_{j+1}/s_j$ ($j = 1, 2, 3, \ldots$) where $n_{j+1}$ denotes the number of photons interacting at least $j+1$ times with the shoot before being absorbed or scattered out from the shoot, and $s_j$ denotes the number of photons scattered at the $j$th interaction. The ratio gives the fraction of the scattered photons at the $j$th interaction that hit the shoot again. The ratios were weighted proportional to $s_j$. The estimated value of $p_{sh}$ for the model shoot was 0.474. Using this value, $\omega_{sh}$ as a function of $\omega_L$ was then predicted by Eq. (6) (Fig. 5). Good agreement was found between predicted and simulated values of $\omega_{sh}$, despite the fact that there was some variation in the ratios $n_{j+1}/s_j$ (i.e. the basic assumption behind the derivation of Eq. (6) did not exactly hold true). Fitting Eq. (6) to the data points in Fig. 5 by the least squares method would have yielded the estimate $p_{sh} = 0.467$, which is negligibly different (1.5% difference) from the value estimated directly by simulation as explained above. (The shoot scattering coefficient $\omega_{sh}$ is 0.98 for the needle scattering coefficient $\omega_L = 1$ (Fig. 4) because sometimes the photons hit the twig which had no transmittance.)

### 3.3. Correspondence between $\overline{STAR}$ and $p_{sh}$

A close to one to one relationship was found between the simulated $p_{sh}$ values, and $1 - 4\overline{STAR}$. (Fig. 6). This result is supported by theoretical considerations (Section 2.4), which also explain why an exact correspondence should not be

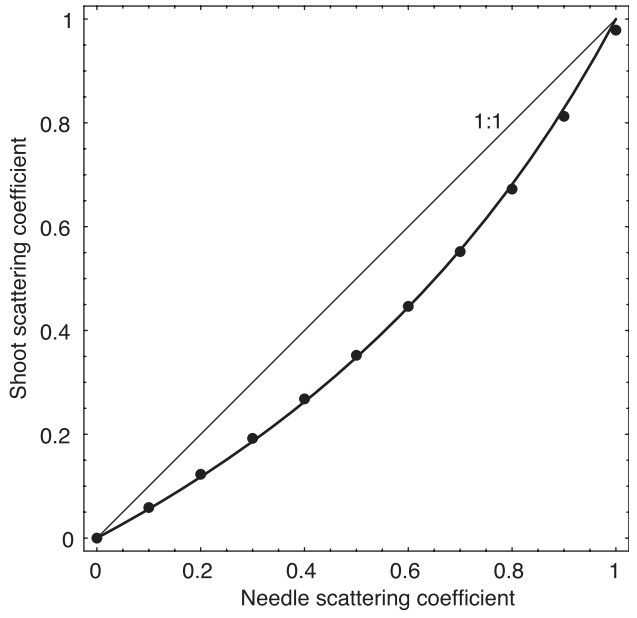


Fig. 5. Predicted (Eq. (5) with $p_{sh} = 0.474$) and simulated shoot scattering coefficient (black dots) for different needle scattering coefficients (wavelengths).

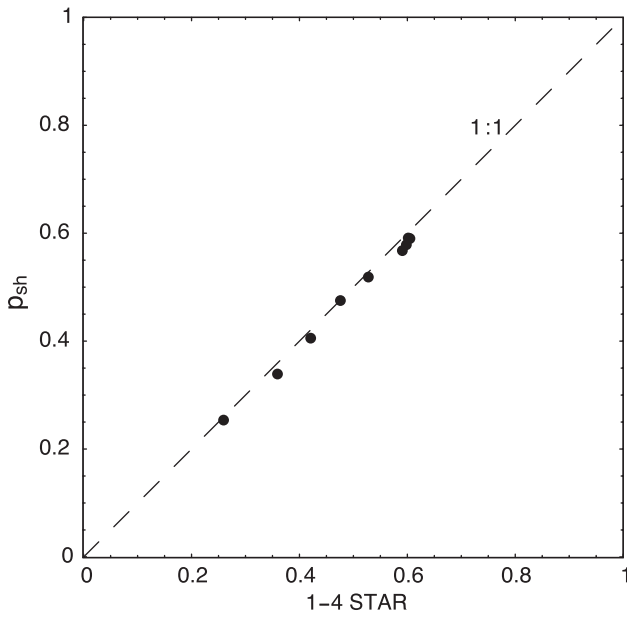


Fig. 6. Relation between $p_{sh}$ and $1 - 4\overline{STAR}$ for nine Scots pine shoots. Shoot structural data from a previous investigation is used (Stenberg et al., 2001).

expected. The formulation of the parameter $p_{sh}$ in Section 2.3 was approximative as it was based on the assumption that the probability of interaction stays constant with successive interactions. In reality, the density of points where scattering occurs varies with the order of interaction, and it is therefore not possible to analytically define the weight on the area over which $p_{sh}$ is averaged.

It should also be recognized that, in contrast to $\overline{STAR}$, $p_{sh}$ is not just a function of shoot geometry but has some dependency on needle optical properties since they affect the directional distribution of scattered photons (here assumed to be Lambertian). Despite this difficulty in finding a strict definition for $p_{sh}$ the correspondence between $p_{sh}$ and $\overline{STAR}$ was in our case good enough to be useful.

Table 2
Parameters used in the canopy simulations

| Canopy | *G*-value | Red | | | NIR | | |
|---|---|---|---|---|---|---|---|
| | | $\omega_L$ | $\rho_L$ | $\tau_L$ | $\omega_L$ | $\rho_L$ | $\tau_L$ |
| Leaf | 0.5 | 0.1 | 0.05 | 0.05 | 0.9 | 0.45 | 0.45 |
| Shoot | 0.266 | 0.1 | 0.05 | 0.05 | 0.9 | 0.45 | 0.45 |
| Shoot-like leaf | 0.266 | 0.059 | 0.034 | 0.025 | 0.81 | 0.47 | 0.34 |

### 3.4. Canopy simulations

In Fig. 7, canopy reflectance (BRF) in red and NIR wavelengths for the model canopies (Table 2), bounded underneath by a black surface, are compared. We notice first

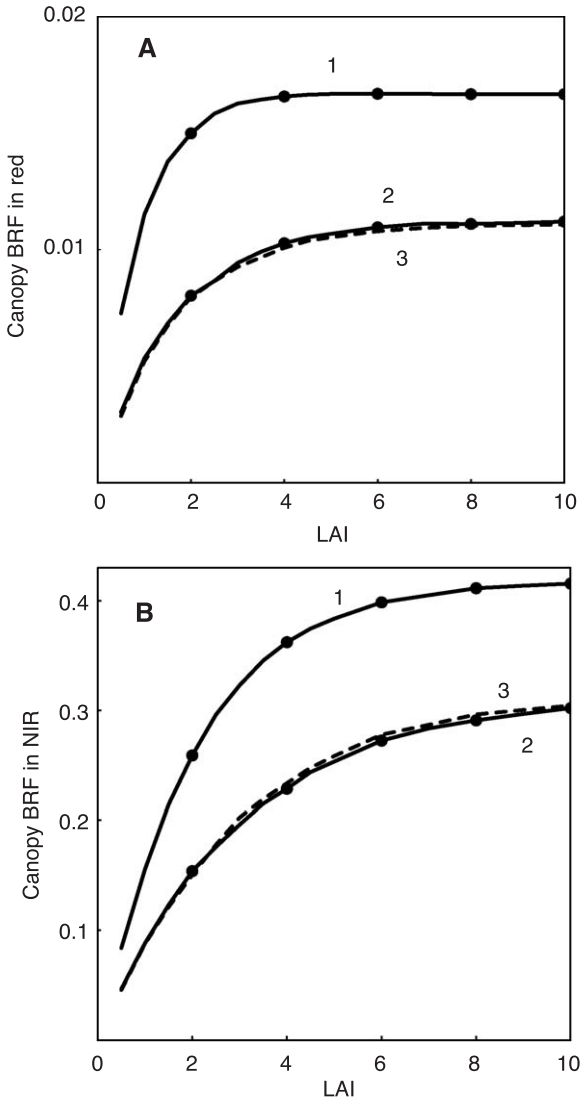


Fig. 7. Canopy bidirectional reflectance factor (BRF) in red and NIR wavelengths as a function of LAI for canopies bounded underneath by black soil. Curve (1) is for leaf canopy, curve (2) for shoot canopy and the dashed curve (3) for "shoot-like leaf" canopy. The black dots denote LAI values of 2, 4, 6, 8 and 10. The solar zenith angle is 45° and the view zenith angle is 0°.

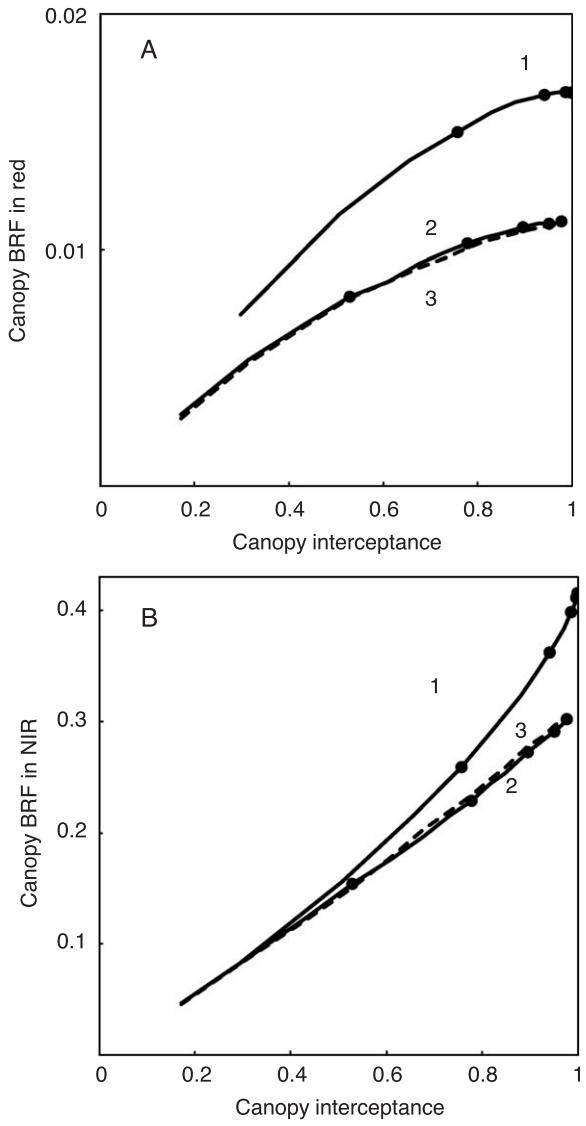


Fig. 8. Canopy bidirectional reflectance factor (BRF) in red and NIR wavelengths as a function of canopy interceptance ($i_0$) for canopies bounded underneath by black soil. Curve (1) is for leaf canopy, curve (2) for shoot canopy, and the dashed curve (3) for "shoot-like leaf" canopy. The black dots denote LAI values of 2, 4, 6, 8 and 10 to facilitate comparison with Fig. 7. The solar zenith angle is 45° and the view zenith angle is 0°.

that the reflectance of the shoot canopy was well approximated by the shoot-like leaf canopy. All curves increased with increasing LAI as they should, since nonreflecting background was assumed in these simulations. At small LAI, canopy reflectance increased more sharply with increasing LAI in the leaf canopy than in the shoot canopy. A reason for this is that the leaf canopy had a higher $G$-value and thus higher canopy interceptance ($i_0$) at similar LAI (see Eq. (8)). When presented as a function of $i_0$ rather than LAI, the reflectance factor of the leaf canopy still remained higher than that of the shoot canopy (Fig. 8). At full canopy cover (represented here by simulations for LAI = 10) the reflectance factor in red was 1.7% in the leaf canopy and 1.1% in the shoot canopy. In NIR, the respective values were 42% for the leaf canopy and 30% for the shoot canopy.

## 4. Discussion

For a fixed LAI, the effect of the clumping of foliage in the canopy is to reduce canopy interceptance (fraction of incoming photons interacting with the leaves or needles in the canopy). In radiative transfer models, clumping at larger spatial scales (e.g. grouping of leaves into tree crowns) can conveniently be handled by dividing the canopy volume in non-foliated and foliated parts (tree crowns) (Kuusk & Nilson, 2000; Nilson & Peterson, 1991). The spatial distribution of leaf area is commonly described by a probability density function, which allows for variation in leaf area density in different parts of the foliated canopy. However, the scale at which variation can be considered by this approach is limited by the size of the smallest unit (the "elementary volume") for which the statistical description is still reasonable. That is, the (imaginary) elementary volume must be large enough to allow the leaf area density to be defined, and contain a sufficient number of statistically independent foliage elements (see an analogue on p. 8 in Mandelbrot, 1983). To overcome the problem of statistical representation of the distribution of needle area within and between the small regions occupied by coniferous shoots, we have used the shoot as the basic structural unit of the canopy. This was done by deriving the interception, absorption, and scattering properties of a shoot as a function of the shoot structure.

When compared to a single leaf, the effect of mutual shading of needles in a shoot is to decrease the radiation interception efficiency ($G$-value) and the scattering coefficient of the shoot, and to change the shape of the scattering phase function to weight it more towards the backscattering directions (Fig. 4). We simulated shoot scattering at different wavelengths and derived the wavelength specific mean shoot scattering coefficient ($\omega_{sh}$), representing the scattering coefficient of a layer of spherically oriented shoots (Fig. 3). It was shown that $\omega_{sh}$ at a specific wavelength could be accurately predicted from the needle scattering coefficient $\omega_L$ at the same wavelength, with the help of a wavelength independent shoot structural parameter, $p_{sh}$ (Fig. 5). The parameter $p_{sh}$—"probability of interaction within the shoot"—depends on the geometrical structure of the shoot. We recall that shoot absorptance ($A_{sh}$) (Eq. (4)) normalized by the needle absorptance ($1-\omega_L$) corresponds to the average number ($n$) of interactions between a photon and the shoot (Eq. (5)), and that the ratio of $\omega_{sh}$ to $\omega_L$ equals $n$ multiplied by the probability of escape ($1-p_{sh}$). The probability of escape, further, was shown to be closely approximated by the shoot shading factor $\kappa = 4\overline{STAR}$ (Fig. 6) and thus we have $\omega_{sh}/\omega_L \approx n\kappa$. The relationship (Eq. (6)) between $\omega_{sh}$ and $\omega_L$ implies that the larger $p_{sh}$ (smaller $\kappa$), the smaller the ratio $\omega_{sh}/\omega_L$. At fixed $p_{sh}$, the ratio $\omega_{sh}/\omega_L$ increases with $\omega_L$, i.e. the decrease in shoot scattering from mutual shading is relatively less at wavelengths with high needle scattering.

Results from the shoot level simulations were applied to show how the clumping of needles into shoots affects canopy reflectance. The relationship of canopy bidirectional reflectance factor (BRF) with LAI was studied in model canopies built of Poisson-distributed and spherically oriented flat leaves and shoots, respectively (Figs. 7 and 8). In the absence of background reflectance, needle clumping decreased the BRF of the shoot canopy as compared to the leaf canopy with similar LAI (Fig. 7) or similar canopy interceptance (Fig. 8). Differences in canopy BRF were relatively larger in the red wavelength (small leaf and needle scattering; $\omega_L = 0.1$) than in NIR (large leaf and needle scattering; $\omega_L = 0.9$). In this study, we have only considered the effect of shoot level clumping in canopies with homogeneous higher level structure. Crown mutual shading can also have an important role in the forest reflectance (Gerard & North, 1997). This kind of higher level clumping would presumably pronounce further the differences between coniferous and broad-leaved forest reflectance. The method introduced in this paper can conveniently be integrated into more realistic forest reflectance models, which take into account the effects of, e.g. background reflectance, crown shape and crown mutual shading.

To parameterize a shoot-like leaf one needs to specify the shoot structural parameter $p_{sh}$ and the shape of the shoot scattering phase function (Fig. 3). The observed tight relationship between $p_{sh}$ and $\overline{STAR}$ is convenient because data on $\overline{STAR}$ are available for many coniferous species (Cescatti & Zorer, 2003; Palmroth, Stenberg, Smolander, Voipio, & Smolander, 2002; Stenberg, Kangas, Smolander, & Linder, 1999; Stenberg et al., 2001; Stenberg, Smolander, Sprugel, & Smolander, 1998). The within-shoot hot spot effect was visible as a peak in the backscattering direction in the shoot scattering phase function (Fig. 4) but cannot be described by the bi-Lambertian distribution (Eq. (9)). Although this peak was not included in the shoot-like leaf scattering phase function, the canopy BRF simulations with shoots and shoot-like leaves were in very good agreement (Figs. 7 and 8). However, the simulated canopy BRF was in the zenith direction and not in the backscattering direction where the

canopy hot spot is seen. The shoot-level backscattering might be important for canopy backscattering.

The shoot scattering coefficient depended on shoot structure ($p_{sh}$) and needle scattering coefficient ($\omega_L$) (Fig. 5), but was not sensitive to the ratio of needle transmittance ($\tau_L$) to reflectance ($\rho_L$) (data not shown). The simplified assumption that $\tau_L$ equalled $\rho_L$ mainly affected the proportions of forward and backward scattering in the shoot scattering phase function (Fig. 4). Changing the ratio of $\tau_L$ to $\rho_L$ (e.g. decreasing $\tau_L$ for visible wavelengths) would change the ratio of shoot forward to backward scattering in the same direction but to a smaller degree. Although the exact shape of the shoot scattering phase function may not have a very large impact on the canopy reflectance, effort should be made to measure realistic spectral values of $\tau_L$ and $\rho_L$ in different species. Similarly, given accurate measurements of needle specular reflectance, this component could be included in the shoot scattering model fairly easily. Finally, to test the model, simulated shoot scattering phase functions should be compared to empirical measurements. To our knowledge such model-based comparison has not been made, although some investigations have involved measurements of the scattering phase function of shoots (Nilson & Ross, 1997; Ross, Meinander, & Sulev, 1994).

The main result of this study was the development of an operational method by which the effect of the small-scale clumping of needles into coniferous shoots could be incorporated into forest reflectance models of different types. For this purpose, it was not considered meaningful to construct model canopies with very complex architecture at higher hierarchical levels, so instead we used simple Poisson-canopies with a homogeneous macroscopic structure. Although our simulations for these hypothetical canopies cannot be meaningfully evaluated against real data, results were in qualitative agreement with empirical observations (Häme et al., 2001; Loechel et al., 1997; Nilson et al., 1999; Tian et al., 2000; Zhang, Tian, Myneni, Knyazikhin, & Woodcock, 2002). That is, it seems that shoot structure can indeed explain large part of the different behavior of coniferous canopy reflectance as compared to broad-leaved canopies. Given relevant data on the geometrical and optical properties of needles and shoots (for the considered species), it would be straightforward to incorporate the approach presented here to radiative transfer models with more realistic description of the macroscopic canopy structure.

*Notation*

| | |
|---|---|
| $\beta$ | divergence angle |
| $\theta$ | polar angle |
| $\Omega$ | a direction (in spherical coordinates) |
| $\omega_L$ | leaf/needle scattering coefficient |
| $\omega_{sh}$ | shoot scattering coefficient |
| $\rho_L$ | leaf/needle surface reflectance |
| $\tau_L$ | leaf/needle surface transmittance |
| $\phi$ | azimuth angle |
| $\psi$ | rotation angle |
| $D$ | canopy depth |
| $G$ | $G$-function, see Ross (1981) |
| $i_0$ | canopy interceptance |
| LAI | leaf area index |
| $n$ | mean number of interactions |
| $p_{sh}$ | shoot structural parameter |
| SSA | shoot silhouette area |
| $\overline{\text{SSA}}$ | spherical average of SSA |
| STAR | silhouette to total area ratio |
| $\overline{\text{STAR}}$ | spherical average of STAR |
| $u_L$ | leaf area density |

## Acknowledgements

The authors are grateful to Prof. Elja Arjas for comments and discussions. The work has been supported by Grants 50178 and 47615 from the Academy of Finland, and by the Graduate School in Computational Biology, Bioinformatics, and Biometry (ComBi).

## References

Bell, C. J., & Rose, D. A. (1981). Light measurement and the terminology of flow. *Plant, Cell and Environment*, *4*, 89–96.

Cannell, M. G. R., & Bowler, K. C. (1978). Phyllotactic arrangements of needles on elongating conifer shoots: A computer simulation. *Canadian Journal of Forest Research*, *8*, 138–141.

Cescatti, A. (1998). Modelling the radiative transfer in discontinuous canopies of asymmetric crowns: I. Model structure and algorithms. *Ecological Modelling*, *101*, 263–274.

Cescatti, A., & Zorer, R. (2003). Structural acclimation and radiation regime of silver fir (*Abies alba* Mill.) shoots along a light gradient. *Plant, Cell and Environment*, *26*, 429–442.

Chen, J. M., & Black, T. A. (1992). Defining leaf area index for non-flat leaves. *Plant, Cell and Environment*, *15*, 421–429.

Chen, J. M., Rich, P. M., Gower, S. T., Norman, J. M., & Plummer, S. (1997). Leaf area index of boreal forests: Theory, techniques and measurements. *Journal of Geophysical Research*, *102*(D24), 29429–29443.

Daughtry, C. S. T., Ranson, K., & Biehl, L. (1989). A new technique to measure the spectral properties of conifer needles. *Remote Sensing of Environment*, *27*, 81–91.

Foley, J. D., van Dam, A., Feiner, S. K., & Hughes, J. F. (1990). *Computer graphics: Principles and practice* (2nd ed.). Reading, MA: Addison-Wesley.

Gates, D. M., & Benedict, C. M. (1963). Convection phenomena from plants in still air. *American Journal of Botany*, *50*, 536–573.

Gerard, F. F., & North, P. R. J. (1997). Analyzing the effect of structural variability and canopy gaps on forest BRDF using a geometric-optical model. *Remote Sensing of Environment*, *62*, 46–62.

Häme, T., Stenberg, P., Andersson, K., Rauste, Y., Kennedy, P., Folving, S., & Sarkeala, J. (2001). AVHRR-based forest proportion map of the Pan-European area. *Remote Sensing of Environment*, *77*, 76–91.

Holman, J. P. (1986). *Heat transfer* (6th ed.). New York: McGraw-Hill.

Knyazikhin, Y., Martonchik, J. V., Myneni, R. B., Diner, D., & Running, S. W. (1998). Synergistic algorithm for estimating vegetation canopy leaf area index and fraction of absorbed photosynthetically active radiation from MODIS and MISR data. *Journal of Geophysical Research*, *103*, 32257–32276.

Kuusk, A., & Nilson, T. (2000). A directional multispectral forest reflectance model. *Remote Sensing of Environment*, *72*, 244–252.

Lang, A. R. G. (1991). Application of some of Cauchy's theorems to estimation of surface areas of leaves, needles and branches of plants, and light transmittance. *Agricultural and Forest Meteorology*, *55*, 191–212.

Loechel, S. E., Walthall, C. L., de Colstoun, E. B., Chen, J., Markham, B. L., & Miller, J. (1997). Variability of boreal forest reflectances as measured from a helicopter platform. *Journal of Geophysical Research*, *102*(D24), 29495–29503.

Mandelbrot, B. B. (1983). *The fractal geometry of nature*. New York: Freeman.

Martonchik, J. V., Bruegge, C. J., & Strahler, A. L. (2000). A review of reflectance nomenclature used in remote sensing. *Remote Sensing Reviews*, *19*, 9–20.

Nilson, T. (1971). A theoretical analysis of the frequency of gaps in plant stands. *Agricultural Meteorology*, *8*, 25–38.

Nilson, T., Anniste, J., Lang, M., & Praks, J. (1999). Determination of needle area indices of coniferous forests canopies in the NOPEX region by ground-based optical measurements and satellite images. *Agricultural and Forest Meteorology*, *98–99*, 449–462.

Nilson, T., & Peterson, U. (1991). A forest canopy reflectance model and a test case. *Remote Sensing of Environment*, *37*, 131–142.

Nilson, T., & Ross, J. (1997). Modeling radiative transfer trough forest canopies: Implications for canopy photosynthesis and remote sensing. In H. L. Gholz, K. Nakane, & H. Shimoda (Eds.), *The use of remote sensing in the modeling of forest productivity* (pp. 23–60). Dordrecht, The Netherlands: Kluwer Academic Publishing.

Norman, J. M., & Jarvis, P. G. (1975). Photosynthesis in sitka spruce (*Picea sitchensis* (Bong.) Carr.). *Journal of Applied Ecology*, *12*(3), 839–878.

Oker-Blom, P., & Kellomäki, S. (1983). Effect of grouping of foliage on the within stand and within-crown light regime: Comparison of random and grouping canopy models. *Agricultural Meteorology*, *28*, 143–155.

Oker-Blom, P., & Smolander, H. (1988). The ratio of shoot silhouette area to total needle area in Scots pine. *Forest Science*, *34*, 894–906.

Palmroth, S., Stenberg, P., Smolander, S., Voipio, P., & Smolander, H. (2002). Fertilization has little effect on light-interception efficiency of *Picea abies* shoots. *Tree Physiology*, *22*, 1185–1192.

Panferov, O., Knyazikhin, Y., Myneni, R. B., Szarzynski, J., Engwald, S., Schnitzler, K. G., & Gravenhorst, G. (2001). The role of canopy structure in the spectral variation of transmission and absorption of solar radiation in vegetation canopies. *IEEE Transactions on Geoscience and Remote Sensing*, *39*, 241–253.

Ross, J. (1981). *The radiation regime and architecture of plant stands*. Hague: Kluwer Academic Publishing.

Ross, J., Meinander, O., & Sulev, M. (1994). Spectral scattering properties of Scots pine shoots. In T. I. Stein (Ed.), *Surface and atmospheric remote sensing: Technologies, data analysis and interpretation. International Geoscience and Remote Sensing Symposium IGARSS'94* (pp. 1451–1454). Piscataway: Institute of Electrical and Electronics Engineers.

Shabanov, N. V., Knyazikhin, Y., Baret, F., & Myneni, R. B. (2000). Stochastic modeling of radiation regime in discontinuous vegetation canopies. *Remote Sensing of Environment*, *74*, 125–144.

Smolander, S., & Stenberg, P. (2001). A method for estimating light interception by a conifer shoot. *Tree Physiology*, *21*, 797–803.

Stenberg, P. (1996). Correcting LAI-2000 estimates for the clumping of needles in shoots of conifers. *Agricultural and Forest Meteorology*, *79*, 1–8.

Stenberg, P., Kangas, T., Smolander, H., & Linder, S. (1999). Shoot structure, canopy openness, and light interception in Norway spruce. *Plant, Cell and Environment*, *22*, 1133–1142.

Stenberg, P., Linder, S., Smolander, H., & Flower-Ellis, J. (1994). Performance of the LAI-2000 plant canopy analyzer in estimating leaf area index of some Scots pine stands. *Tree Physiology*, *14*, 981–995.

Stenberg, P., Palmroth, S., Bond, B. J., Sprugel, D. G., & Smolander, H. (2001). Shoot structure and photosynthetic efficiency along the light gradient in a Scots pine canopy. *Tree Physiology*, *21*, 805–814.

Stenberg, P., Smolander, H., & Kellomäki, S. (1993). Description of crown structure for light interception models: Angular and spatial distribution of shoots in young Scots pine. *Studia Forestalia Suecica*, *191*, 843–850.

Stenberg, P., Smolander, H., Sprugel, D., & Smolander, S. (1998). Shoot structure, light interception, and distribution of nitrogen in an *Abies amabilis* canopy. *Tree Physiology*, *18*, 759–767.

Tian, Y., Zhang, Y., Knyazikhin, Y., Myneni, R. B., Glassy, J. M., Dedieu, G., & Running, S. W. (2000). Prototyping of MODIS LAI and FPAR algorithm with LASUR and LANDSAT data. *IEEE Transactions on Geoscience and Remote Sensing*, *38*, 2387–2401.

Zhang, Y., Tian, Y., Myneni, R. B., Knyazikhin, Y., & Woodcock, C. E. (2002). Assessing the information content of multiangle satellite data for mapping biomes I: Statistical analysis. *Remote Sensing of Environment*, *80*, 418–434.

V

Available online at www.sciencedirect.com

SCIENCE DIRECT®

Remote Sensing of Environment 94 (2005) 355–363

Remote Sensing of Environment

www.elsevier.com/locate/rse

# Simple parameterizations of the radiation budget of uniform broadleaved and coniferous canopies

Sampo Smolander[a], Pauline Stenberg[b,*]

[a]Department of Mathematics and Statistics, P.O. Box 68, FIN-00014, University of Helsinki, Finland
[b]Department of Forest Ecology, University of Helsinki, P.O. Box 27, FIN-00014, Finland

Received 12 August 2004; received in revised form 28 October 2004; accepted 30 October 2004

**Abstract**

Simulations of the different components of the spectral radiation budget of structurally simple leaf and shoot canopies with varying canopy leaf area index (LAI) were performed. The aims were (1) to test a proposed parameterization of the budget using two spectrally invariant canopy structural parameters ($p$ and $p_t$) governing canopy absorption and transmittance, respectively, and (2) to incorporate the effect of within-shoot scattering in the parameterization for shoot canopies. Results showed that canopy spectral absorption and scattering were well described by a single parameter, the canopy $p$ value or 'recollision probability', which was closely related to LAI. The relationship between $p$ and LAI was however different in leaf and shoot canopy: e.g., at the same LAI the recollision probability was larger in the shoot canopy. It was shown that the $p$ value of the shoot canopy could be decomposed into the $p$ value of an individual shoot ($p_{sh}$) and the $p$ value of the leaf canopy with the same effective LAI ($LAI_e$). The canopy $p$ value allows calculation of canopy absorption and scattering at any given wavelength from the leaf (or needle) scattering coefficient at the same wavelength. To calculate canopy reflectance, separation of the downward and upward scattered parts is needed in addition. The proposed parameter $p_t$ worked rather well in the leaf canopy at moderate values of LAI, but not in the coniferous shoot canopy nor at high values of LAI. However, the simulated fraction of upward scattered radiation increased in a straightforward manner with LAI, and was not particularly sensitive to the leaf (or needle) scattering coefficient. Judged by this 'smooth' behavior, the existence of another kind of simple parameterization for this separation remains an interesting possibility.


*Keywords:* LAI; Vegetation canopy; Parameterization; Spectra; Radiative transfer

## 1. Introduction

The basic premises for optical remote sensing of vegetation are that the solar radiation received by a remotely located sensor (e.g., on a satellite) upon interaction with the vegetation canopy carries in it the signature of the canopy, and that this spectral signature can be deciphered to obtain the information of interest (Goel, 1988, 1989). Physically based methods for the assessment or monitoring of vegetation parameters (e.g., structural and biophysical characteristics) have progressively become more and more attractive since they are better suited for many current large-scale applications than the traditionally used statistical (empirical) techniques (Knyazikhin et al., 1998b). The parameters of interest vary with the area of application (production ecology, global change monitoring, climate models, etc.); however, for all applications good models of the shortwave radiation budget of vegetation canopies are needed to interpret the remotely sensed signal. The shortwave 'radiation budget' describes how the fractions of radiation absorbed by or scattered out from the canopy to the underlying soil and understorey or back to space (canopy reflectance or albedo) are related to the structural and optical properties of canopy and background.

Given a detailed description of a single canopy, the radiation budget can be calculated using Monte Carlo simulation models (Disney et al., 2000). However, the simulation results are case specific and difficult to generalize

* Corresponding author. Tel.: +358 9 191 58105.
*E-mail address:* pauline.stenberg@helsinki.fi (P. Stenberg).

0034-4257/$ - see front matter © 2004 Elsevier Inc. All rights reserved.
doi:10.1016/j.rse.2004.10.010

in lack of knowledge on which of the various canopy characteristics used as input are the most important. To be more generally and operationally applicable, models should build upon a canopy representation with only a small set of basic parameters which govern the radiation budget with sufficient accuracy.

Knyazikhin et al. (1998a,b) analyzed the multiplication factor eigenvalues of the radiative transfer equation for vegetation canopies to find such set of parameters (see Bell & Glasstone, 1970, Section 1.5e). They proposed that, to a good approximation, the amount of radiation absorbed by a canopy should depend only on the wavelength and a canopy structural parameter ($p$), which is wavelength independent. The parameter $p$ can be interpreted as the probability that a photon scattered from a leaf in the canopy will interact within the canopy again—the "recollision probability". Knowing the $p$ value of a canopy, the scattering coefficient of the canopy at any wavelength can be predicted from the leaf scattering coefficient at the same wavelength. Knyazikhin et al. (1998a,b) also introduced a similar parameter ($p_t$) relating canopy transmittances at two different wavelengths to the leaf scattering coefficients at these wavelengths. Given the absorption ($p$ value) and transmission ($p_t$ value), total reflectance (the upward scattered part of the incident radiation) is also known (because they all sum up to one). The eigenvalue theory thus states that the radiation budget of a vegetation canopy can be parameterized using only two parameters ($p$ and $p_t$) which, however, depend on canopy structure in a rather complex manner (Panferov et al., 2001; Shabanov et al., 2003; Wang et al., 2003). Although both parameters are related to the canopy leaf area index (LAI), the relationships between $p$, $p_t$ and LAI in addition may vary with a set of other parameters, including leaf orientation and spatial distribution, and the degree of grouping of the leaves.

In this paper, we study the behavior of the spectral radiation budget of structurally simple model canopies and demonstrate the effect within-shoot scattering has on the budget. We first estimate the canopy spectral scattering coefficient, defined as the ratio of photons exiting the canopy to those initially hitting leaves or needles in the canopy, for simulated canopies of varying leaf area index (LAI) and composed of randomly distributed single leaves ("leaf canopy") or shoots ("shoot canopy"). This is done by photon tracing (Jensen, 2001), where photons of specified wavelength fired into the canopy are followed until they are absorbed or exit the canopy. The structural parameter ($p$) is estimated by recording the number of interactions between the photons and the canopy.

The shoot canopy differs from the leaf canopy in that a photon hitting a needle on a shoot may undergo several interactions within the shoot before being absorbed or scattered out from the shoot. In a previous paper (Smolander & Stenberg, 2003), we introduced the recollision probability within a coniferous shoot ($p_{sh}$) and showed that the shoot scattering coefficient could be predicted from $p_{sh}$ using the same relationship as the one proposed to hold true at the canopy level. The result offers a means to account for the within-shoot scattering in models developed primarily for broadleaved canopies. Here, we show that in the shoot canopy, the canopy level recollision probability can be decomposed into $p_{sh}$ and the $p$ value of a leaf canopy with the same "effective LAI". In two canopies with the same effective LAI, the collided and uncollided part of incoming photons (canopy interceptance and zero order transmittance) are the same for both canopies. We derive the relationship between $p$ and canopy LAI in the two model canopies, allowing the total amount of scattered (or absorbed) radiation to be calculated as a function of LAI. Finally, the proposed $p_t$-method of separating the scattered radiation into downward and upward scattered (i.e. reflected) parts as well as the two-stream model by Ross (1981) is evaluated using the simulation results.

## 2. Theoretical background and aim of study

### 2.1. Canopy absorption and scattering

We use the following terminology to separate the fates of photons arriving in a vegetation canopy, assumed to be bounded underneath by a black surface. The portion of photons which do not interact with leaves at all but are transmitted directly to the ground through gaps in the canopy is called the zero order canopy transmittance ($t_0$). Canopy interceptance ($i_0$) correspondingly denotes the portion of incoming photons hitting a leaf, and thus we have $i_0+t_0=1$. Notice that $i_0$ and $t_0$ depend on the incoming direction of the photons but do not depend on their wavelength ($\lambda$). Part of $i_0$ will be absorbed by the leaves in the canopy, this wavelength dependent part is the canopy spectral absorption ($a(\lambda)$), while another part ($s(\lambda)$) is scattered out from the canopy ($i_0=a+s$). Note that, at this point, $s$ contains both the upward (to the sky) and downward (to the ground) scattered photons. The canopy radiation budget can now be written as:

$$a(\lambda) + s(\lambda) + t_0 = 1 \tag{1}$$

Panferov et al. (2001) introduced the canopy structural parameter ($p$), which can be interpreted as the (mean) probability by which a photon scattered from a leaf in the canopy will interact within the canopy again. We call this the recollision probability. On the assumption that the recollision probability remains constant in successive interactions, canopy absorption ($a$) and scattering ($s$), normalized by canopy interceptance ($i_0$, the part of incoming photons not transmitted directly to the ground), are then obtained as:

$$\begin{aligned} a(\lambda)/i_0 &= (1-\omega_L(\lambda)) + \omega_L(\lambda)p(1-\omega_L(\lambda)) \\ &\quad + \omega_L(\lambda)^2 p^2(1-\omega_L(\lambda)) + \ldots = \frac{1-\omega_L(\lambda)}{1-p\omega_L(\lambda)} \end{aligned} \tag{2}$$

and

$$s(\lambda)/i_0 = \frac{\omega_L(\lambda) - p\omega_L(\lambda)}{1 - p\omega_L(\lambda)} \quad (3)$$

where $\omega_L$ denotes the leaf scattering coefficient (leaf reflectance plus transmittance). Schematically, the fate of the incoming photons can be thought to follow the four-state Markov chain model presented in Fig. 1.

The ratios $a(\lambda)/i_0$ and $s(\lambda)/i_0$ (Eqs. (2) and (3)) represent the portions of photons absorbed and scattered out from the canopy from those initially hitting the canopy, i.e. they can be interpreted as the absorption and scattering coefficients of the canopy. The average number of interactions ($n$) between a photon and (leaves in) the canopy, furthermore, is obtained as the ratio of canopy to leaf absorption coefficients, that is:

$$n(\lambda) = \frac{1}{1 - p\omega_L(\lambda)} \quad (4)$$

Eq. (4) describes the simple relationship between the recollision probability ($p$) and the degree of multiple scattering within the canopy.

In our previous paper, the $p$ value of an individual coniferous shoot ($p_{sh}$) was introduced and was successfully used to describe the absorption and scattering coefficients of the shoot by means of Eqs. (2) and (3) with $p$ replaced by $p_{sh}$ and with $\omega_L$ denoting the needle scattering coefficient (Smolander & Stenberg, 2003, Eqs. (4) and (6), p. 366). The shoot scattering coefficient ($\omega_{sh}$) is smaller than that of its needles ($\omega_L$) (except at completely absorbing or completely scattering wavelengths) but the relationship is nonlinear so that the ratio of $\omega_{sh}$ to $\omega_L$ increases with $\omega_L$ and decreases with increasing $p_{sh}$. It was shown, also, that close to perfect linear relationship existed between $p_{sh}$ and the spherically averaged ratio of shoot silhouette area to total needle area ($\overline{STAR}$), allowing $p_{sh}$ to be calculated as $1 - 4\overline{STAR}$. In this study, we test the relationships (Eqs. (2) and (3)) at the canopy level using simulated model canopies composed of randomly distributed and spherically oriented leaves and shoots, respectively. The canopy $p$ values are denoted $p_{LC}$ (leaf canopy) and $p_{CC}$ (coniferous canopy). Further, we derive the relationship between $p$ and canopy leaf area index (LAI) and test the hypothesis that $p_{CC}$ can be decomposed into $p_{sh}$ and the $p_{LC}$ of a leaf canopy with the same effective leaf area index ($LAI_e$) as:

$$p_{CC} = p_{sh} + (1 - p_{sh})p_{LC}(LAI_e) \quad (5)$$

In the way presented above (Eqs. (1)–(5)), we can relate the canopy spectral absorption and scattering to a single parameter, the canopy $p$ value, which is a function of LAI.

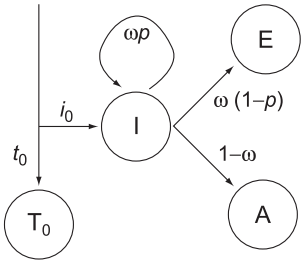


Fig. 1. An illustration of the four-state Markov chain model for canopy absorption and scattering. The photon, coming from the sky, can go through the canopy without interactions with probability $t_0$, and end up in $T_0$ (assuming black soil and thus no further scattering). With probability $i_0=1-t_0$ it will interact with the canopy (state I). With probability $1-\omega$ it will be absorbed (state A). With probability $\omega p$ it will be scattered by the phytoelement and then hit the canopy again. With probability $\omega(1-p)$ the photon will be scattered by the phytoelement and not hit the canopy again, it will escape (state E).

### 2.2. Upward and downward scattering

Canopy scattering is divided into upward and downward scattering, of which the former component is of special interest here being the one registered by remote sensing instruments. The upward scattered part of $s$ is called canopy spectral reflectance ($r(\lambda)$). Canopy spectral transmittance ($t(\lambda)$), in turn, is composed of the downward scattered part of $s$ ($t_s(\lambda)$) plus the (wavelength independent) zero order transmittance ($t_0$). We have then:

$$a(\lambda) + s(\lambda) + t_0 = a(\lambda) + r(\lambda) + t_s(\lambda) + t_0 = 1 \quad (6)$$

When leaves have nonzero absorption, that is $\omega_L<1$, it is easy to decompose the total absorption ($a$) into first order ($a_1$) and higher order ($a_s$) absorption: $a=a_1+a_s$. The photons that are absorbed at the first interaction constitute $a_1$. The total radiation budget is then:

$$a_1(\lambda) + a_s(\lambda) + r(\lambda) + t_s(\lambda) + t_0 = 1 \quad (7)$$

and, actually, $a_1$ is easy to calculate: $a_1=(1-t_0)(1-\omega_L(\lambda))$.

Panferov et al. (2001) defined the other structural canopy parameter, $p_t$, by a simple algebraic combination of leaf and canopy spectral transmittances which, based on both empirical and theoretical analyses, was proposed to eliminate the dependency on wavelength. Using the parameter $p_t$, canopy transmittance at any given wavelength ($\lambda$) is related to that at a reference wavelength ($\lambda_{ref}$) by the equation:

$$t(\lambda) = t(\lambda_{ref})\frac{1 - p_t\omega_L(\lambda_{ref})}{1 - p_t\omega_L(\lambda)} \quad (8)$$

Interpretation of the parameter $p_t$ is not as straightforward as that for the parameter $p$, however, using $\omega_L(\lambda_{ref})=0$, Shabanov et al. (2003, Eq. (3), p. 413) arrived at the relationship:

$$\frac{t(\lambda) - t_0}{t(\lambda)} = \frac{t_s(\lambda)}{t(\lambda)} = p_t\omega_L(\lambda) \quad (9)$$

according to which the product $p_t\omega_L$ is equal to the portion of collided radiation ($t_s$) from the total canopy transmittance ($t$).

Using Eqs. (3) and (9), canopy scattering ($s$) and its division into upward ($r$) and downward components ($t_s$) can be solved as a function of the parameters $p$ and $p_t$:

$$\frac{r(\lambda)}{s(\lambda)} = \frac{s(\lambda) - t_s(\lambda)}{s(\lambda)} = 1 - \frac{t_0 p_t \omega_L(\lambda)(1 - p\omega_L(\lambda))}{i_0(\omega_L(\lambda) - p\omega_L(\lambda))(1 - p_t\omega_L(\lambda))} \quad (10)$$

In this paper, the performance of Shabanov's method of separating the total canopy scattering into upward and downward scattered components is tested. We also test the applicability of the model by Ross (1981, Section II.6.4), derived for uniform leaf canopies, on our shoot canopies by incorporating a correction for within-shoot scattering. In the two-component model by Ross, the upward and downward components of radiation inside a canopy are modeled by a pair of differential equations, which in the case of a homogeneous Poisson canopy with spherically oriented Lambertian leaves, yields a good approximate analytical solution.

### 2.3. Simulation method

Simulations of the different components of the radiation budget (Eq. (7)) were performed for the model canopies with different values of LAI. The aim was to test the proposed parameterization of the radiation budget (Eqs. (1)–(10)), which can be solved knowing the two canopy structural parameters ($p$ and $p_t$) together with the leaf (needle) scattering coefficient ($\omega_L$) and, in case of the shoot canopy, the parameter $p_{sh}$ related to shoot structure. The canopies were composed of randomly distributed and spherically oriented foliage elements (leaves or shoots), and the underlying soil was assumed black. In the simulations, the incident angle of incoming photons was set to 45°. In addition, the effect of differing incoming angles was studied separately.

The simulation algorithm is as described in Smolander and Stenberg (2003). In short, a number of photons at different wavelengths are fired into the canopy and every photon is followed by photon tracing (a computer graphics method similar to ray tracing, but following a photon in the direction it actually moves; see Jensen, 2001) until it is absorbed by a leaf or a shoot, or exits the canopy. The lengths of the free paths for photons are taken from the exponential distribution, and successive paths are treated independently. (Thus, the model does not include the backscattering hot spot effect.) Zero order canopy transmittance ($t_0$) and interceptance ($i_0$) in the model canopies are given by:

$$t_0 = \exp(-GLAI/\cos\theta) \quad (11a)$$

and

$$i_0 = 1 - \exp(-GLAI/\cos\theta) \quad (11b)$$

where LAI denotes the leaf area index, $\theta$ is the angle of incidence for photons (solar zenith angle), and $G$ is the extinction coefficient, taking the value 0.5 in the leaf canopy. In the shoot canopy, the $G$ value corresponds to $2\overline{STAR}$, where $\overline{STAR}$ is the spherically averaged ratio of shoot silhouette area to total needle area (Oker-Blom & Smolander, 1988). In this study, we used the values $\overline{STAR} = 0.133$ and $p_{sh} = 1 - 4\overline{STAR} = 0.47$ representative of a Scots pine (*Pinus sylvestris* L.) shoot (Smolander & Stenberg, 2003). The value used here for $\overline{STAR}$ implies that the LAI of the shoot canopy must be 88% higher (0.5/0.266=1.88) than the LAI of the leaf canopy to get similar $t_0$ and $i_0$ (or that, for similar values of LAI, the effective LAI ($LAI_e$) of the shoot canopy is 47% smaller (0.266/0.5=0.53) than that of the leaf canopy).

## 3. Results

The basic spectral behavior of the canopy radiation budget is presented in Fig. 2. The most obvious difference between the leaf canopy (Fig. 2A) and the shoot canopy

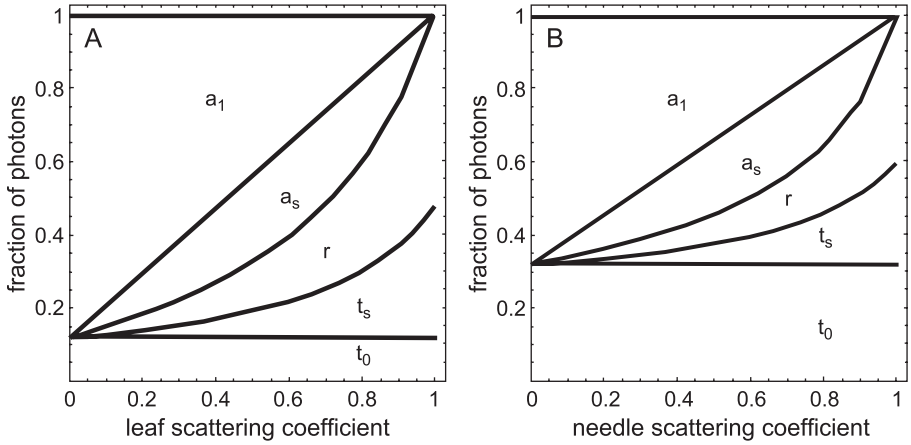


Fig. 2. Schematic presentation of the different components of radiation as a function of the leaf (needle) scattering coefficient for the two model canopies ((A) leaf canopy, (B) shoot canopy) with LAI=3.

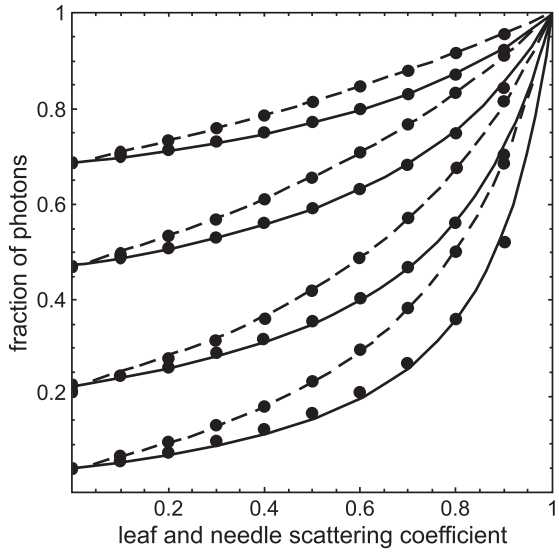


Fig. 3. The non-absorbed component, $1-a=t_0+t_s+r$ (see Fig. 2) of the canopy radiation budget as a function of the leaf (needle) scattering coefficient. The black dots denote values obtained from simulations, and the curves for the shoot canopies (solid lines) and leaf canopies (broken lines) were fitted using Eq. (3). Values of LAI for the shoot canopies were LAI=1 (uppermost curve), 2, 4, and 8 (lowest curve). The leaf canopy LAI values were chosen so, that the effective LAI ($LAI_e$) was the same for each pair of leaf and shoot canopies.

(Fig. 2B) of the same LAI (here LAI=3) is that because the shoot canopy has a smaller $LAI_e$, a larger part of the incoming photons goes straight through (larger $t_0$). This of course causes the other components to be, respectively, smaller for the shoot canopy. Another difference is that, in the leaf canopy, the total absorption ($a=a_1+a_s$) and scattering ($s=r+t_s$) respond more linearly to the element scattering coefficient than in the shoot canopy.

At the same $LAI_e$, the zero order transmittance ($t_0$) is equal for the two canopies but the scattered part of $i_0$ is smaller in the shoot canopy except at completely absorbing or completely scattering wavelengths (Fig. 3). At all other wavelengths the shoot canopy absorbs more than a leaf canopy with the same $LAI_e$. In both the leaf and the shoot canopy, the fraction of scattered photons as a function of $\omega_L$

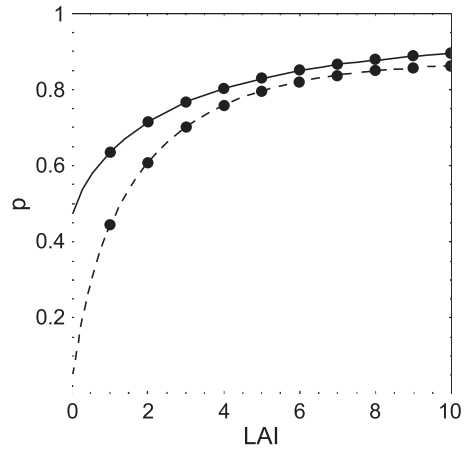


Fig. 5. Parameter $p$ ($p_{LC}$ and $p_{CC}$) for the leaf and shoot canopy as a function of LAI. Black dots denote the $p$ values solved by Eq. (2) using the simulated absorption data (see Fig. 3). The curve fitted for the leaf canopy (broken curve) is $p_{LC}=p_{LC,max}(1-\exp(-k\mathrm{LAI}^b))$, with $p_{LC,max}=0.88$, $k=0.7$ and $b=0.75$. The curve for the shoot canopy (solid curve) was produced independently using the decomposition formula (Eq. (5)).

(plotted in Fig. 3) shows good agreement with Eq. (3), but with different $p$ values.

Estimated $p$ values of the leaf canopy ($p_{LC}$) and the shoot canopy ($p_{CC}$) for different values of LAI are shown in Fig. 4A and B. The parameter $p$ was estimated in two different ways: by fitting Eq. (3) to the simulated canopy and leaf scattering coefficients for different $\omega_L$ ("fitted $p$", shown in Fig. 4), and independently, by calculating the recollision probability by directly counting the interaction events in a single photon tracing simulation with $\omega_L=1$ ("direct $p$"). As shown in Fig. 4A and B, there is close to perfect agreement (one to one relationship) between the fitted and directly counted values of $p$. This indicates that to estimate the canopy $p$ value one needs only to perform the photon tracing simulations with one wavelength, instead of performing them for a number of wavelengths and then applying a curve fitting procedure to the data. In Fig. 4C, the value of $p_{CC}$ calculated using the decomposition formula (Eq. (5)) is compared to the fitted $p_{CC}$, showing good agreement.

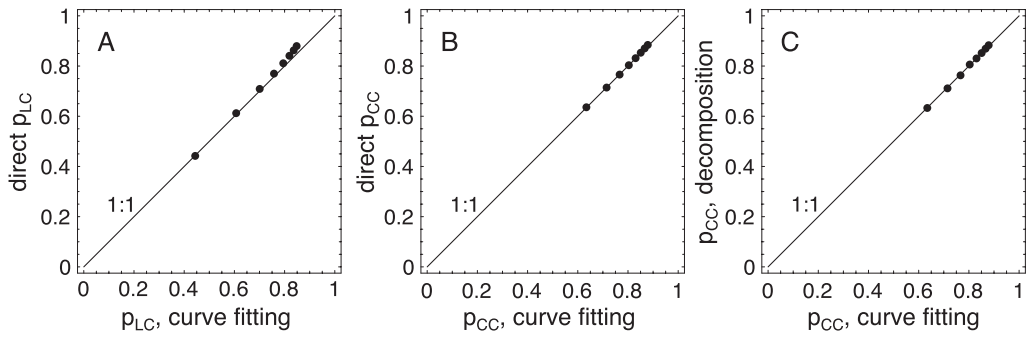


Fig. 4. (A, B) Comparison of $p$ values obtained by fitting Eq. (3) to simulations performed for different $\omega_L$ (see Fig. 3), and by direct counting of the photon interaction events for simulations with $\omega_L=1$ ((A) leaf canopy, (B) shoot canopy). (C) Shoot canopy, $p_{CC}$ calculated with the decomposition formula (Eq. (5)) plotted against the fitted values of $p_{CC}$. The dots represent LAI=1, 2, 3,..., 8.

Fig. 5 presents (i) how the leaf canopy $p$ value ($p_{LC}$) changes as a function of LAI, and (ii) how the dependence between LAI and the $p$ value of the shoot canopy ($p_{CC}$) can be predicted from $p_{sh}$ and $p_{LC}$ using the decomposition formula (Eq. (5)). The parameter $p_{LC}$ as a function of LAI was well approximated by the relationship $p_{LC}=p_{LCmax}(1-\exp(-k\mathrm{LAI}^b))$, with $p_{LCmax}=0.88$, $k=0.7$ and $b=0.75$. The $p$ value of the shoot canopy ($p_{CC}$) in turn was very well predicted by the decomposition formula evaluated using $p_{LC}$ of the leaf canopy with similar $\mathrm{LAI_e}$ and $p_{sh}=0.47$. This confirms our hypothesis that in the shoot canopy the recollision probability can be decomposed into within-shoot and between-shoot recollision probabilities.

Simulations made for different directions (zenith angles) of incoming photons showed that the zenith angle, because it changes the distribution of the points of first interaction within the canopy, has some effect on $p_{LC}$ (Fig. 6). However, for zenith angles less than ca. 50°, the variation in $p_{LC}$ was less than 1.2%. This means that the $p$ value is practically insensitive to the solar zenith angle in the range of solar angles commonly used in satellite remote sensing.

The canopy $p$ value provides the key for calculating canopy absorption and scattering, respectively, but not for separating between the upward ($r$) and downward ($t_s$) components of the scattered radiation ($s$). For this purpose, we tested the applicability of the model by Ross (1981) and the parameterization proposed by Shabanov et al. (2003).

In the two-component model by Ross, the upward and downward components of radiation inside a canopy are modeled by a pair of differential equations, shown to give a good approximate analytical solution in the case of a homogeneous Poisson canopy with spherically oriented Lambertian leaves, i.e. corresponding to the leaf canopy in this study. In Fig. 7, simulated values of $r$ and $t_s$ in the shoot canopy with LAI=4 are compared to results obtained by the model of Ross (1981). When $\mathrm{LAI_e}$ (=2.13) was used as an input value for the model (instead of the true LAI), the simple components, zero-order transmittance ($t_0$) and interceptance ($i_0$), were obtained correctly but the canopy scattering and thus its upward and downward components ($r$ and $t_s$) were overestimated by the model (Fig. 7, broken lines). However, when the correction for within-shoot scattering was included in the model by replacing the needle scattering coefficient (transmittance and reflectance) by that of the shoot (see Smolander & Stenberg, 2003), the curves shifted and the model agreed well with the simulations (Fig. 7, solid line).

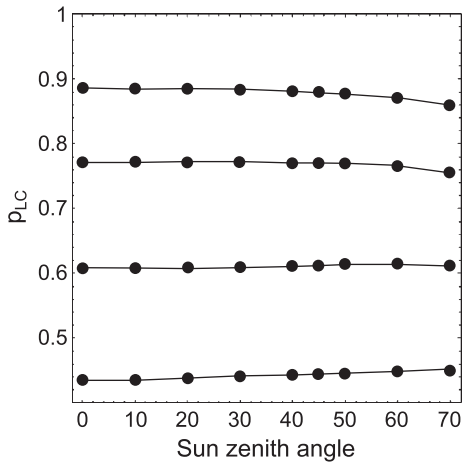


Fig. 6. The effect of solar zenith angle on $p_{LC}$ for LAI=1 (lowest curve), 2, 4, and 8 (highest curve). Black dots denote simulated values.

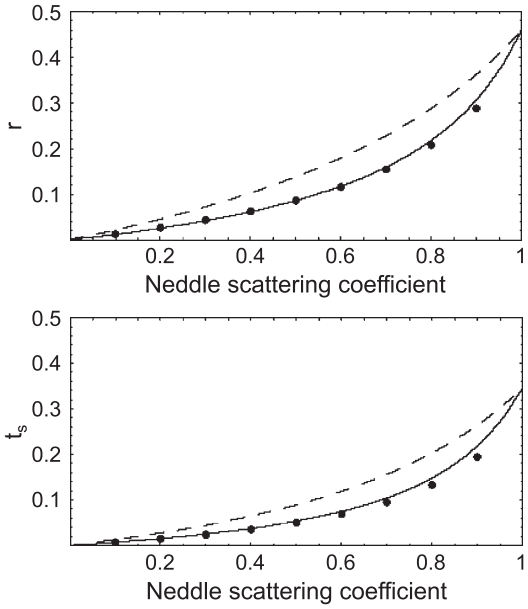


Fig. 7. Demonstration of the effect of including within-shoot scattering in the leaf-based model by Ross (1981). Black dots denote the reflected ($r$) and transmitted scattered radiation ($t_s$) for the shoot canopy with LAI=4. When the model was used with the effective LAI ($\mathrm{LAI_e}$=2.13) as input, zero order transmittance ($t_0$) was obtained correctly (not shown here) but components $r$ and $t_s$ were overestimated (broken curves). When, additionally, the element scattering coefficient was corrected for by including within-shoot scattering, as suggested by Smolander and Stenberg (2003), the curves shifted and the model fitted well to the simulation data (solid curves).

Simulated values of the ratio of upward to total scattering, $r/(r+t_s)$ for the leaf and shoot canopy, as a function of the leaf (needle) scattering coefficient ($\omega_L$), are presented in Fig. 8, and compared to results obtained by the models of Ross (1981) and Shabanov et al. (2003). The fraction of upward scattered radiation increased with LAI: for LAI=2 (the lowest curve), approximately 60% of the scattered photons escaped upwards in both the shoot and the leaf canopy, and for LAI=8, the upwards escaping fraction was more than 90% in the leaf canopy (Fig. 8A) and about 80% in the shoot canopy (Fig. 8C). (Notice that values of the effective LAI are smaller in the shoot canopy.) A slight decrease in $r/(r+t_s)$ with increasing $\omega_L$ can be observed. This pattern was correctly mimicked by Ross' model, which generally showed good agreement with the simulations both in the leaf canopy and the shoot canopy (when the shoot level correction was applied). Shabanov's parameterization worked rather well for the leaf canopy at moderate values of

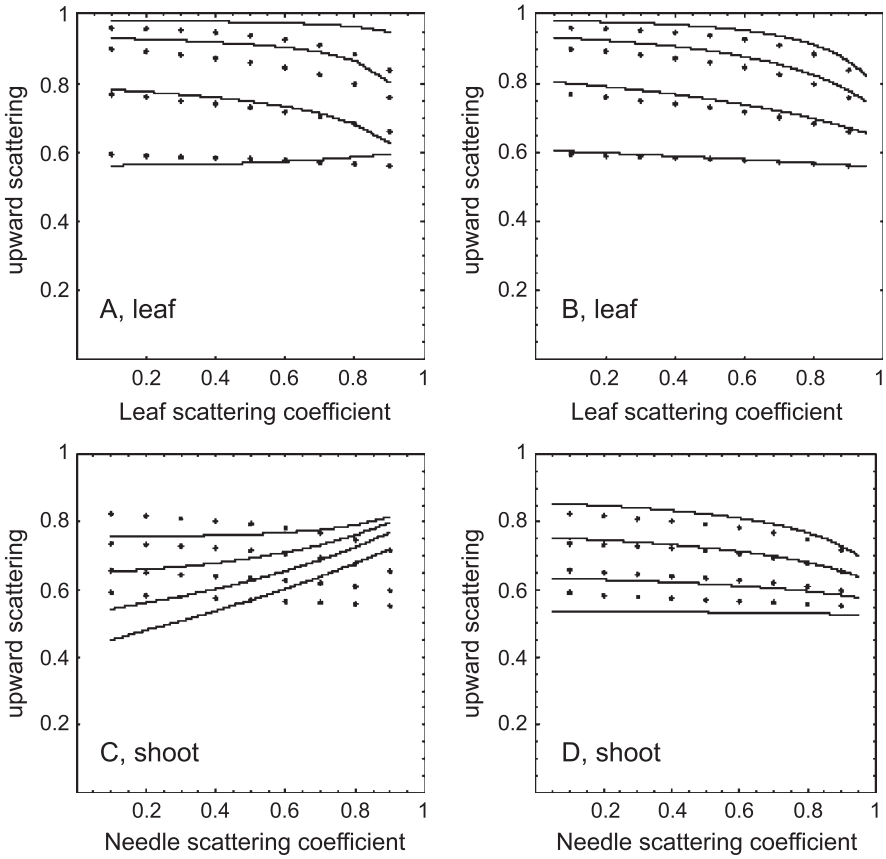


Fig. 8. Simulated values (black dots) of the upward fraction of the total scattered radiation $r/(r+t_s)$ for the leaf and shoot canopies with LAI=2 (lowest dot-line), 4, 6, and 8 (highest dot-line). (A, B) Leaf canopy. (C, D) Shoot canopy. The curves present the results obtained by the $p_t$-method described by Shabanov et al. (2003) (A and C) and the two-stream model by Ross (1981) (B and D).

LAI (LAI=2 and 4) but not so well for the shoot canopy or for high values of LAI. The curves were produced by Eq. (10), using fixed (i.e. the simulated) values of $s$ and $t_0$ and the value for $p_t$ giving the best fit to the simulations. Despite this fitting procedure, poor results for the shoot canopy were obtained due to the different shapes of the simulated and calculated curves. The shape of the curve described by Eq. (10) depends in a complex manner on the relation between $p$ and $p_t$, which explains the different outlook of the curves in Fig. 8A and C. At similar LAI, the shoot canopy has larger $p$ value but smaller $p_t$ value.

To demonstrate the relevance of the shoot-level correction for the interpretation of remote sensing data, we used Ross' (1981) model, with shoot-level correction, to calculate canopy hemispherical reflectance in red and near-infrared (NIR) wavelengths. The leaf (needle) scattering coefficients were set to $\omega_L$=0.1 for red, and $\omega_L$=0.9 for NIR, and the canopies were assumed to be bounded underneath by two different soils with reflectance values of 0.05 and 0.15. Trajectories of leaf and shoot canopy hemispherical reflectance as functions of increasing LAI in the red–NIR plane are presented in Fig. 9. The shoot canopy spectral reflectances change in a different manner and more slowly with increased LAI than those of the leaf canopy, and thus the shoot canopy trajectories occupy a different space in the red–NIR plane than the leaf canopies. Also, an identical signal can result from different canopy and soil combinations. (Note that the hemispherical reflectance values of Fig. 9 are not directly

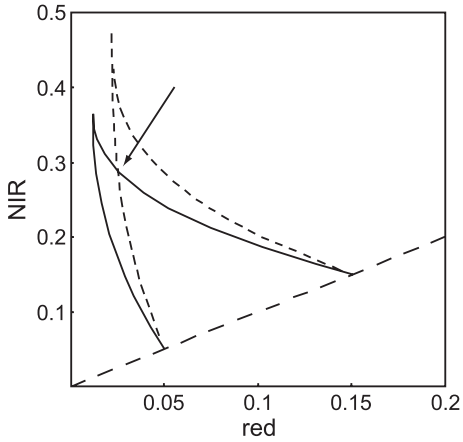


Fig. 9. Trajectories of the hemispherical reflectances of homogeneous leaf canopies (broken curve) and shoot canopies (solid curve) in the red–NIR plane. The trajectories start from the 1:1 soil line at two different soil reflectances: 0.05 and 0.15 (soil reflectance assumed to be the same in red and NIR). A trajectory crossing is indicated by an arrow, where leaf and shoot canopies with different LAI and soil reflectance produce an identical signal in the red–NIR plane: leaf canopy LAI=1.3 and soil reflectance 0.05; shoot canopy LAI=2.7 and soil reflectance 0.15.

comparable to the directional values measured by satellites, but the difference between leaf and shoot canopies should remain approximately the same.)

## 4. Discussion

The canopy $p$ value holds promising potential to be the single parameter needed to describe the canopy spectral absorption. The results presented here (Figs. 3 and 4) show that the approach works well in the case of simple homogeneous canopies. Based on our previous simulation study (Smolander & Stenberg, 2003), a similar approach works well in describing the spectral absorption of a coniferous shoot. Since also the combination of shoot-level and canopy-level recollision probabilities (Eq. (5), Figs. 4C and 5) worked well, it seems possible that also more complicated canopy structures could be handled in a similar manner. An important part of the usefulness of the $p$ value is its stability under different solar zenith angles (Fig. 6).

The inclusion of the within-shoot scattering, as described by the shoot level $p$ value ($p_{sh}$), seems to be crucial for realistic modeling of the radiation budget in a coniferous canopy. The effect of the within-shoot scattering is to increase canopy absorption when compared to a broad-leaved canopy with the same effective LAI (and thus equal zero order transmittance, $t_0$). With increased absorption, the scattered components ($r$ and $t_s$) decrease in such a way that in a coniferous canopy they respond more slowly to the increased leaf/needle scattering coefficient than in a broad-leaved canopy. Fig. 7 demonstrates this effect: When the model of Ross (1981) was applied to the shoot canopy, parameterized with effective LAI to get the direct component right, the scattered components were too large; but when the element scattering coefficient was corrected using the model by Smolander and Stenberg (2003), the curves "shifted" and matched the simulations well. Application of the model to demonstrate the relevance of the shoot-level correction for the interpretation of remote sensing data (Fig. 9) showed that the inclusion of within-shoot scattering changes the spectral behavior of coniferous forests, as compared to broadleaved forests, in a manner conforming to empirical observations (Tian et al., 2000).

The proposed simple parameterization of the canopy radiation budget included two parameters or "spectral invariants", $p$ and $p_t$. The canopy $p$ value can intuitively be understood to govern canopy absorption through its definition as the "recollision probability", i.e. the probability that a photon scattered from a leaf element will interact in the canopy again. As noted above, the parameter $p$ performed well in estimating the absorption of both homogeneous leaf canopies and homogeneous shoot canopies, and it is reasonable to believe that it should work also in canopies of still more complicated structure.

The other invariant, $p_t$, controls the part of the scattered radiation that exits the canopy downwards. No intuitively simple interpretation such as given for the $p$ value exists, or has yet been found for $p_t$, which can be defined as 'the eigenvalue (normalized by leaf albedo) of the linear operator that assigns downward radiances at the canopy bottom to incoming radiation' (Shabanov et al., 2003). For the simulated leaf canopies, the parameter $p_t$ performed relatively well, although the model of Ross (1981) performed slightly better (Fig. 8A and B). The situation was different for shoot canopies, where the $p_t$-based approach predicted that the upwards portion of scattered radiation should increase with increasing needle scattering coefficient, when it was actually decreasing (Fig. 8C). Ross' model, when corrected for effective LAI and for within-shoot scattering, on the other hand performed quite well in explaining the upwards portion of the scattered radiation (Fig. 8D).

It should be noted that Ross' model is formulated only for simple Poisson canopies, and thus is not directly applicable to canopies with nonuniform higher level structure. However, since the shoot-level correction of Smolander and Stenberg (2003) was able to extend the applicability of the model from Poisson leaf-canopies to Poisson shoot-canopies, it seems possible that a similar correction could work also for models with nonuniform higher level structure. The 'smooth' behavior of the simulated fraction of upward scattered radiation with increasing LAI (Fig. 8) moreover suggests that the parameterization approach for this separation remains an interesting possibility.

## 5. Conclusions

In short, results from this study confirmed that the spectral absorption and scattering of structurally simple uniform canopies can indeed be well described by a single parameter, the canopy $p$ value, which furthermore showed a close relationship with the LAI but insensitivity to the solar zenith angle. Shabanov et al. (2003) have proposed a similar parameter for separating the upward and downward parts of the scattered radiation. Unfortunately, based on the model simulations, this parameter does not seem to work when the shoot-level complexity is added to the canopy structure. The existence of another kind of simple parameterization for this separation however appears as a realistic assumption judged by the straightforward dependence of the ratio of upward to total scattered radiation on LAI, and its insensitivity to the leaf (needle) scattering coefficient. Another matter, not treated in this study, is what controls the directional distribution of the upward scattered (i.e. reflected) radiation. Ultimately, the goal would be a parameterization including tools also for calculating the bidirectional reflectance factor (BRF) of the canopy.

Many satellite instruments measure canopy reflectance from nadir only, and even though there are instruments that produce multidirectional data that can be used to estimate the total upwards component (see Zhang et al., 2002), one

would usually like to work with a model that accepts one-directional satellite data as input. Since the directional distribution of reflected radiation is not uniform, the satellite nadir readings do not as such contain enough information to estimate the total upwards scattered portion. Or, the other way around, nondirectional models for canopy radiation budget are not as such sufficient for use in satellite image interpretation. This issue is further complicated by the effect of crown shape on the directional reflectance distribution (Gerard & North, 1997; Rautiainen et al., 2004).

We think that simple parameterizations, when possible, will help to conceptualize and summarize the behavior of more complicated radiation budget models. They may also be useful when one tries to invert the more complicated models for operational satellite image interpretation purposes.

## Acknowledgements

The authors are grateful to Professor Elja Arjas for valuable scientific discussions on the topic as well as for providing the computing facilities for S. Smolander. We also wish to thank MSc Miina Rautiainen and the journal reviewers for useful comments on the manuscript. The work has been supported by Grant 50178 from the Academy of Finland.

## References

Bell, G. I., & Glasstone, S. (1970). Nuclear reactor theory. Malabar, FL: Robert E. Krieger Publishing.

Disney, M. I., Lewis, P., & North, P. R. J. (2000). Monte Carlo ray tracing in optical canopy reflectance modelling. *Remote Sensing Reviews*, *18*, 163–196.

Gerard, F. F., & North, P. R. J. (1997). Analyzing the effect of structural variation and canopy gaps on forest BRDF using a geometric-optic model. *Remote Sensing of Environment*, *62*, 46–62.

Goel, N. S. (1988). Models of vegetation canopy reflectance and their use in the estimation of biophysical parameters from reflectance data. *Remote Sensing Reviews*, *4*, 1–212.

Goel, N. S. (1989). Inversion of canopy reflectance models for estimation of biophysical parameters from reflectance data. In G. Asrar (Ed.), *Theory and applications of optical remote sensing* (pp. 205–251). New York: Wiley.

Jensen, H. W. (2001). Realistic image synthesis using photon mapping. Wellesley, MA: AK Peters.

Knyazikhin, Y., Kranigk, J., Myneni, R. B., Panferov, O., & Gravenhorst, G. (1998a). Influence of small-scale structure on radiative transfer and photosynthesis in vegetation cover. *Journal of Geophysica Research, D: Atmospheres*, *103*, 6133–6144.

Knyazikhin, Y., Martonchik, J. V., Myneni, R. B., Diner, D. J., & Running, S. W. (1998b). Synergistic algorithm for estimating vegetation canopy leaf area index and fraction of absorbed photosynthetically active radiation from MODIS and MISR data. *Journal of Geophysica Research, D: Atmospheres*, *103*, 32257–32276.

Oker-Blom, P., & Smolander, H. (1988). The ratio of shoot silhouette area to total needle area in Scots pine. *Forest Science*, *34*, 894–906.

Panferov, O., Knyazikhin, Y., Myneni, R. B., Szarzynski, J. Engwald, Schnitzler, K. G., & Gravenhorst, G. (2001). The role of canopy structure in the spectral variation of transmission and absorption of solar radiation in vegetation canopies. *IEEE Transactions on Geoscience and Remote Sensing*, *39*, 241–253.

Rautiainen, M., Stenberg, P., Nilson, T., & Kuusk, A. (2004). The effect of crown shape on the reflectance of coniferous stands. *Remote Sensing of Environment*, *89*, 41–52.

Ross, J. (1981). The radiation regime and architecture of plant stands. The Hague: Dr. W. Junk Publishers 391 pp.

Shabanov, N. V., Wang, Y., Buermann, W., Dong, J., Hoffman, S., Smith, G., et al. (2003). The effect of spatial heterogeneity in validation of the MODIS LAI and FPAR algorithm over broadleaf forests. *Remote Sensing of Environment*, *85*, 410–423.

Smolander, S., & Stenberg, P. (2003). A method to account for shoot scale clumping in coniferous canopy reflectance models. *Remote Sensing of Environment*, *88*, 363–373.

Tian, Y., Zhang, Y., Knyazikhin, Y., Myneni, R. B., Glassy, J. M., Dedieu, G., et al. (2000). Prototyping of MODIS LAI and FPAR algorithm with LASUR and LANDSAT data. *IEEE Transactions on Geoscience and Remote Sensing*, *38*, 2387–2401.

Wang, Y., Buermann, W., Stenberg, P., Smolander, H., Häme, T., Tian, Y., et al. (2003). A new parameterization of canopy spectral response to incident solar radiation: Case study with hyperspectral data from pine dominant forest. *Remote Sensing of Environment*, *85*, 304–315.

Zhang, Y., Tian, Y., Myneni, R. B., Knyazikhin, Y., & Woodcock, C. E. (2002). Assessing the information content of multiangle satellite data for mapping biomes: I. Statistical Analysis. *Remote Sensing of Environment*, *80*, 418–434.